Search for SM Higgs Boson in $ZH \to \mu\bar{\mu} + b\bar{b}$ Channel in $p\bar{p}$ Collisions at $\sqrt{s} = 1.96$ TeV

Huishi Dong, John D. Hobbs

December 13, 2006

Abstract

This note describes a search for the standard model Higgs boson produced with a Z boson at DØ based on an integrated luminosity of $L = 370$ pb^{-1}of data. We study $p\bar{p} \to ZH \to \mu\bar{\mu}b\bar{b}$ channel where Z decays to $\mu\bar{\mu}$ and H decays to $b\bar{b}$. In order to boost the the signal rate we first introduce the optimized di-muon isolation probability for separating the Z+2j signal from the multi-jet background, then use the ExtraLoose JLIP b-tag to enhance the double b-tag signal significance. We set at 95% C.L. upper limits on the $\sigma(p\bar{p} \to ZH) \times \mathrm{Br}(H \to b\bar{b})$ for Higgs mass between 105 GeV and 145 GeV.

1 Introduction

We present a search for the standard model Higgs boson produced with a Z boson at the DØ experiment with Tevatron $\sqrt{s} = 1.96$ GeV, using an integrated luminosity of 370 pb^{-1}of data collected between April 2002 and June 2004. We study the $p\bar{p} \to ZH \to \mu\bar{\mu}b\bar{b}$ channel where Z decays to $\mu\bar{\mu}$ and H decays to $b\bar{b}$. For the *Standard Model* this channel has among the best signal to noise because of the $Z \to \mu\mu$ signal.[1]

The final state of the channel is characterized with 2 high p_{T} isolated muons from Z decay and 2 energetic b-jets from H decay. One major source of background can be classified as the $Z + qq$ processes The 2 final state jets could be either b flavor, or c or mis-tagged light flavor jets. The other main backgrounds are $t\bar{t}, ZZ, WZ$ and QCD.

The theoretical expectation of the total cross section times branching ratio for the signal is 0.0028 *pb* for *Standard Model* Higgs mass 115 GeV. With about 300 pb^{-1}data, about one

event should be produced. With various detector and event reconstruction and selection inefficiencies previously measured, the signal efficiency as low as approximately 1%, it seems to be hopeless to observe the Higgs boson with the current data set. Yet we introduce a set of optimized event selection algorithms in order to boost the signal efficiency so that we can still try to set a better upper limit on the cross section, and lay the ground work for analyses with significantly larger data sets. These algorithms are the definition of muon isolation probability, the topological analysis method on the di-muon system, and the optimized working point for the b-jet tagger. Compared with the unoptimized method where the standard muon isolation cut on pT_{rel}, track cone p_{T} and track halo and the standard tight b-tag operation point were used, the combined optimizations could give about 2-5 times more signals[2]. This enables us to set the better limit on the ZH cross section, and increase the chance of observing the signal in the DØ RunIIb.

The organization of the note is the following: sections 2 and 3 describe the data and MC samples used in this analysis, section 4 shows how the events are selected using the standard and optimized cuts and how to measure the efficiencies of various cuts. Section 5 gives the details of how QCD background is subtracted from the selected events. In section 6 to section 8 we discuss the systematic uncertainties that come into the analysis. The ZH cross section upper limit is set in section 9, and the conclusions are in section 10.

2 Data Set

The data used in this analysis is collected at the DØ experiment between April 2002 and June 2004. For our study the common sample group (CSG) 2MUhighPt skim is used[7] which simply requires the presence of 2 loose muons with $p_{\mathrm{T}} > 15.0$ GeV. The events are reconstructed with different versions of p14 d0reco. All events have been fixed for different reconstruction deficits with pass2 TMB fixing. Object level corrections are done with d0correct v8. The analyze package is based on the top group Ipanema top_analyze package and top_trees [8].

The runs flagged as "bad" by SMT, CFT or MUON detectors are rejected from the analysis. We also reject events flagged as "bad" by the Calorimeter Data Quality Group[9].

We require events to have fired triggers listed in Table 1. To simplify the analysis, the L1 muon trigger is required to be unprescaled. The events within the luminosity blocks flagged as "bad" by lm_tools utility getLuminosity using these triggers are also removed from the analysis[10].

Finally the events flagged as "coherent noise", "missing crate", "noon noise" or "ring of fire" are rejected by cal_daq_quality package.

Table 1: Triggers used for the analysis. The run range is divided into 3 ranges. The first 2 ranges contain the trigger version less than 12. The last one contains trigger version that is greater or equal to 12. The division of the first 2 ranges is due to the L2CFT and L3 tracking improvement mentioned in [11].

Run Range	Trigger Name	$\int \mathcal{L}$ (pb^{-1})
173522-175517	MUW_W_L2M3_TRK10	17.8
175518-194566	MUW_W_L2M3_TRK10	312
194567-196584	MUH1_TRK10	39.4

After the above cuts, a total number of 128874 events are left, corresponding to the integrated luminosity of 370 pb^{-1}. The integrated luminosity is lower than the other p14 Higgs searches because of the simplified muon trigger selection.

We introduced the muon isolation discriminant and muon isolation probability[2] in this analysis in order to optimize the di-muon isolation cut. To construct the muon isolation discriminant JetTrigger skimmed events were used. About 6 million events were selected after requiring 2 or more jets and only 1 reconstructed muon(with the same kinematic cuts as applied to event selection, see section 4).

3 MC Samples

Table 2 lists the Higgs signal samples, Table 3 lists the the background samples. The cross section for the Higgs channel is based on the NLO calculations in [3]. The cross sections for the background samples are based on the NLO MCFM calculations[4][5]. The PDG'04[6] branching ratios are used in the calculations. These MC samples were run thought the same DØ RECO and top analyze packages as the data but not through the trigger simulation.

4 Event Selection

The final state of the processes studied contains 2 high p_{T} muons from Z boson decay and 2 b jets from Higgs boson decay. The event selection criteria on the jets, muons and the Z candidate are listed below:

- 2 or more good jets, where a good jet is defined as [12]

Table 2: PYTHIA generated MC Higgs events for the channel $ZH \to \mu\bar{\mu}b\bar{b}$.

M_H GeV	$\sigma\times$Br (pb)	SAM req. ID	# of events
105	0.0040	11667	5000
115	0.0028	11668	5000
125	0.0018	11669	5000
135	0.0011	11670	5000
145	0.0005	11671	5000

Table 3: PYTHIA (+Alpgen) generated MC events for the backgrounds of the channel $ZH \to \mu\bar{\mu}b\bar{b}$.

Process	$\sigma\times$Br (pb)	SAM req. ID	Generator	# of events
$Zbb \to \mu\bar{\mu}b\bar{b}$	0.533	11409, 11410	Alpgen+Pythia	96500
$Zcc \to \mu\bar{\mu}b\bar{b}$	1.15	15553-15560	Alpgen+Pythia	46250
$Zjj \to \mu\bar{\mu}b\bar{b}$	29.4	10721-10724	Alpgen+Pythia	188000
ZZ inclusive	1.56	15528	Pythia	53500
WZ inclusive	3.68	15527	Pythia	34250
$t\bar{t} \to \ell\nu b\ell\nu\bar{b}, M_t = 175$ GeV	0.671	15385	Alpgen+Pythia	36000
$t\bar{t} \to \ell b\bar{b}jj, M_t = 175$ GeV	2.676	15326, 15343, 15344	Alpgen+Pythia	1353000
$Z \to \mu\mu$	266.7	12014, 12016	Pythia	202000

  - T42 and L1 confirmation
  - $0.05 < EMF < 0.95$
  - $CHF < 0.4$
  - $n90 > 1$
  - Jet energy scale corrections
  - $E_T > 20.0$ GeV
  - $|\eta| < 2.5$
- Jet taggability selection: require jet match to a trackjet by $\Delta R \equiv \sqrt{\delta\eta^2 + \delta\phi^2} < 0.5$
- Jet B-tagging selection [13], using the JLIP b-tagger at the ExtraLoose (0.04 mistag rate) operating point.
- Muon Selection
  - 2 or more muons with loose muon quality requirement [14]
  - Each muon has a central track match
  - Number of SMT hits > 0
  - $p_{\mathrm{T}} > 15$ GeV
  - $|\eta| < 2.0$
  - Track $r - \phi$ DCA < 0.25 cm w.r.t the primary vertex.
  - The muons are required to be isolated, see detail in section 4.2
- Z candidates
  - The 2 candidate muons have opposite charge
  - The dimuon's opening angle in the transverse plane $\delta\phi > 0.4$
  - Di-muon invariant mass window is 65 GeV $\leq M_{\mu_1,\mu_2} \leq$ 115 GeV

The optimizations come into the muon isolation which is used to suppress the QCD background and the JLIP b-tag operating point which is used to select the b flavor jets.

At each cut stage an inefficiency on the signal and background is introduced. Figure 1 shows the cut flow chart and all the efficiencies that need to be measured and what events they are measured with respect to. The following sections will deal with the efficiency measurements.

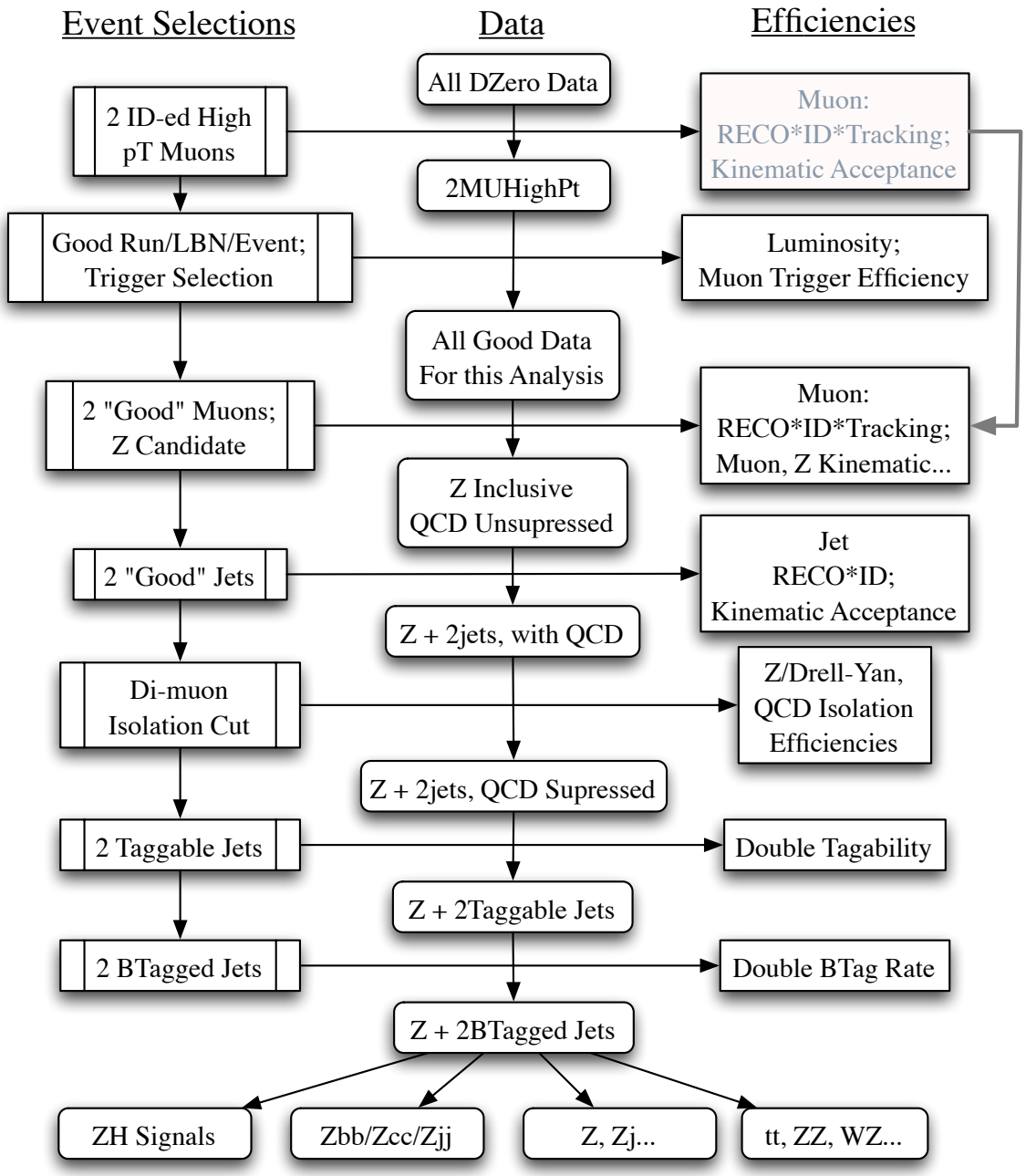

Figure 1: The cut flow of the event selection. All the efficiencies are measured with respect to the data before the corresponding cut, for example, the isolation efficiency is measured w.r.t $Z + 2j$ events, *eg.* the number of $Z + 2$ jets events after the isolation cut divided by the number of $Z + 2$ jets events before the isolation cut. There are two muon selection efficiencies, the first one is gray since the second one is more tighter than the it, the efficiency will be measured at the second stage.

4.1 Muon Trigger×ID×Tracking×SMT Efficiency

Trigger, ID, tracking and SMT hit efficiencies for a single muon are measured using muo_cert package[15]. The data sample used to measure the efficiencies is the 1MULoose skim [16].

The measured efficiencies of L1/L2/L3 muon trigger terms, L3 tracking times muon-track matching, the loose muon ID and SMT hit are given as functions of various variables as shown in Figures 2–8.

These efficiencies need to be applied to all the MC samples for the data and MC comparisons since the MC events are not run through the trigger simulations. In doing that we need to calculate the event average by convoluting the single muon efficiencies measured above. As discussed in the appendix, the convolution is done using Eq. 19 where ζ is replaced with the following for trigger efficiency, (ID×Tracking) and SMT hit efficiency respectively:

$$\begin{aligned} \zeta_{trig} &= L1_{mu}(\eta,\phi)\cdot L2_{mu}(\eta,\phi)\cdot L3_{mu}(\eta,\phi) && (1)\\ \zeta_{ID\ \cdot Trk} &= ID_{mu}(\eta,\phi)\cdot Trk_{mu}(\eta,\phi) && (2)\\ \zeta_{SMTHit} &= SMT(\eta,\phi) && (3) \end{aligned}$$

where $L1, L2, L3$ are the single muon L1/L2/L3 trigger efficiencies respectively, ID, Trk are the ID and tracking efficiencies, SMT is the efficiency of a muon producing a SMT hit.

According to Figure 1, the convolution should be done over all the good events without any muon or jet selection applied.[1] Yet in order to get the efficiency values in Eq. 1 and 2, the muons must have been RECO-ed and this will introduce the muon RECO efficiency. So in order not to double count the RECO efficiency the convolution is done over all the good events that have 2 or more RECO-ed muons, and the efficiencies are measured with respect to the number of events that 2 or more muons are found instead of the number of all good events.[2] Due to the statistical limitations the various single muon efficiencies are expressed just as functions of muon η and ϕ.

The convoluted efficiencies are the (expected) data efficiency for each of the MC samples. For the trigger efficiency Eq. 22 is used since we required single muon trigger; for the (ID×tracking) and SMT hit efficiencies Eq. 23 is used since we required two or more loose muons that have central track matching and both muon has at least one SMT hit in a event.

[1] For MC samples, the good event selection also need to be applied as shown in Figure 1, namely there is a small potion of events that are labeled as having the 4 kind of CAL noises, so the total number of effective MC events are slightly smaller than those listed in Tables 2 and 3.

[2] An alternative and better way is to use the muon ID×Tracking efficiency data/MC scale factor, the difficulty is that there is no priori knowledge of the $Zjj, Zcc, Zbb, t\bar{t}$... composition of data, and the muon ID×Tracking efficiencies are notably different as shown in Table 4, so we cannot determine the data/MC scale factor directly.

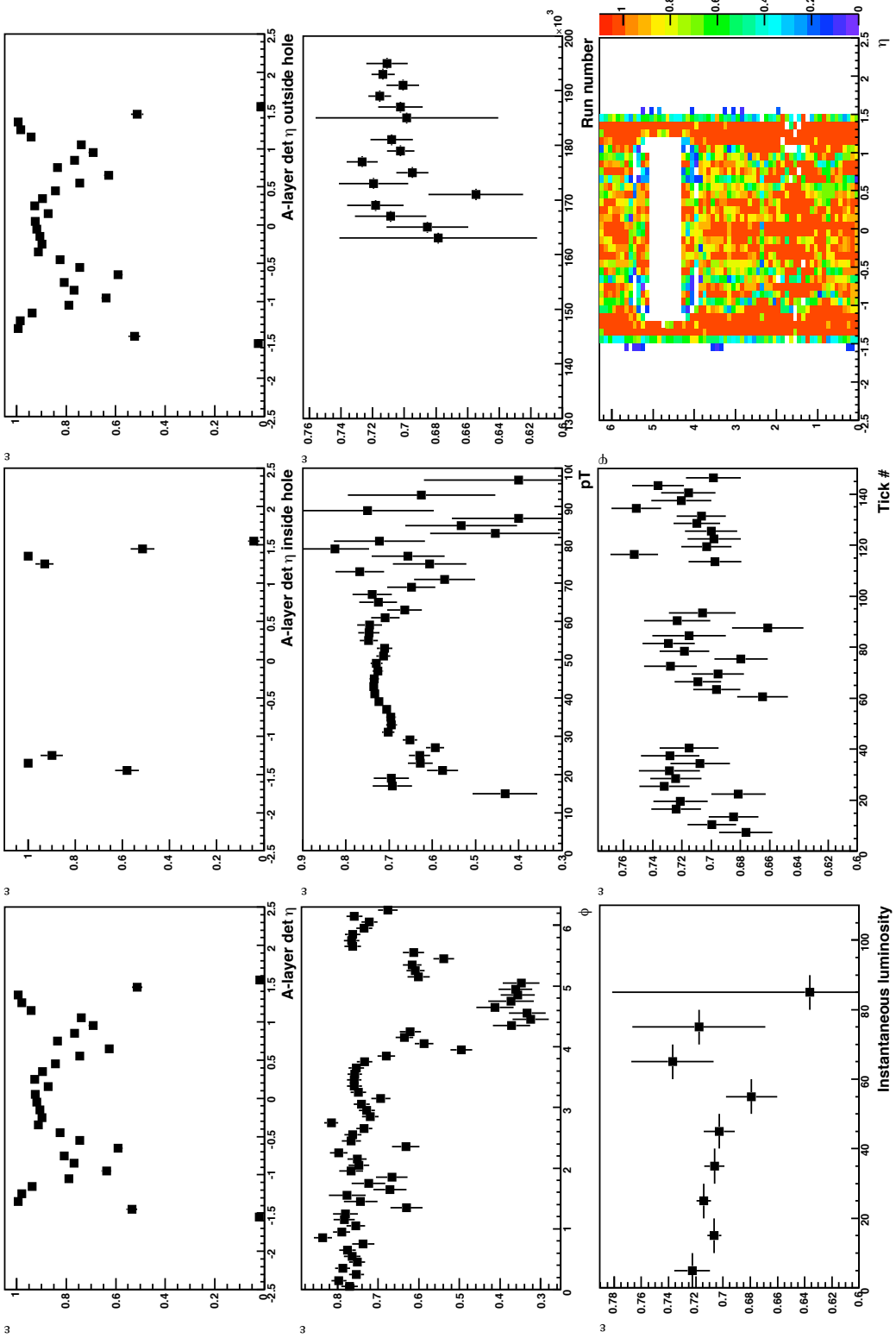

Figure 2: Muon L1 scint. wide trigger efficiencies.

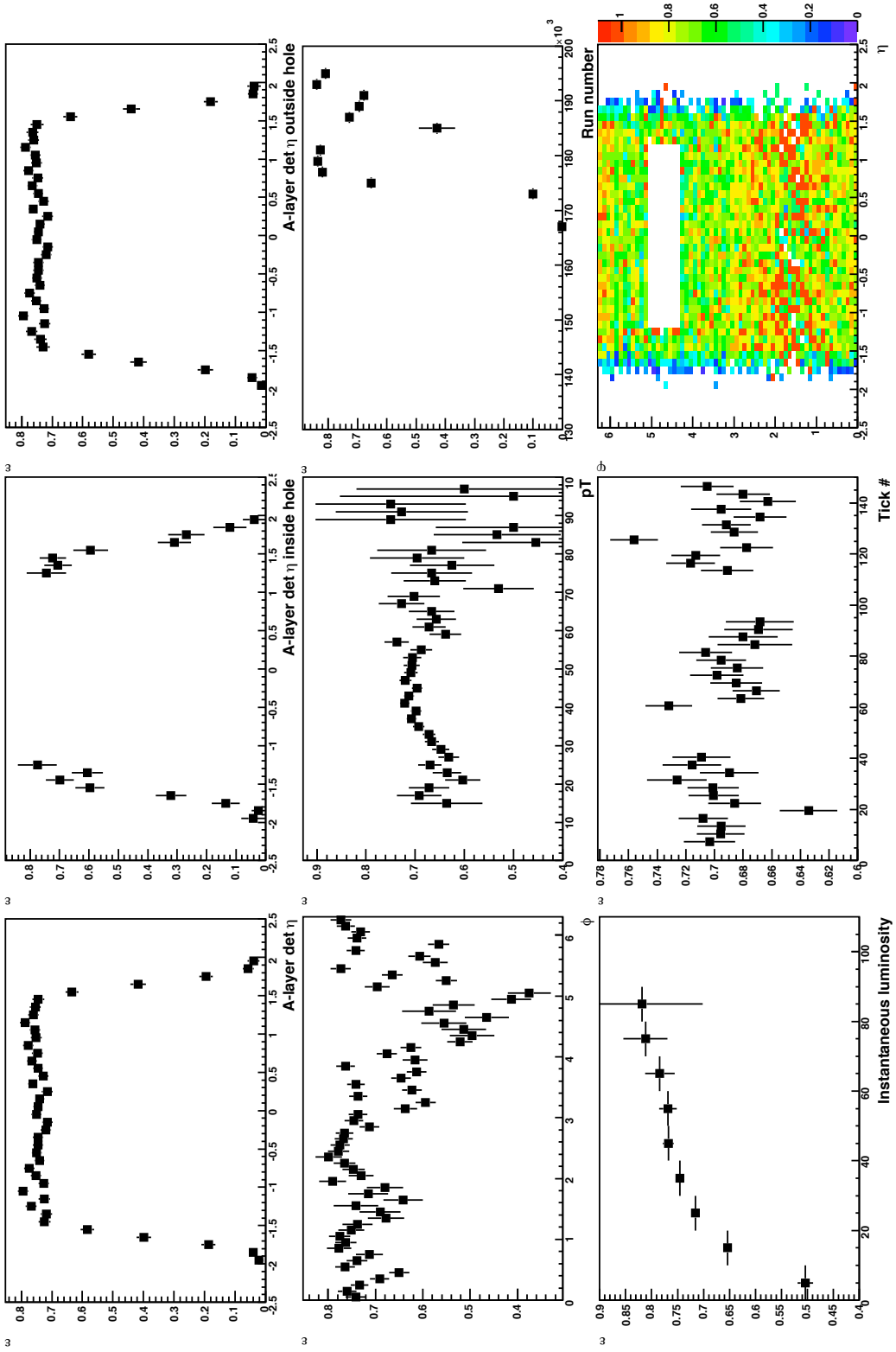

Figure 3: Muon L1 track $p_{\mathrm{T}} > 10$ GeV trigger efficiencies.

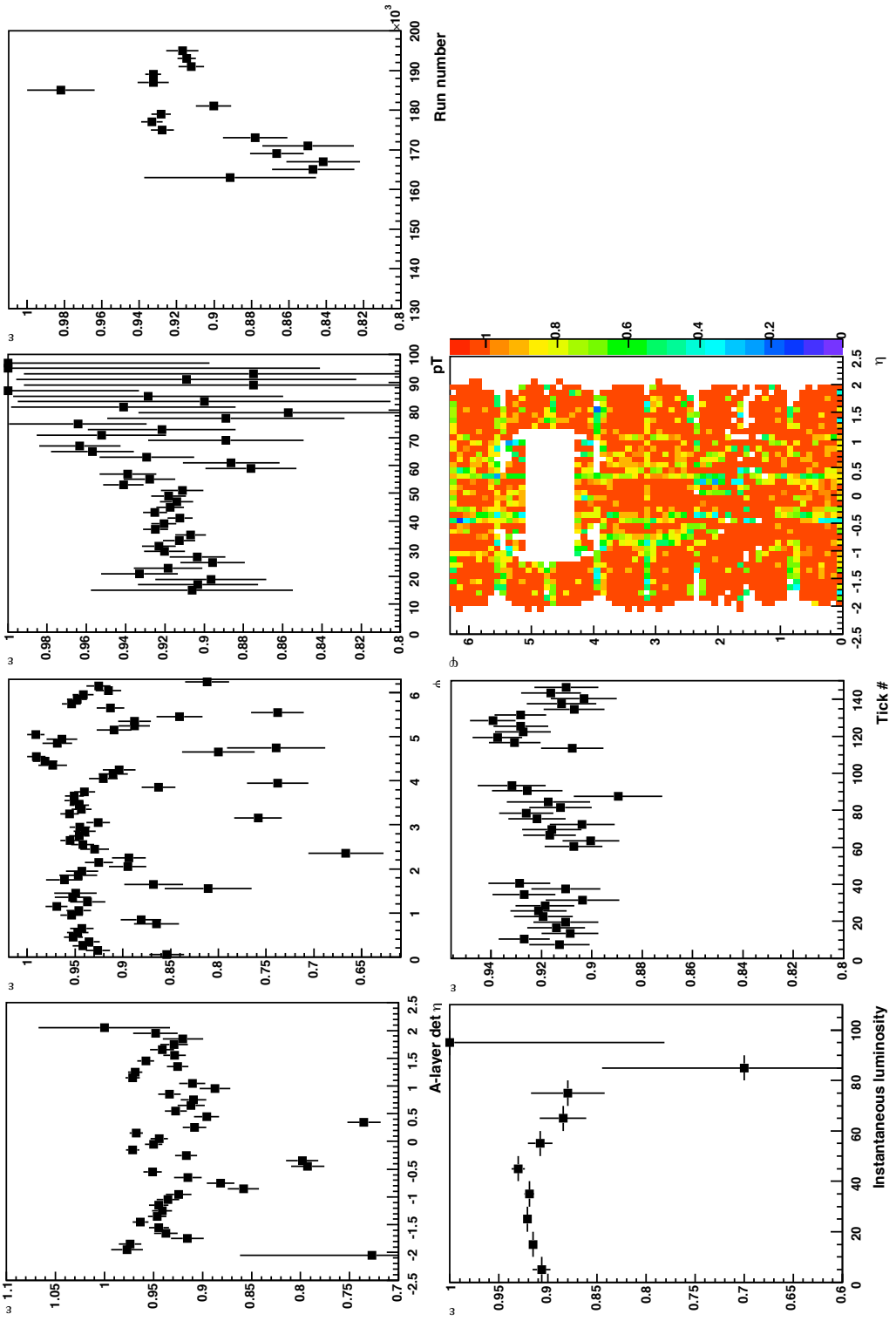

Figure 4: Muon L2M3 trigger term efficiencies. This level 2 trigger term requires a medium quality muon candidate with $p_{\mathrm{T}} > 3$ GeV

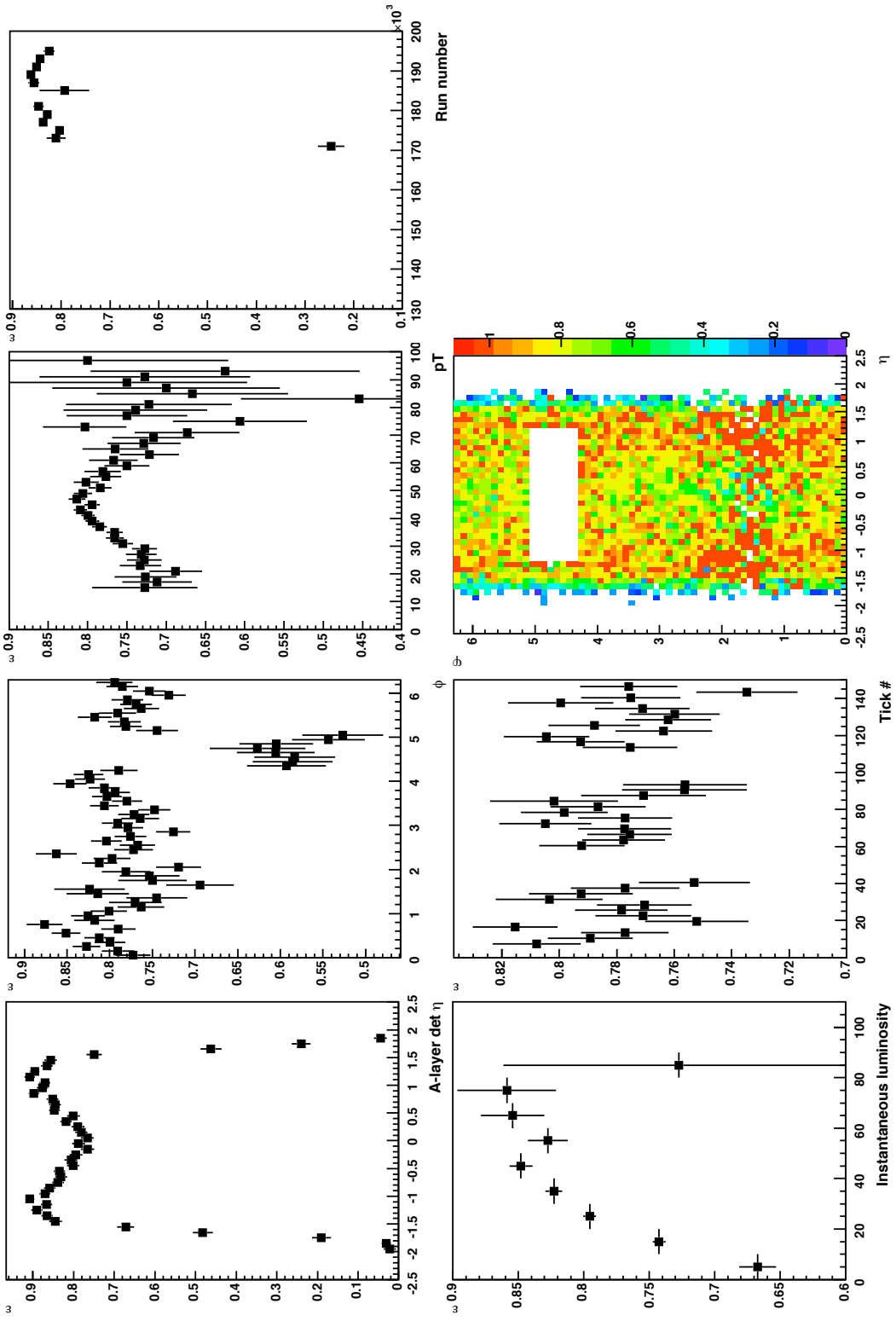

Figure 5: Muon L3TRK10 trigger term efficiencies.

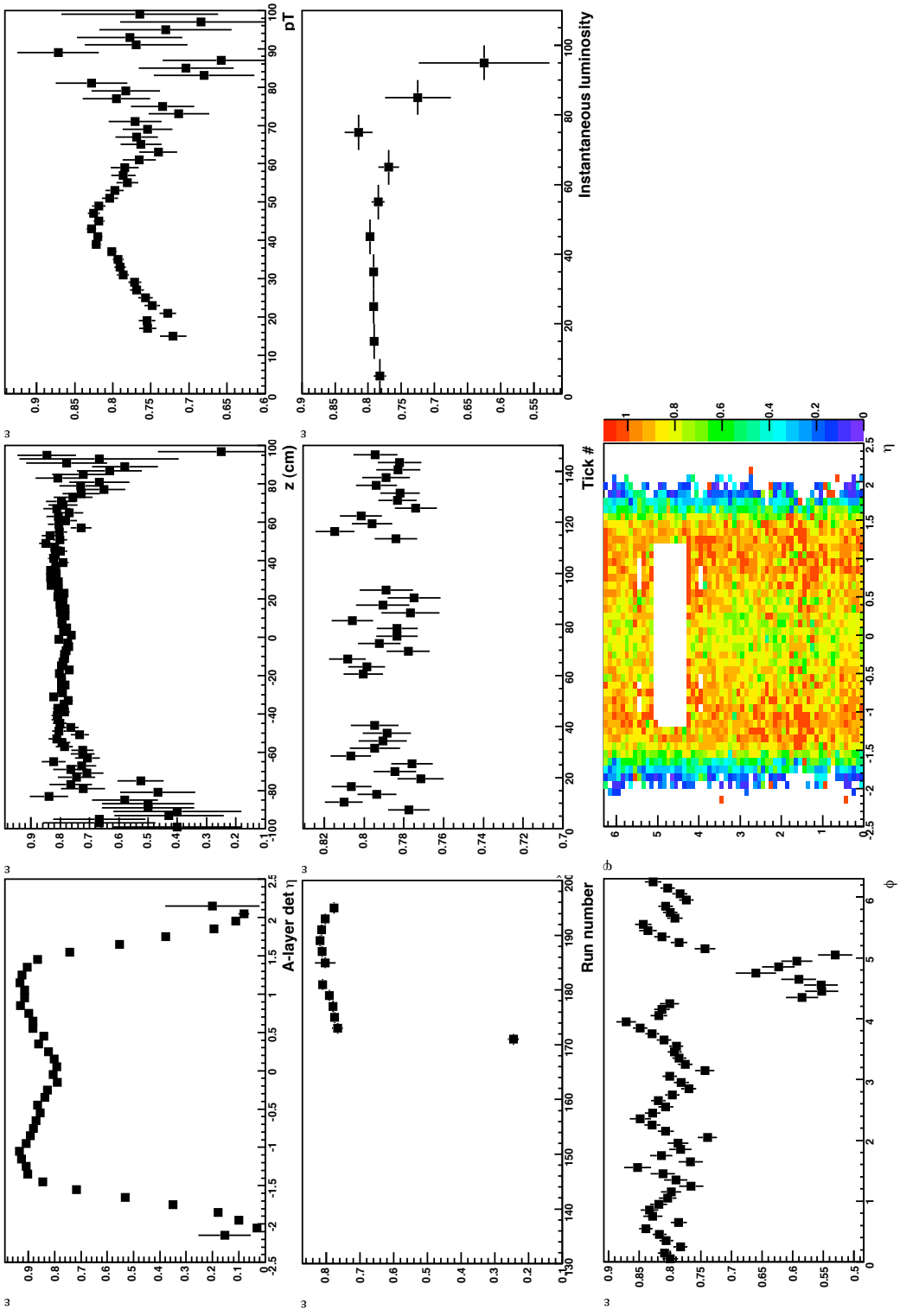

Figure 6: Muon L3 tracking and track matching efficiencies.

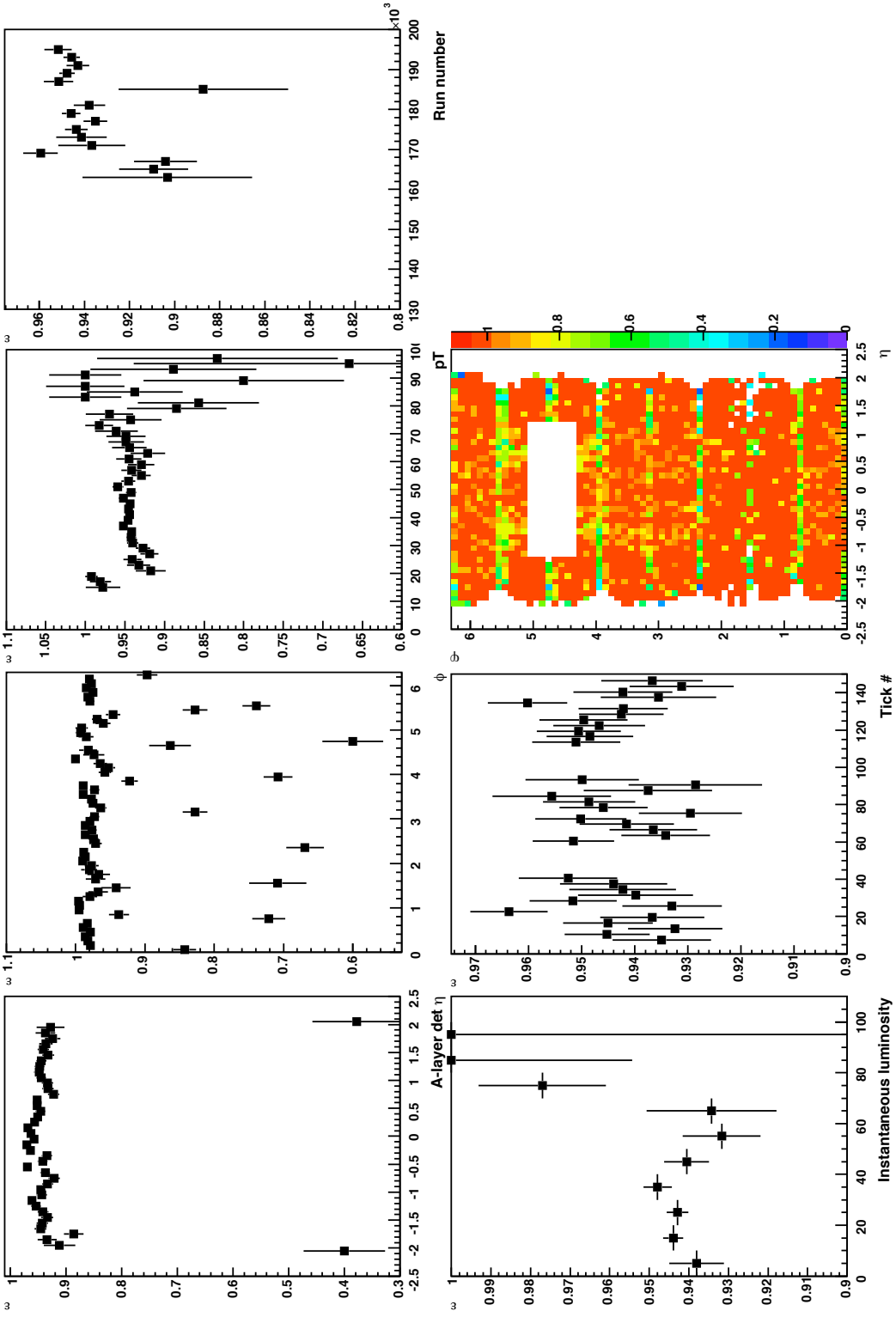

Figure 7: Muon RECO×ID efficiencies.

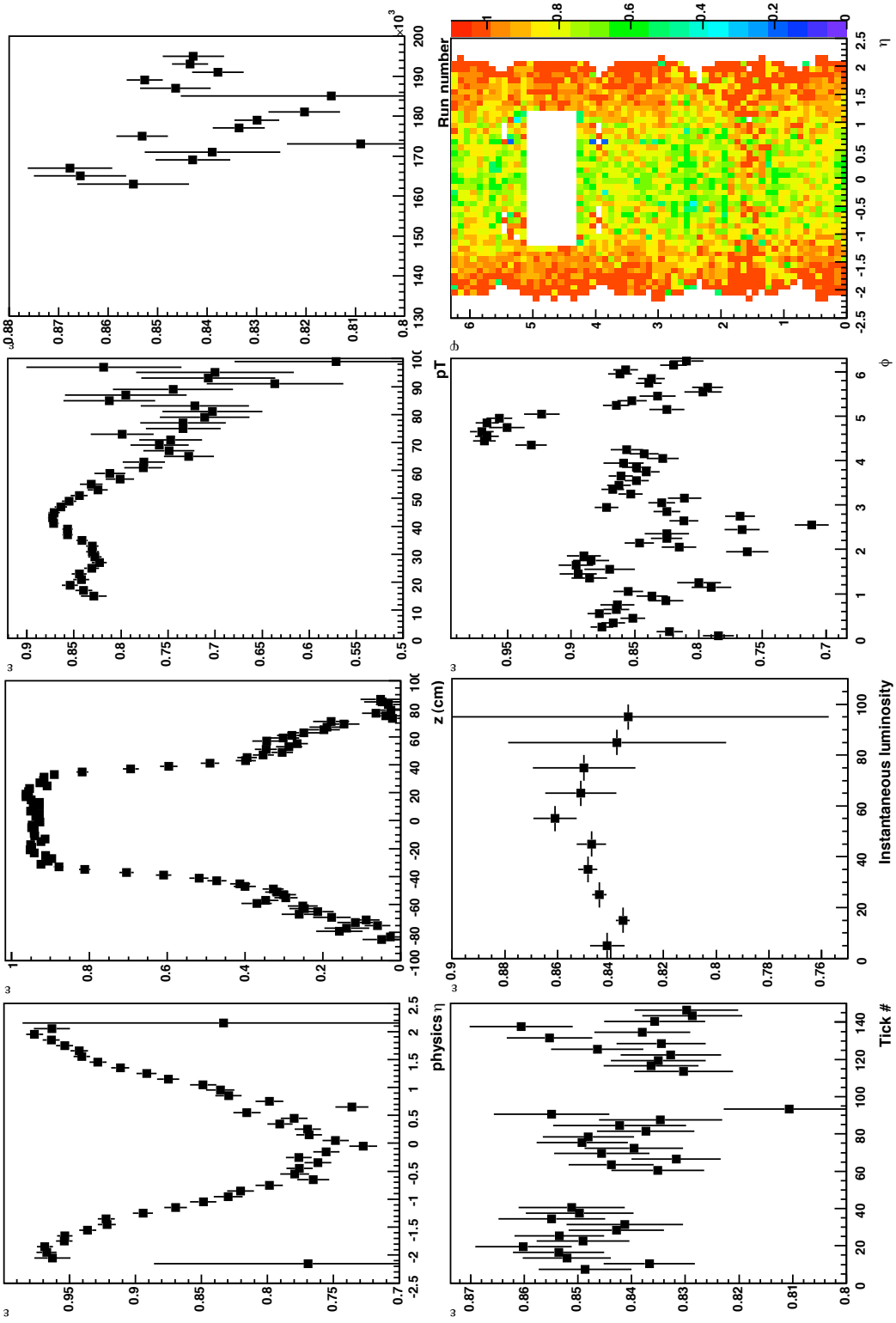

Figure 8: Muon SMT hit efficiencies.

We did not try to fit the efficiencies, instead the bin values in the efficiency plots are used. The results for all MC samples are listed in Table 4.

The MC muon (ID×Tracking) and SMT hit efficiencies for each of the MC samples are calculated by the ratio of the number of events that have at least 2 loose muons with central track match or that have at least 2 muons with at least a SMT hit and the total number of events respectively, as shown in Figure 1.

The muon p_{T} , η and ϕ distributions of the selected $Z \to \mu\bar{\mu}$ events from the MC samples in Table 2, 3 are compared with those from the data sample as shown in Figure 9. It is clear the MC describes the kinematic variables of muons from $Z \to \mu\bar{\mu}$ events well, so the efficiencies convoluted over the MC sample are reliable descriptions of efficiencies for real data.

Table 4: Event average of muon (trigger × ID × tracking × SMT Hit) efficiency and muon ID×Tracking, SMT hit data/MC scale factor(SF) for the di-muon events for each MC sample. The branching ratio is also included automatically in these efficiencies for WZ, ZZ and $t\bar{t}$ processes. *ttsl* and *ttdl* stand for $t\bar{t}$ single leptonic and di-leptonic decay channel respectively. The systematic and statistic uncertainties in this and the following tables that has no explicitly listed the uncertainties are listed in the Section 8.

Process	Zbb	Zcc	Zjj	*ttdl*	*ttsl*	ZZ	WZ	Z
Trigger	0.831	0.839	0.806	0.873	0.908	0.828	0.802	0.782
$(\mathrm{ID}\times\mathrm{Trk})_{data}$	0.606	0.645	0.557	0.502	0.487	0.478	0.465	0.513
$(\mathrm{ID}\times\mathrm{Trk})_{MC}$	0.673	0.636	0.573	0.405	0.34	0.562	0.406	0.504
(ID×Trk) SF	0.901	1.01	0.972	1.24	1.43	0.85	1.15	1.02
$(\mathrm{SMT\ Hit})_{data}$	0.679	0.727	0.642	0.747	0.822	0.717	0.701	0.613
$(\mathrm{SMT\ Hit})_{MC}$	0.823	0.842	0.805	0.85	0.873	0.836	0.827	0.784
(SMT Hit) SF	0.824	0.863	0.798	0.879	0.942	0.858	0.847	0.782

Process	$ZH(105)$	$ZH(115)$	$ZH(125)$	$ZH(135)$	$ZH(145)$
Trigger	0.875	0.876	0.876	0.878	0.882
$(\mathrm{ID}\times\mathrm{Trk})_{data}$	0.686	0.704	0.695	0.7	0.711
$(\mathrm{ID}\times\mathrm{Trk})_{MC}$	0.775	0.778	0.783	0.791	0.797
(ID×Trk) SF	0.886	0.905	0.888	0.885	0.892
$(\mathrm{SMT\ Hit})_{data}$	0.734	0.74	0.735	0.736	0.743
$(\mathrm{SMT\ Hit})_{MC}$	0.84	0.831	0.848	0.846	0.842
(SMT Hit) SF	0.874	0.89	0.866	0.87	0.883

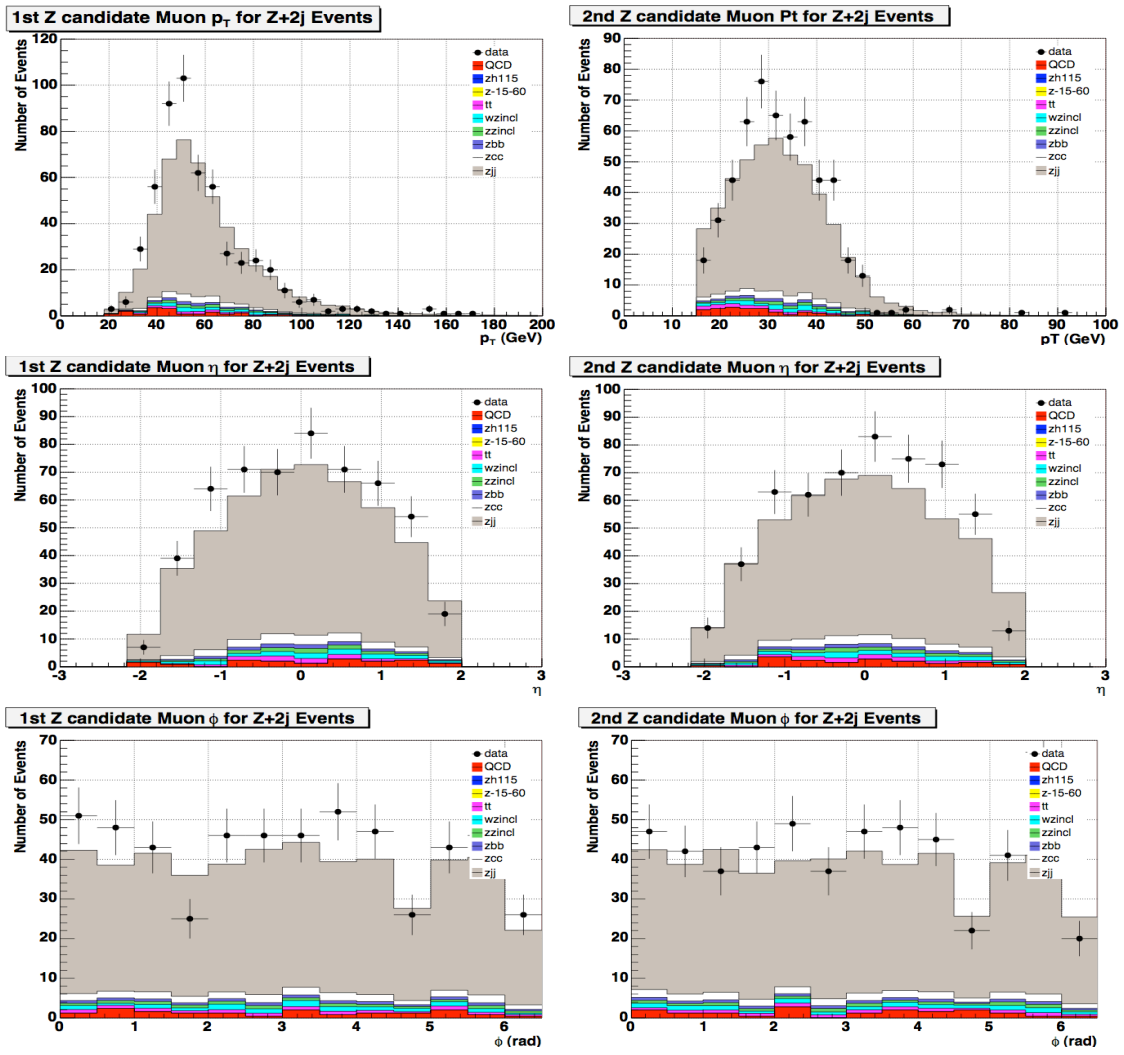

Figure 9: p_{T} , η, ϕ distributions of the first and second Z candidate muon for $Z + 2$ jet 0 btag events.

4.2 Muon isolation Optimization

We introduced a muon isolation probability[2] in order to optimize the di-muon isolation cut for Z event selection. In short we first introduce a muon isolation discriminant f_{iso}:

$$f_{iso} = \frac{\sum\limits_{0.1<dR<0.4}^{N_{cell}} E_{\mathrm{T}} + \sum\limits_{dR<0.5}^{N_{track}} p_{\mathrm{T}}}{p_{\mu}} \tag{4}$$

where p_{μ} is the muon's 3-D momentum. The first term in the numerator is the muon halo which is the sum over all the calorimeter cell's transverse energy deposition between a cone of $R = 0.1$ and a cone of $R = 0.4$ around the muon. The second term is the muon track cone p_{T} which is the sum over all the tracks around the the muon within a cone of $R = 0.5$, muon not included.

We then get the discriminant distribution for the QCD background of the $Z \to \mu\mu$ events, *eg.* for muon that is UNLIKELY to be isolated by studying the multi-jet events (the skimmed 6 million JetTrigger events mentioned in Section 2). This distribution is shown in Figure 10. The same distribution with 1 and 2 b-tag requirements are shown in Figures 11 and 12.

Based on this distribution, we construct the isolation probability $P_{iso}(f_{iso})$ for a given muon as a function of its isolation discriminant:

$$P_{iso}(f_{iso}) = \frac{\int_0^{f_{iso}} f_{iso}(x)dx}{\int_0^{\infty} f_{iso}(x)dx} \tag{5}$$

The distribution of single muon isolation probability behaves differently for isolated muons (from $Z \to \mu\mu$ events) and non-isolated muons(from QCD process). On the one hand, for the muon that is likely to be isolated, the probability is more populated at 0 due to the smaller halos and track kernels in Eq. 4 compared to the non-isolated muons. On the other hand, for a muon that is not isolated, the probability is randomly distributed from 0 to 1. Particularly, since QCD (and other non-Z) process dominates those events where only single muon and single muon trigger presents together with 2 jets and the muons from these events are likely to be non-isolated, the isolation probability distribution for these muons is evenly distributed between 0 and 1 by the construction of the isolation probability in Eq. 5.

The difference in the isolation probability distribution is more obvious when dimuons are considered together. The two muons from the Z are generally isolated, while the two muons from the multi-jet background are usually non-isolated because these are produced by decay of particles contained in hadronic jets. As shown in Figures 13, 14 and 15 the Z muons' 2-D isolation probability distribution concentrates around the axes, while the QCD muons' distribution is evenly scattered in the unit square. So instead of cutting on the isolation

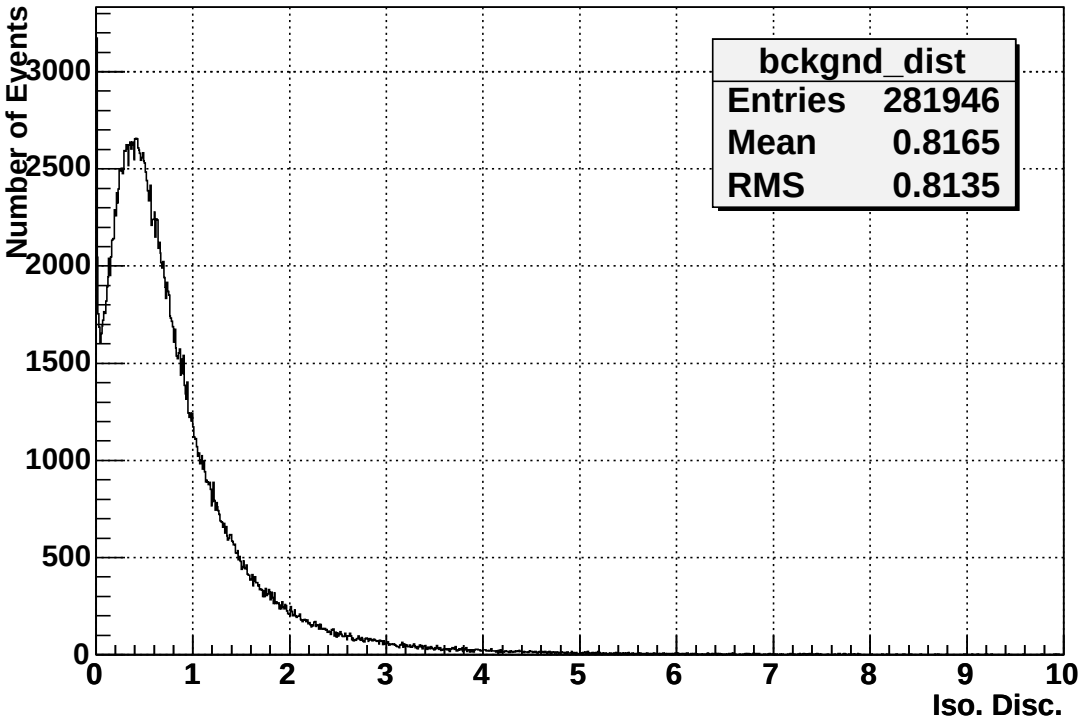

Figure 10: Muon isolation discriminant distribution for the multi-jet events from JetTrigger skimmed data with additional requirement of 1 muon and 2 or more jets. The muon and the jets passed the same kinematic cuts as used in the event selection. This discriminant describes the muon behavior of the $Z \rightarrow \mu\mu$ process's QCD background. It is used to construct the muon isolation probability.

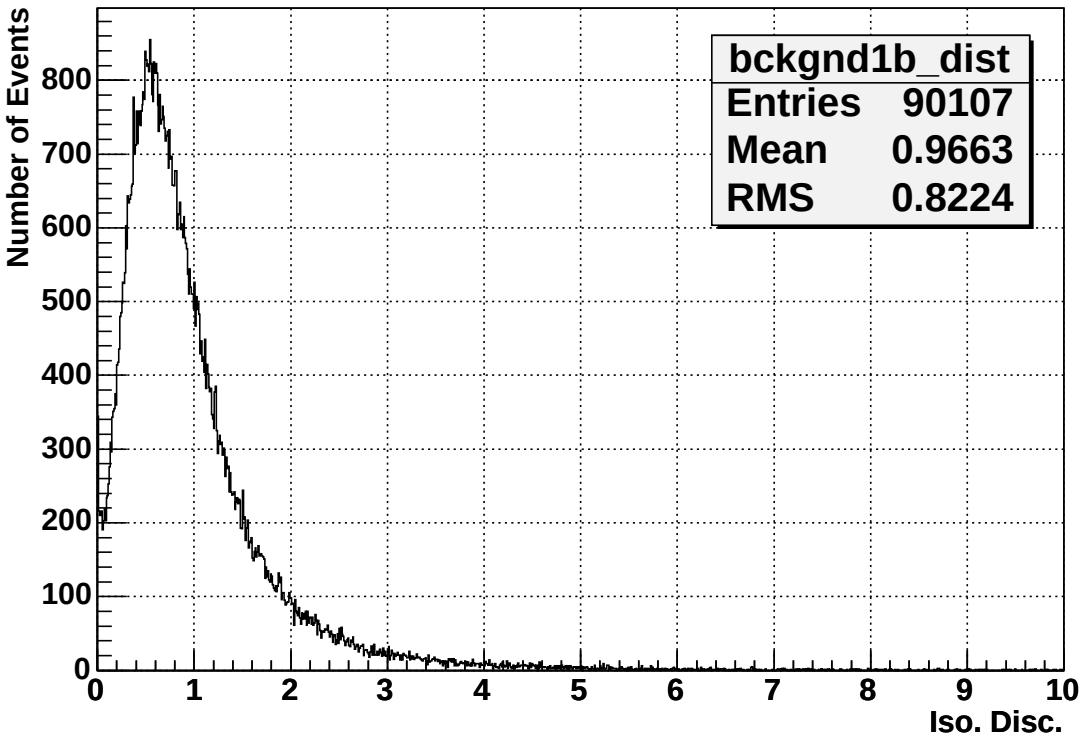

Figure 11: The same distribution as in Figure 10 except 1 b-tag jet is required.

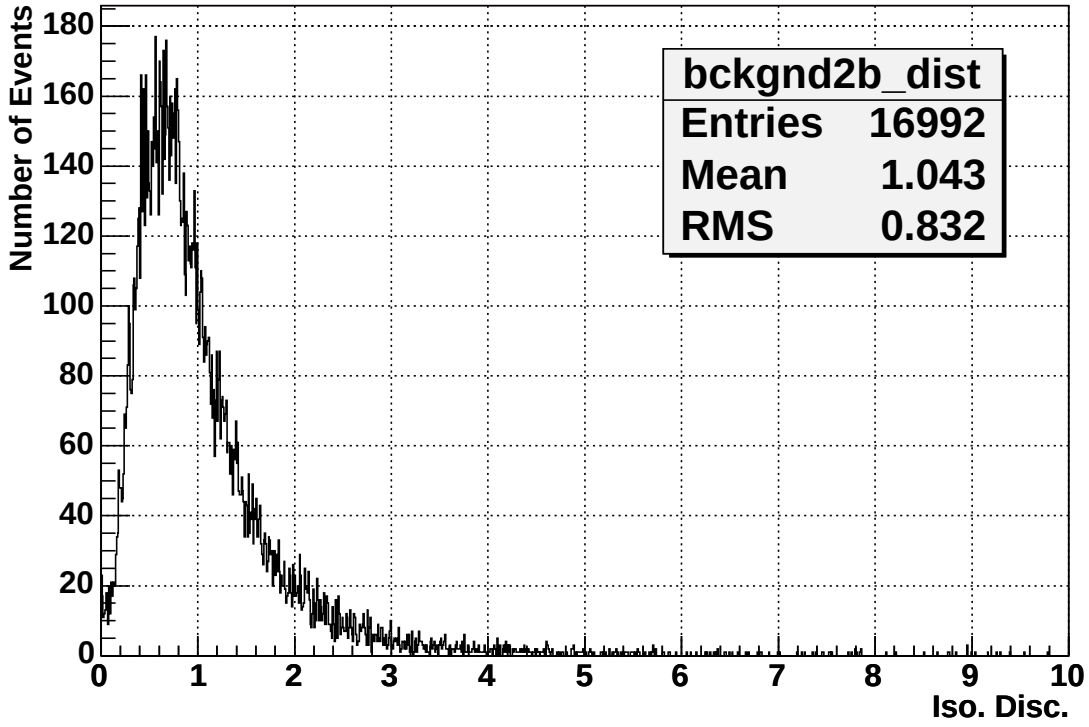

Figure 12: The same distribution as in Figure 10 except 2 b-tag jet is required.

probability on each of the muon, we cut on the product of the probabilities of the 2 muons. Obviously this cut is more efficient for the Z signals than cut on a single muon, and less efficient for the background muons that are not correlated with each other.

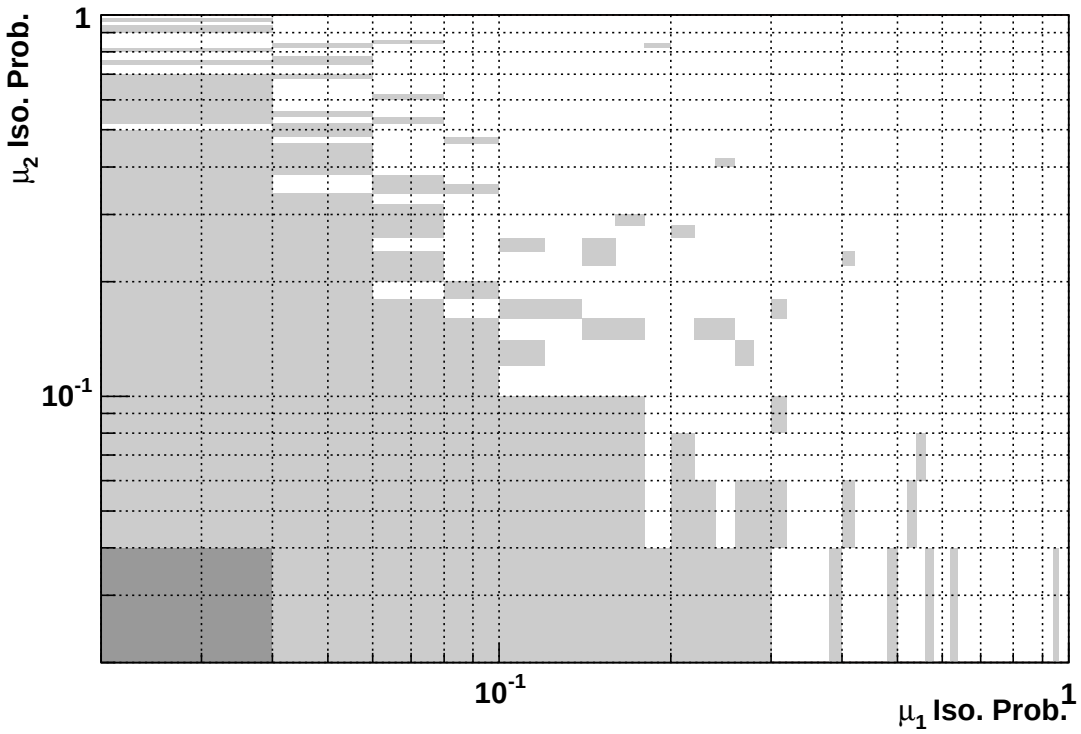

Figure 13: 2-D di-muon isolation probability distribution for the MC $Z \to \mu\mu$ events. Clearly the cut on the product of 2 muons' isolation probability yield higher signal efficiency than a cut on each muon when keeping the background rate at about the same level.

The isolation cut efficiency ϵ_{iso} is defined as the ratio of the event number after and before the di-muon isolation cut. In the following 3 sections, ϵ_{iso} is calculated for both $Z/\gamma^* \to \mu\bar{\mu}$, $t\bar{t}$ and the QCD background w.r.t the events which contain $\mu\bar{\mu}$+2 or more jets as shown in Figure 1.

4.2.1 Di-muon isolation cut efficiency for $Z/\gamma^* \to \mu\bar{\mu}$

There are three direct ways to measure the Z and/or Drell-Yan process di-muon isolation cut efficency:

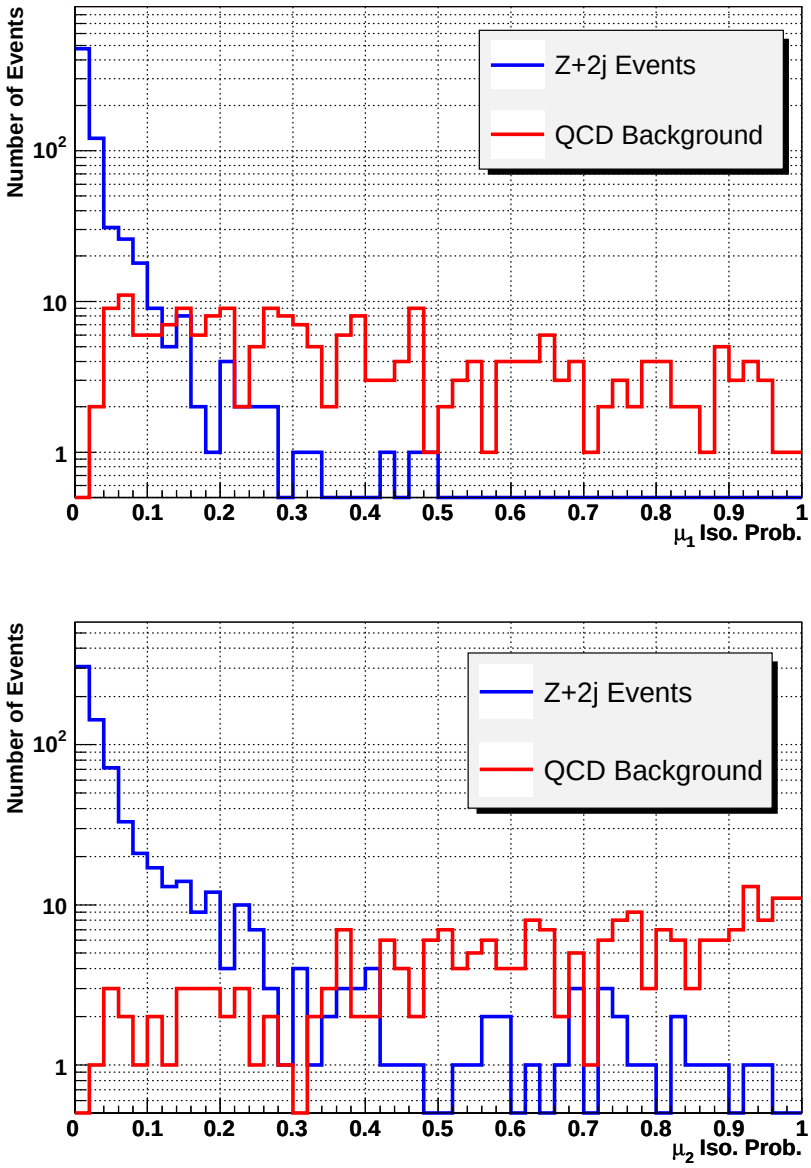

Figure 14: Isolation probability distributions for the first(upper panel) and the second(lower panel) Z muon candidates (blue lines) from $Z + 2$ jets events in data compared with the isolation probabilities of the first and second muons from the multi-jet plus 2 muon events(red lines)–these events satisfy the same event selection cut as $Z + 2$ jet events except for that they fail the di-muon isolation probability cut. Referring to Figures 16 and 17 these anti-isolated($p_1 \times p_2 \geq 0.02$) $Z + 2$ jet events are mostly the QCD background of the $Z + 2$ jet events. Clearly Z muon's isolation probability distribution is distinctly different from the muons from multi-jet events.

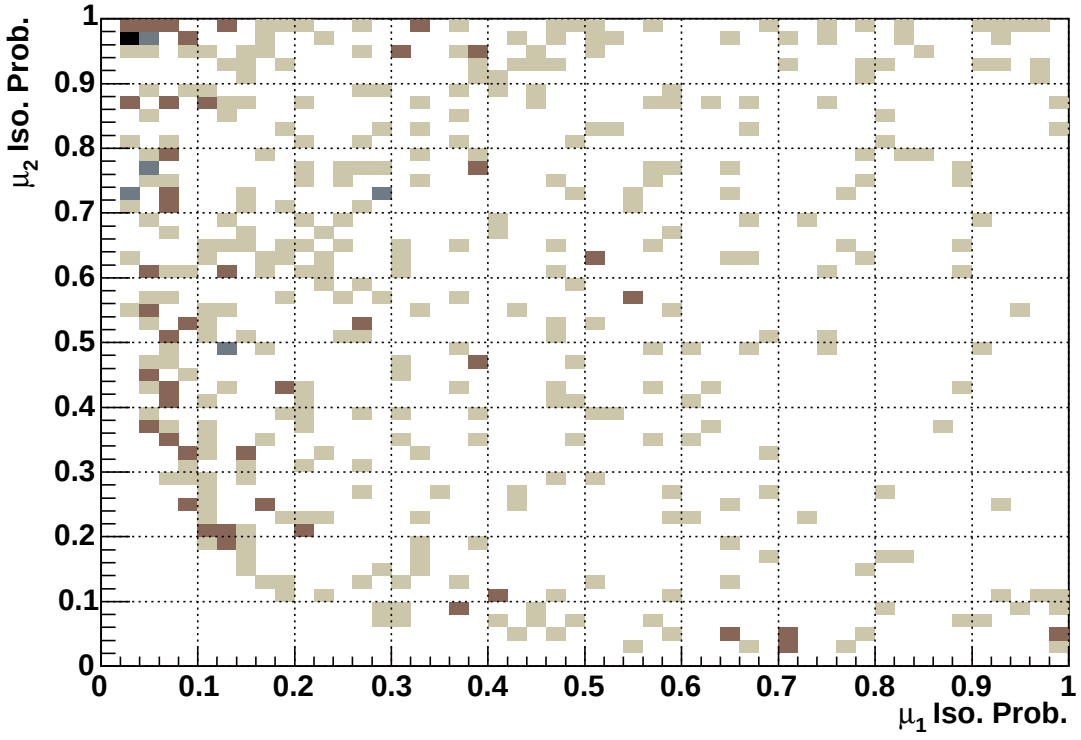

Figure 15: 2-D di-muon isolation probability distributions for the QCD background of 2 $Z + 2$ jets. Clearly the di-muon isolation probability from the QCD background are evenly distribution within the unit square.

1. Use the Z+2j events from the data sample. Fit the Z peak and the background–which contains both the QCD and Drell-Yan processes–within the mass window. The efficiency for a given isolation cut is obtained by taking the ratio of the number of the fitted Z signals at that isolation cut to the number of fitted Z signals when there is no isolation cut.

2. Use the MC Z+nj sample. Still fit the Z peak and the background–in this case only Drell-Yan process is involved in the background–and the isolation cut efficiencies of both Z and Drell-Yan processes can be calculated by using the same techniques above.

3. Use the MC Z+nj sample. Don't fit the Z peak and the Drell-Yan background, instead assume Z and Drell-Yan processes have the same isolation cut efficiencies due to the similarity of the kinematics. Count the total number of events within the mass window, the efficiency is given by the ratio of the number of events with and without the isolation cut.

For data we can only use the first method, while for MC samples the second and the third methods are suitable. Figures 16–21 show the fitting results for data with and without the isolation cut for 0,1 and 2 b-tagged jets. The MC fits resemble that of data with the isolation cut.

The second way and the third way gives similar efficiencies for the MC samples. The third way is used in order to avoid the need for fitting to the background thus achieved smaller statistical uncertainties. The measured Z and Drell-Yan isolation cut efficiencies for different Z MC samples are shown in Figure 22, along with the data isolation cut efficiency measured using the first way. It is obvious the MC Z processes and data have the same isolation cut efficiencies at the isolation cut region we are interested in(~ 0.02). Also the plot shows that the isolation cut is independent of the jet and b-jet multiplicity. The averaged isolation cut efficiency are listed in Table 5.

Table 5: Di-muon isolation cut efficiencies for Z/Drell-Yan for different isolation cut points. This efficiency is an average for all the MC samples which contain the Z boson. The relative uncertainties is around 2%.

Cut	0.1	0.07	0.05	0.03	0.02	0.01	0.007	0.005	0.003	0.001
ϵ^{Z}_{iso}	0.996	0.995	0.992	0.987	0.981	0.960	0.940	0.918	0.875	0.743

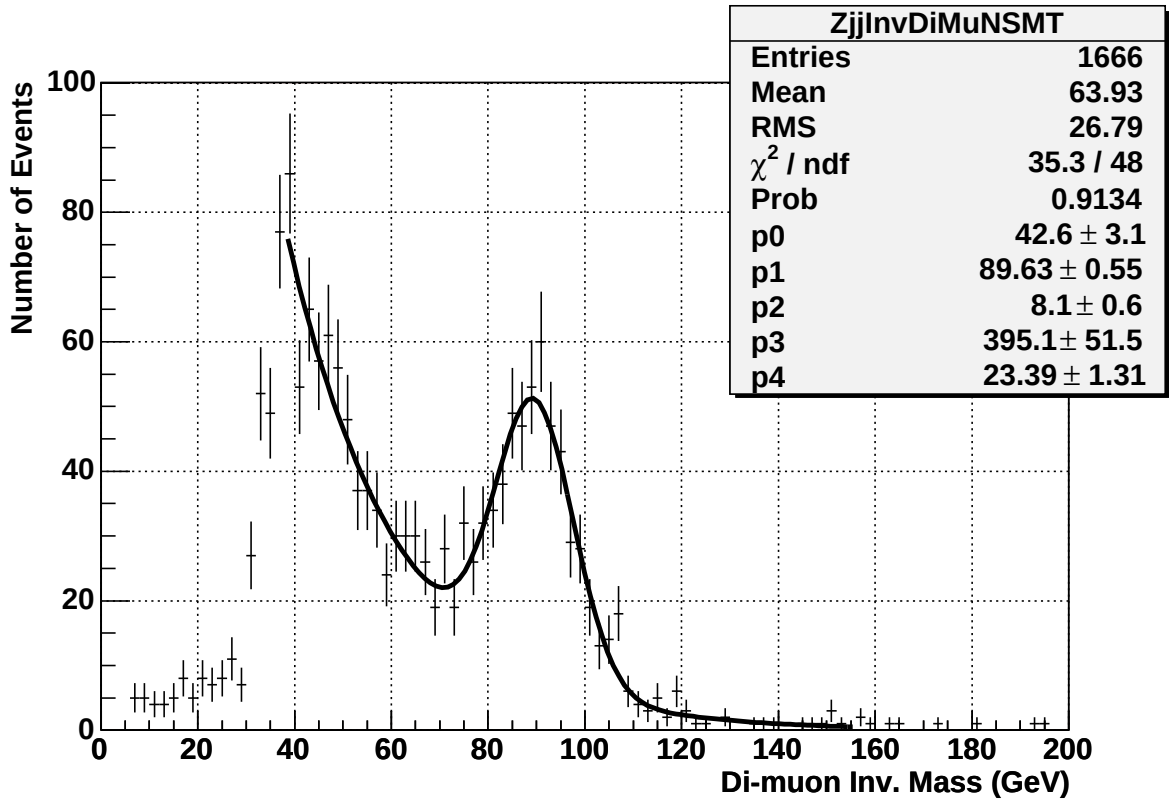

Figure 16: Di-muon invariant mass distribution for $Z+2$ jet with 0 btag events. No isolation cut is applied. Z peak is modelled by Gauss function $p0 \cdot e^{\frac{(x-p1)^2}{2p2^2}}$ for simplicity. It has almost the same fit result as the convoluted function of Gauss function and Breit-Wigner function. The QCD and Drell-Yan is modelled by $p3 \cdot e^{-p4 \cdot x}$. The total number of QCD + Drell-Yan events is the integration of the fit function within the Z mass window. The Z signal is the total number of events within the Z mass window subtracted by the total number of QCD and Drell-Yan process with the constraint of the measured γ_1 and γ_2 (defined in Eq. 12 and 13 in section 5.1.)

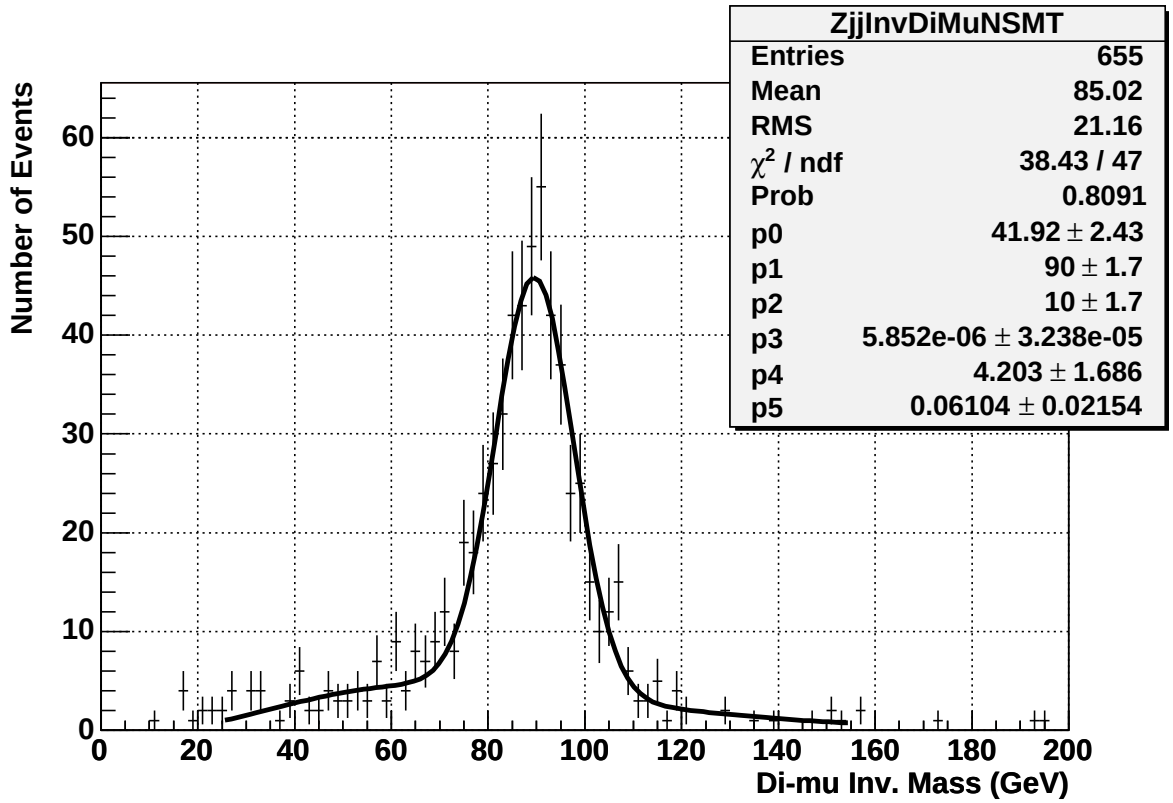

Figure 17: Di-muon invariant mass distribution for $Z+2$ jet with 0 btag events. Isolation cut 0.02 is applied. Z peak is modelled by Gauss function $p0 \cdot e^{\frac{(x-p1)^2}{2p2^2}}$. The QCD and Drell-Yan is modelled by $p3 \cdot x^{p4} \cdot e^{-p5 \cdot x}$.

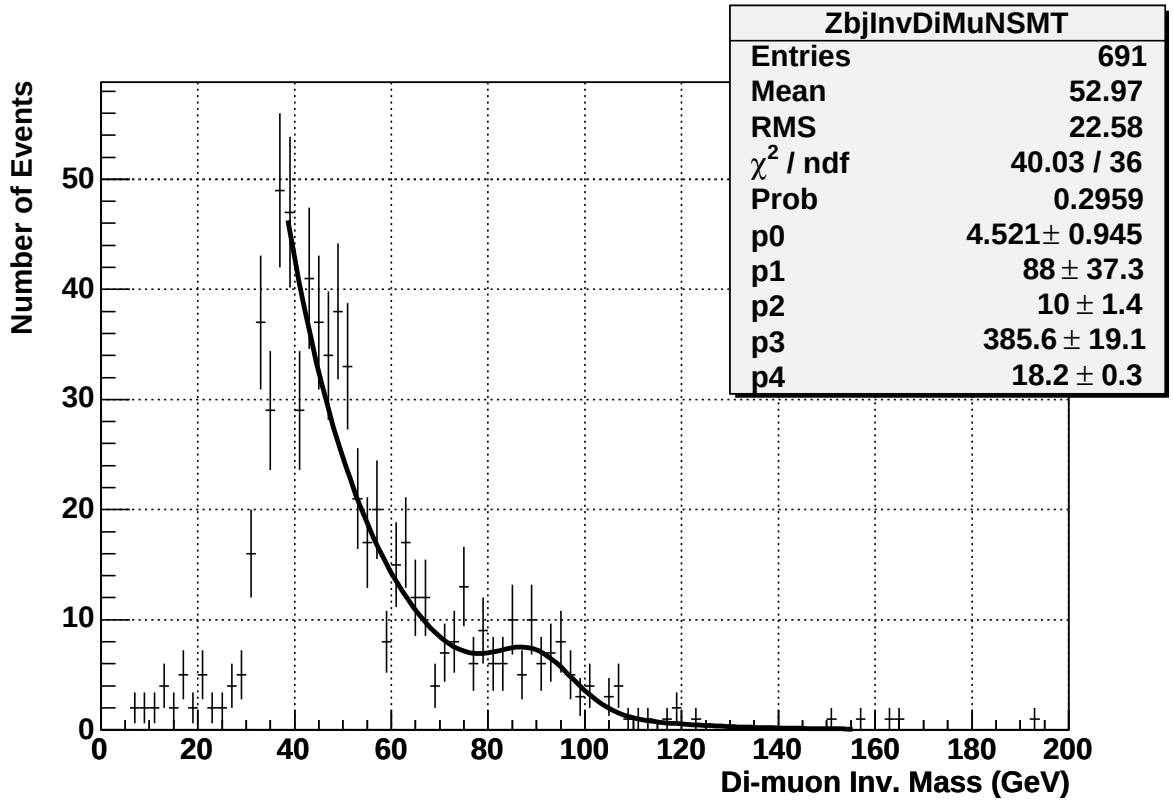

Figure 18: Di-muon invariant mass distribution for $Z+2$ jet with 1 btag events. No isolation cut is applied. Z and Drell-Yan+QCD are modelled using the same functions as in 0 btag case with p1 and p2 forced to be the same values as the fit results of the 0 btagged events. The numbers of QCD + Drell-Yan and Z are calculated using the same method as in 0 btag too.

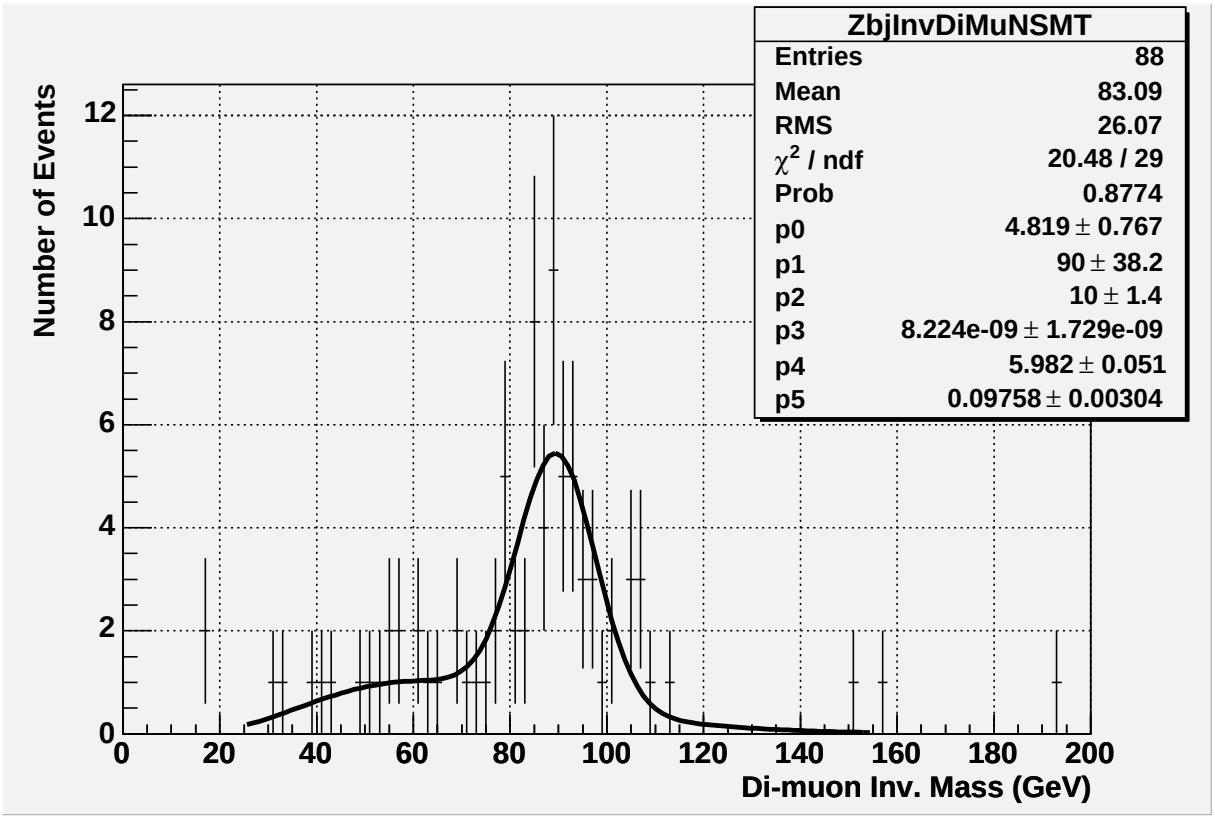

Figure 19: Di-muon invariant mass distribution for $Z + 2$ jet with 1 btag events. Isolation cut 0.02 is applied. Z and Drell-Yan+QCD are modeled using the same functions as in 0 btag case with p1 and p2 forced to be the same values as the fit results of the 0 btagged events.

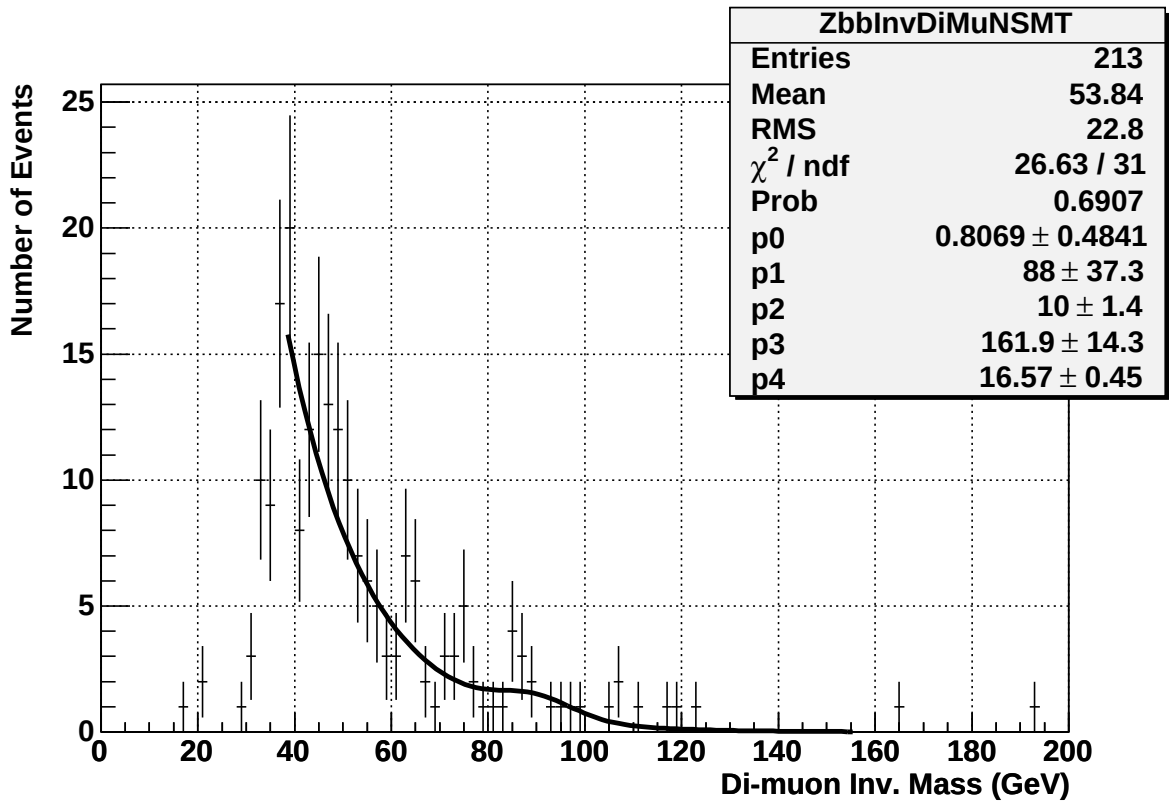

Figure 20: Di-muon invariant mass distribution for $Z+2$ jet with 2 btag events. No isolation cut is applied. Z and Drell-Yan+QCD are modeled using the same functions as in 1 btag case. The number of Z is calculated by integrating the fit function, the number of QCD+Drell-Yan is the total number of events within the Z mass window subtracted by the number of Z.

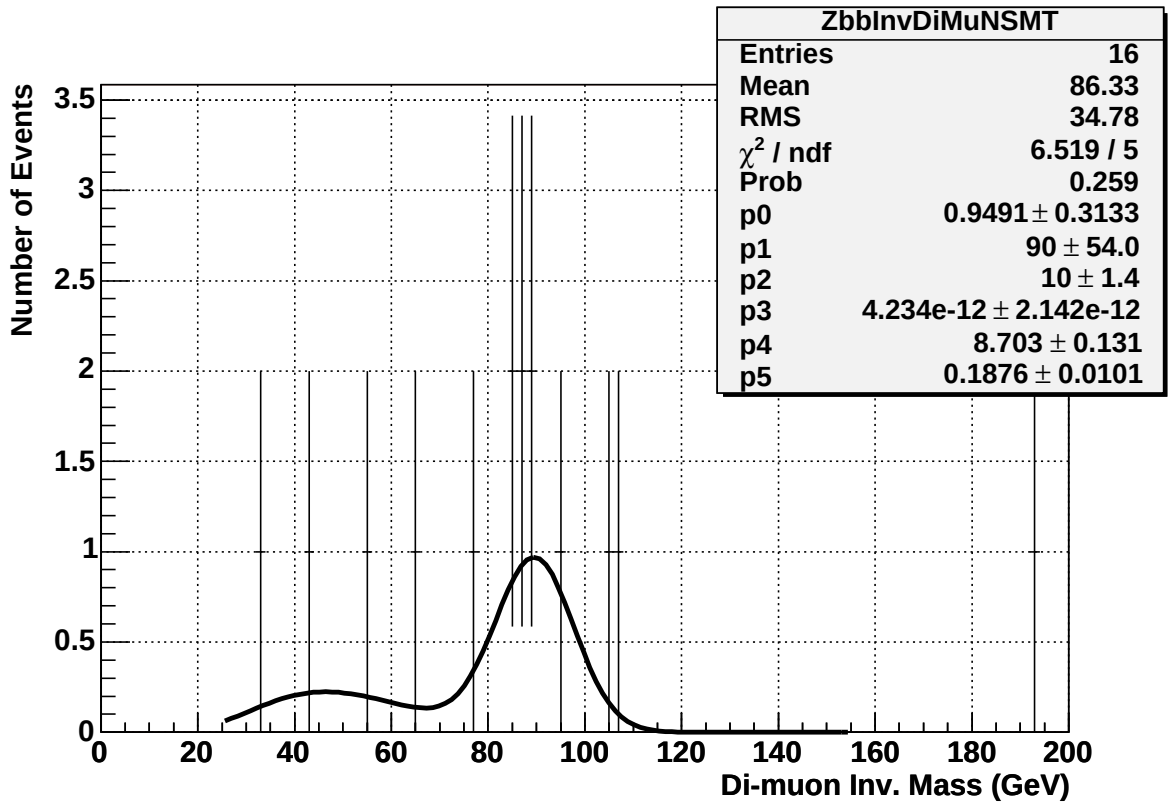

Figure 21: Di-muon invariant mass distribution for $Z + 2$ jet with 2 btag events. Isolation cut 0.02 is applied. Z and Drell-Yan+QCD are modeled using the same functions as in 1 btag case.

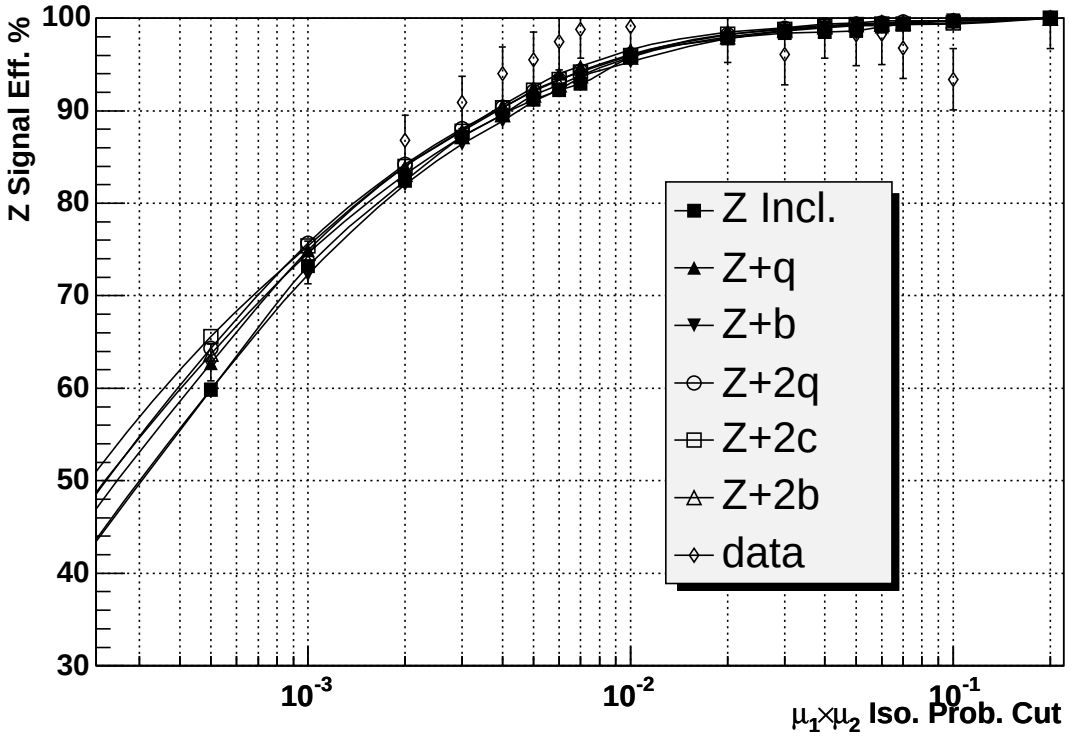

Figure 22: Di-muon isolation probability cut efficiencies for $Z + 2j$ events selected from MC $Z + nj$ and $Z + nb$ samples and data. For the MC samples, the third method is used; for the data sample, the first method is used. As one can see within uncertainties the efficiency from data agrees with those from MC calculations. The average of the MC efficiencies are used in this analysis.

4.2.2 Di-muon isolation cut efficiency for $t\bar{t}$.

The ttbar decay process does not contain a Z, but two muons can come from independent decay of the two W's produced in top pair decay and thus fake the Z signal. The third method is used to measure the isolation cut efficiency and the results is listed in Table 6. As one would expected for the di-leptonic decay channel the efficiency is similiar but slightly lower than the process which contains Z, for the single lepton decay mode the efficiency is much lower due to the un-isolated muon from b decay..

Table 6: The di-muon isolation cut efficiencies for $t\bar{t}$ processes with 0, 1, 2 btagged jets at isolation cut = 0.02. The efficiency is as expected to be lower than the MC Z samples, and it is weakly dependent on the number of b-tagged jets.

	0 btag	1 btag	2 btag
$t\bar{t} \to \mu\mu + 2j$	0.952 ± 0.01	0.944 ± 0.01	0.949 ± 0.01
$t\bar{t} \to \mu + 2b + 2j$	0.713 ± 0.02	0.702 ± 0.02	0.668 ± 0.03

4.2.3 Di-muon isolation cut efficiency for QCD background

Contrary to the Z/Drell-Yan which has the isolation cut efficiency independent of the number jets/b-jets, the QCD isolation cut efficiency is expected to be dependent on the b-jet requirement. We will show in detail in section 5 how we use the matrix equation method to subtract the QCD background from the Z/Drell-Yan signal and calculate the QCD efficiency for different number of final b-jets.

The di-muon isolation cut efficiency for QCD background without b-tagged jet is the simplest to calculate. As discussed before, the single muon isolation probability in this case is a evenly distributed number from 0 to 1. Assuming there is no correlation between the 2 muons in the QCD background, one can model the di-muon QCD isolation probability distribution by using the product of 2 random numbers. This method has been tested using the anti-isolated samples[17]. The isolation cut efficiency for QCD with 2 muon and 2 jets without b-tag is summarized in Table 7.

The optimized isolation cut is determined by maximize the the signal significance $Z/\sqrt{Z + QCD}$ as a function of isolation cut. It is detailed in section 5. The result cut is set to $f_{iso} = 0.02$.

Table 7: Di-muon isolation cut efficiencies for 2μ+2 jets QCD background without b-tagged jet requirement.

Cut	0.1	0.07	0.05	0.03	0.02	0.01	0.007	0.005	0.003	0.001
ϵ_{iso}^{QCD}	0.330	0.256	0.200	0.134	0.098	0.056	0.042	0.032	0.021	0.008

4.3 Jet RECO×ID Efficiency

The data and MC jet (RECO×ID) efficiencies and scale factors have been measured in [18]. Since the top_trees for the MC samples do not contain enough information to get the particle jet of a RECO-ed jet, we cannot use the parameterizations for the jet (RECO×ID) efficiency as the function of jet p_{T} in different η regions. Instead the data/MC scale factor which is also measured in [18] will be used to correct the MC jet RECO×ID efficiency.

The parameterization of the data/MC scale factor is given as a function of jet p_{T} :

$$j_{SF} = 1.00 \times Erf(0.0285 * Z_{p_{\mathrm{T}}} + 0.262) \quad (6)$$

$$j_{SF}^{+\sigma} = 0.0199 + 0.0750 \times e^{1.97-0.0286*Z_{p_{\mathrm{T}}}} \quad (7)$$

$$j_{SF}^{-\sigma} = 0.0172 + 0.217 \times e^{-0.0503*Z_{p_{\mathrm{T}}}} \quad (8)$$

where $j_{SF}, j_{SF}^{+\sigma}, J_{SF}^{-\sigma}$ are the scale factor central value, central value+1σ and -1σ, and $Z_{p_{\mathrm{T}}}$ is the MC smeared calorimeter jet p_{T} :

$$Z_{p_{\mathrm{T}}} = 0.719 + 0.953 \times p_{\mathrm{T}} \quad (9)$$

where p_{T} is the jet p_{T} measure in calorimeter.

The event average of the MC jet RECO×ID efficiency is calculated by the ratio of the number of events that have $Z + 2$ or more jets(no good jet cut applied) to the number of the events that have passed the Z selection.

For each MC sample the jet RECO×ID data/MC scale factor of a single jet is convoluted with the selected Z events as shown in Figure 1 to get the event average. Since 2 or more jets are required for each event, Eq. 23 is used to calculate the event average, where ζ is replaced with j_{SF}.

The event average of the MC jet (RECO×ID) efficiencies, the data/MC scale factor and the data efficiencies for ZH signal and backgrounds are listed in Table 8.

To ensure the MC samples model the jet well, jet multiplicity, p_{T} , η and ϕ distributions are compared with those of jets in data. All of them requires the presence of a $Z \to \mu\bar{\mu}$ signal. The plots are shown in Figures 23-26. It is clear the MC agrees with data well.

Table 8: Event averages of jet RECO×ID efficiencies for the selected Z candidates with 2 or more jets for ZH signals and the backgrounds. The branching ratio for the double jet production is also included in these efficiencies.

Process	Zbb	Zcc	Zjj	$ttdl$	$ttsl$	ZZ	WZ	Z
MC Eff.	0.361	0.375	0.363	0.812	0.989	0.528	0.516	0.0509
Data Eff.	0.281	0.29	0.28	0.761	0.987	0.458	0.422	0.0341
Data/MC SF	0.777	0.774	0.77	0.938	0.997	0.868	0.818	0.669

Process	$ZH(105)$	$ZH(115)$	$ZH(125)$	$ZH(135)$	$ZH(145)$
MC Eff.	0.809	0.827	0.84	0.87	0.877
Data Eff.	0.716	0.751	0.769	0.814	0.819
Data/MC SF.	0.885	0.908	0.915	0.935	0.934

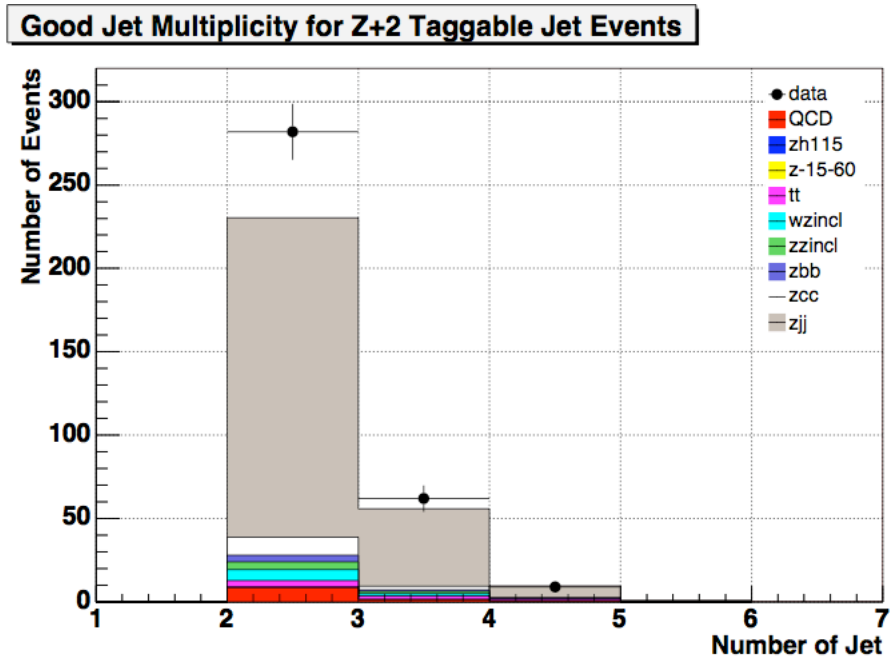

Figure 23: Exclusive jet multiplicity distribution for the $Z+ \geq 2$ jet events with 0 btag.

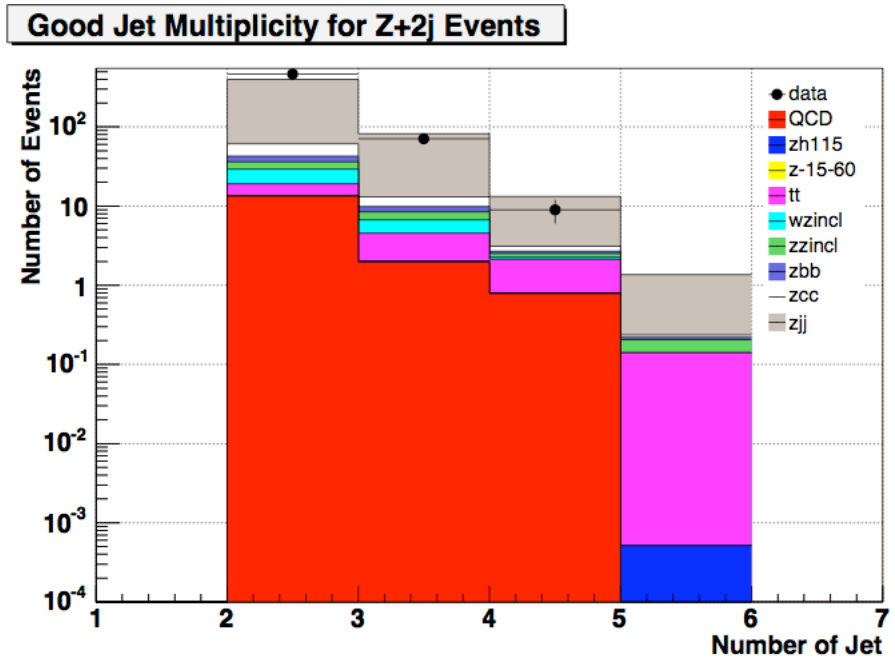

Figure 24: Exclusive jet multiplicity distribution for the $Z+ \geq 2$ jet events with 0 btag in log scale.

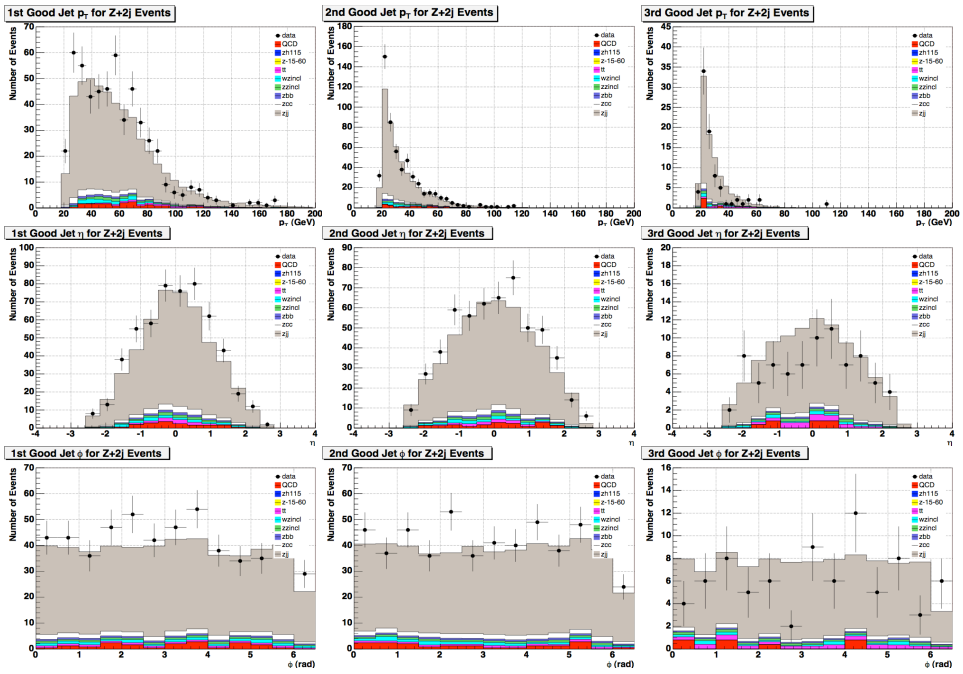

Figure 25: The 1st, 2nd and 3rd good jet p_{T} , η, ϕ distribution for the $Z+ \geq 2$ jet events.

4.4 Jet Taggability and B-tag Optimization

We use JLIP b-tagger with JES v5.3 [13] to find the b jets in the selected $Z + 2j$ events. The JLIP tagger has 6 operating points. As discussed in [2], the optimized operating point with respect to the Higgs signal significance is the ExtraLoose mistag rate.

We would like to use the double b-jet JLIP probability the same way we use the isolation probability for the di-muon system, *e.g.* we could cut on the product of the JLIP probability of the 2 b jets instead of cutting on the probability on each of the jet. But this turns out to be unpractical for the time being. One of the problems is that the optimized operation point for single jet b-tag for our study is already the loosest one. In order to make the most of the topological method, we need a much looser mistag rate beyond the current available operation points. Another problem is that TRF is only available for the 6 operating points, yet in order to use the topological method and calculate the tag rate for each of the jet flavor, we will need TRF's as functions of mistag rate. With this in mind we will simply use the extra loose cut to identify b-tagged jets. The topological method will be implemented in the future.

In order to reduce the background, the JLIP b-tagger makes the jet taggability requirement on the jet to be tagged, *eg.* a trackjet matches the jet with $\Delta R < 0.5$.[13]. Then the JLIP

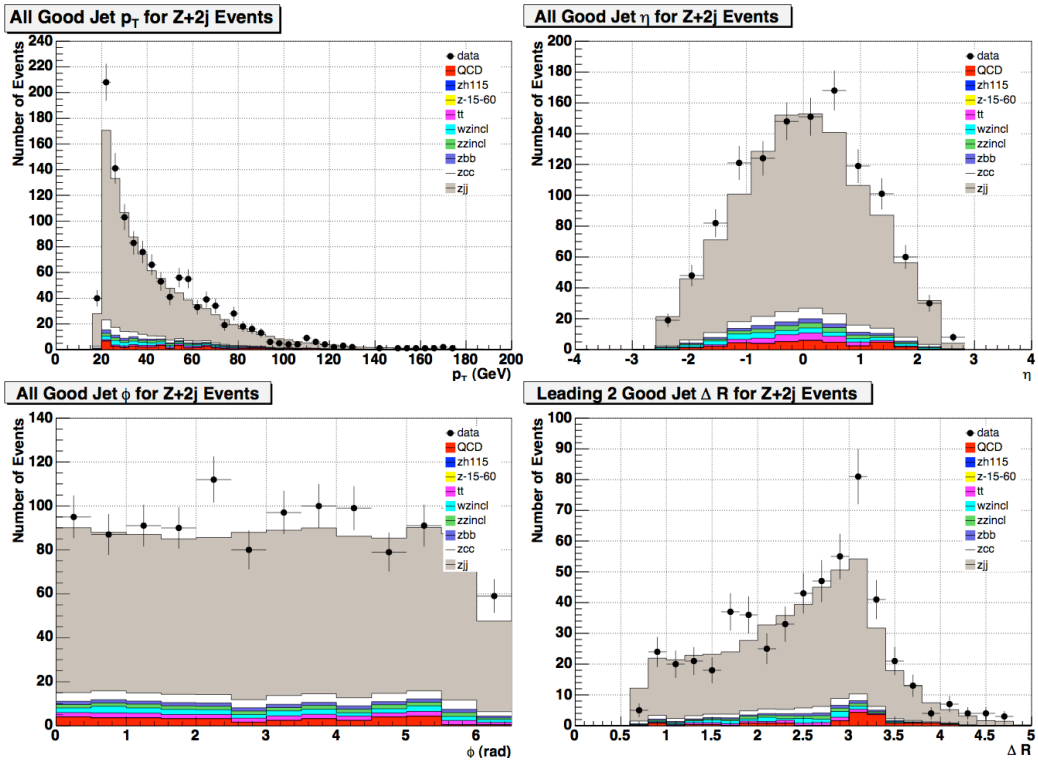

Figure 26: All good jet p_{T} , η, ϕ and the leading 2 good jets' dR distribution for the $Z+ \geq 2$ jet events.

b-tagger provides a probability for each taggable jet for b-tag selection. The event average of data and MC jet taggability and b-tag rate need to be calculated in order to get the data/MC scale factor.

The JLIP b-tagger provides the b-tag rate data/MC scale factor for a single b-jet and c-jet. The same convolution technique is used to get the event average of the b-tag TRF data/MC scale factor.

The event average of the MC taggability for each of the MC sample is the ratio of the number of $Z + 2$jet events with and without jet taggability requirement as shown in Figure 1. The event average of the data taggability for the $Z + 2$ jets events in data measured in the same way. Both MC and data tagabilities are measured as functions of jet p_{T} and η. The results are shown in Figures 27-36. The event average of b-tag rate is done in the same way.

There are some behaviors of the jet taggability worth mentioning:

- The taggability in the multi-jet sample may be biased because the found muon(s) often occur within a jet, so at least one track is already provided by the muon. The taggability computation must exclude jets with muons when those muons are used to select the event. With the standard muon isolation cut which normally cut on the ΔR between the muon and jet, this bias is excluded automatically. For this analysis the muon isolation cut does not explicitly cut on the muon and jet distance, so the taggability can actually be quite different from the taggability calculated using the standard muon isolation cut.
- The taggability could be slightly process dependent due the un-standard muon isolation cut which could introduce process dependent bias.
- Taking into consider the big uncertainties, the jet taggability is not sensitive to the jet flavor, for example Zbb, Zcc and Zjj have the similar taggability as in Figures 27-29.
- The data taggability is independent of the di-muon isolation cut.
- The difference in taggability between data without and with the trigger selection is shown in Figure 37. Apparently the 2 tagabilities are identical within uncertainty.

According to Figure 1 in order to calculate the data jet taggability, we need to use the $Z + 2$ jets events with trigger selection and muon isolation cut. However, with the above mentioned points in mind, one can improve the statistics by loosening the events selection Z inclusive events without the di-muon isolation cut or the trigger selection.

Since the Zbb, Zcc and Zqq events compose most of the selected $Z+2$ jets events in data(with or without b-tag requirement), and they have almost identical taggability, we can calculate

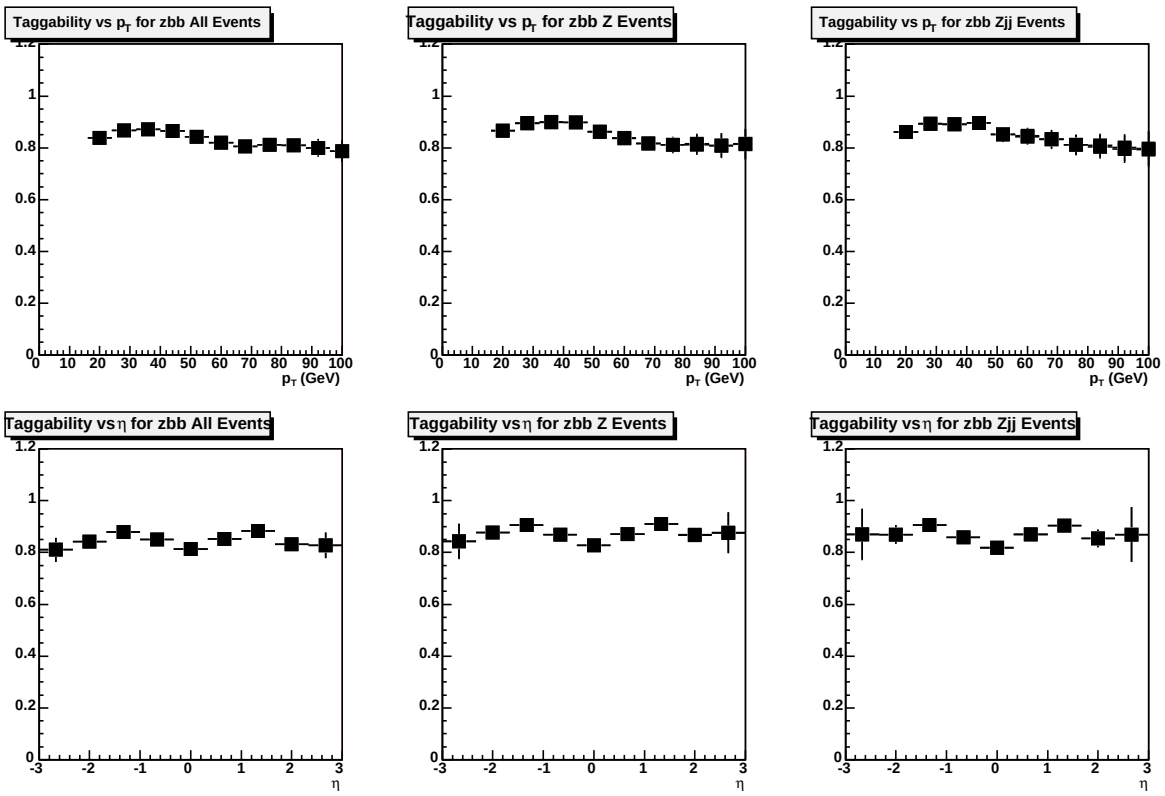

Figure 27: The jet taggability calculated for Zbb MC sample. In this plot, as in Figures 28-**??**, the upper and lower rows are taggablity as a function of jet p_{T} and η respectively; the first, second and third columns are the taggability measured w.r.t all good jets in events without Z event selection, all good jets in events with a Z candidate and all good jets in events with $Z + 2$ or more jets. For the second and third columns each plot contains taggabilities of both Z event with and without the di-muon isolation cut, since they have very small difference we will not differentiate them explicitly. The 3 types of events have slightly different taggability as shown in this and the following taggabilities for MC samples. The third column is the one we should use in the analysis according to Figure 1.

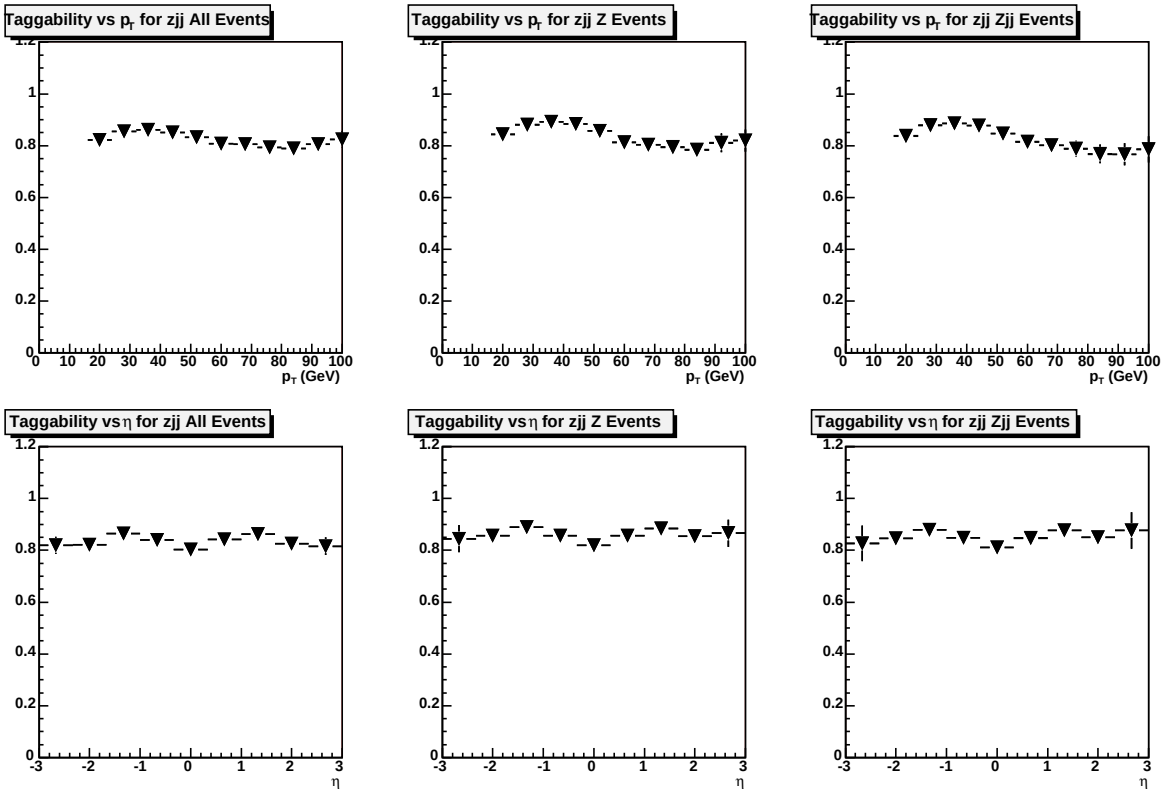

Figure 28: The jet taggability calculated for Zjj MC sample. Compared to Figure 27 , it is clear that the jet taggability is jet flavor independent as one would expect.

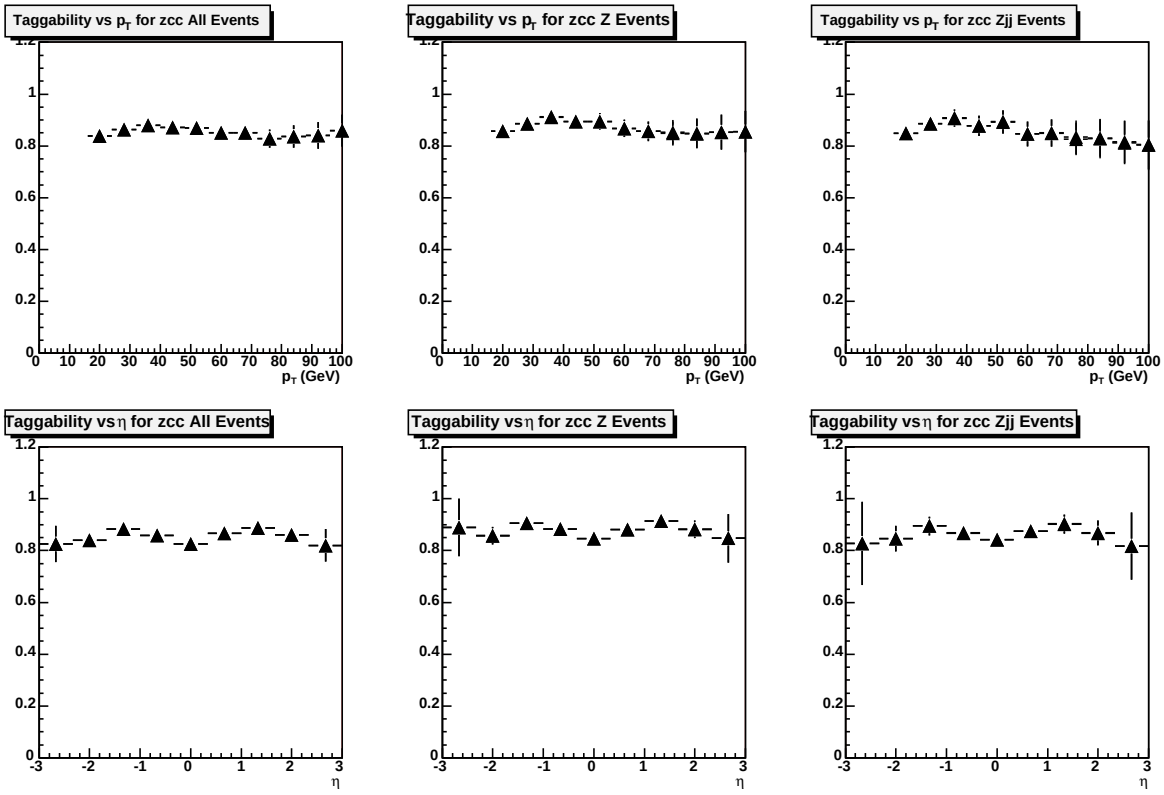

Figure 29: The jet taggability calculated for *Zcc* MC sample.

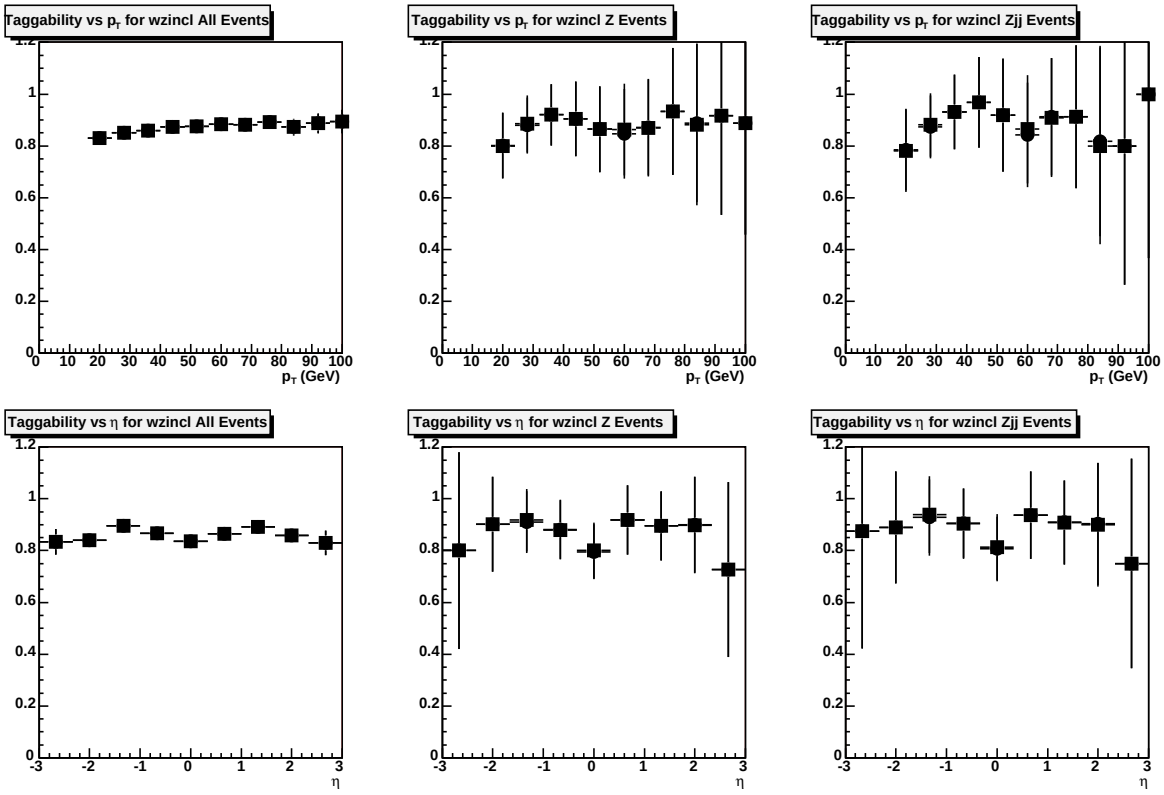

Figure 30: The jet taggability calculated for WZ inclusive MC sample..

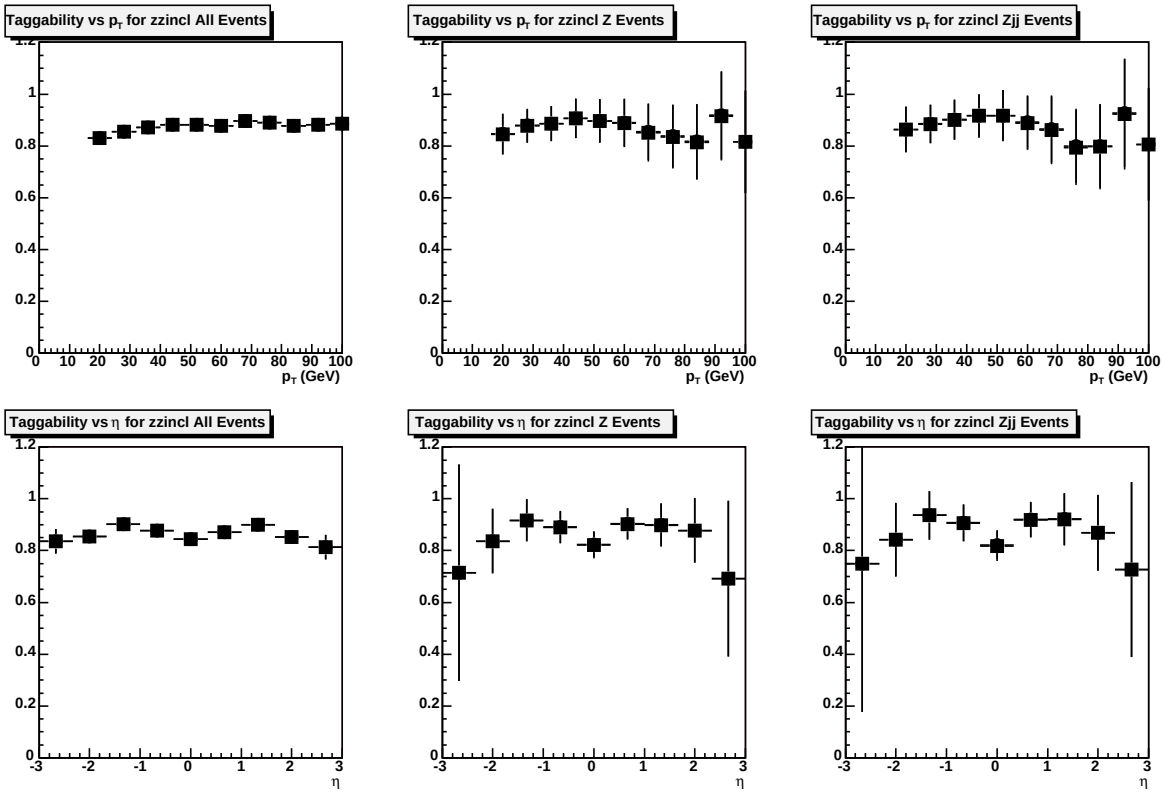

Figure 31: The jet taggability calculated for ZZ inclusive MC sample.

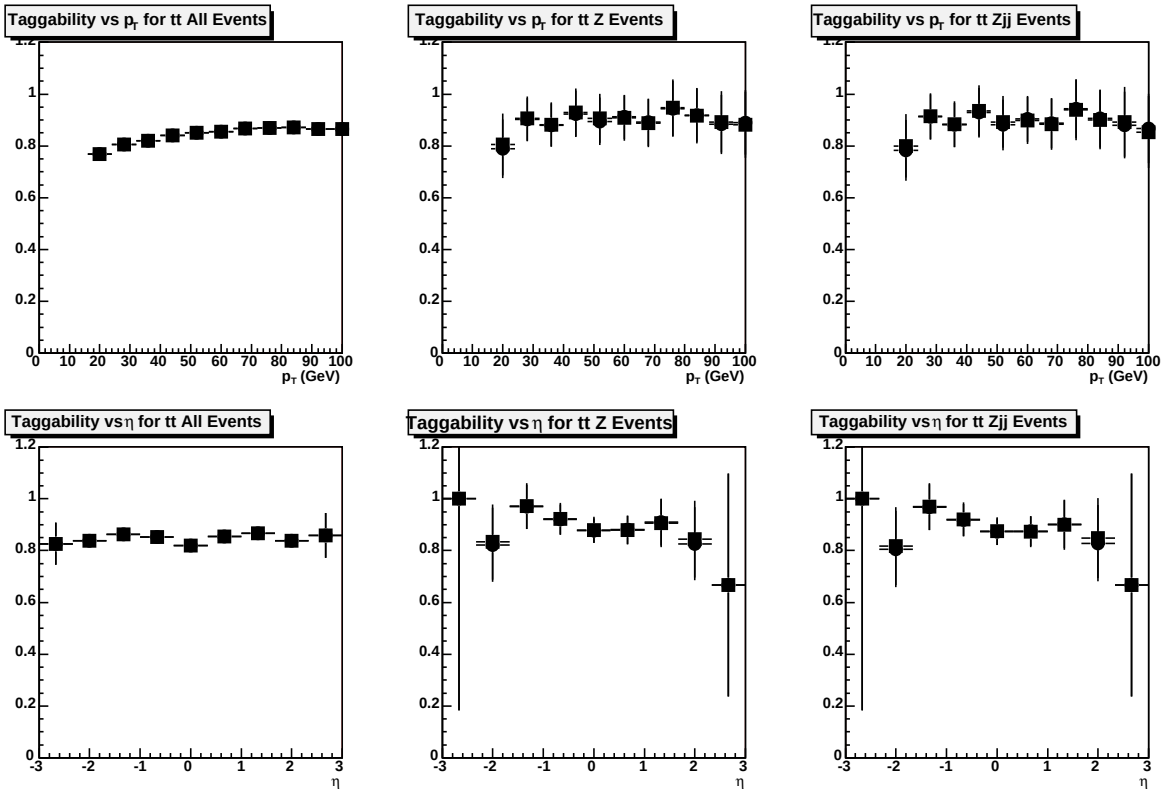

Figure 32: The jet taggability calculated for $t\bar{t}$ di-leptonic channel MC sample.

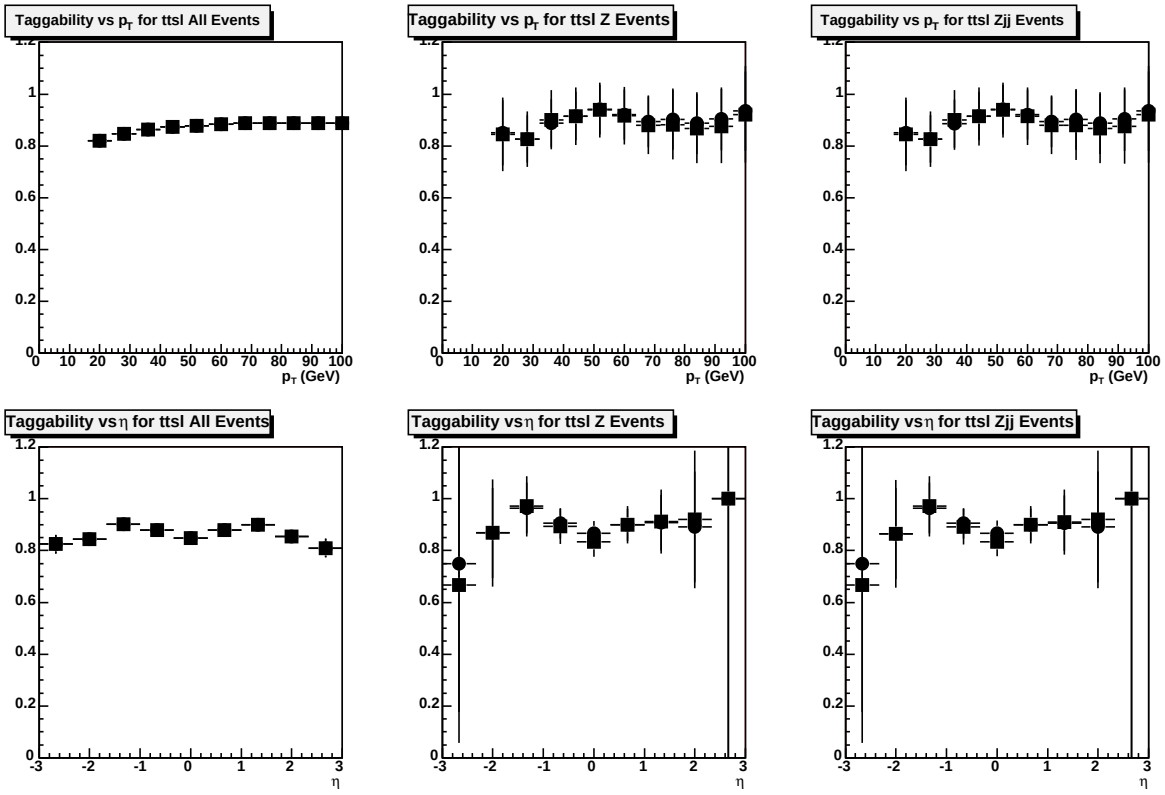

Figure 33: The jet taggability calculated for $t\bar{t}$ single leptonic channel MC sample.

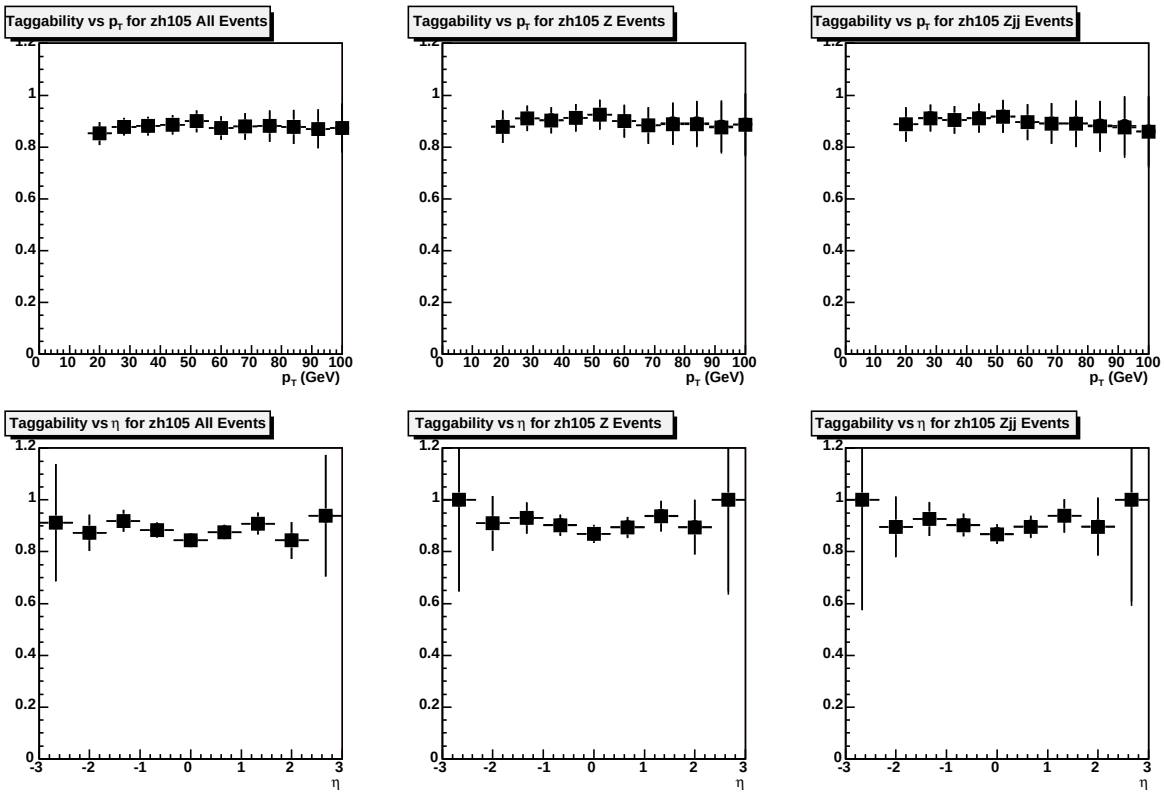

Figure 34: The jet taggability calculated for $ZH(105)$ MC sample.

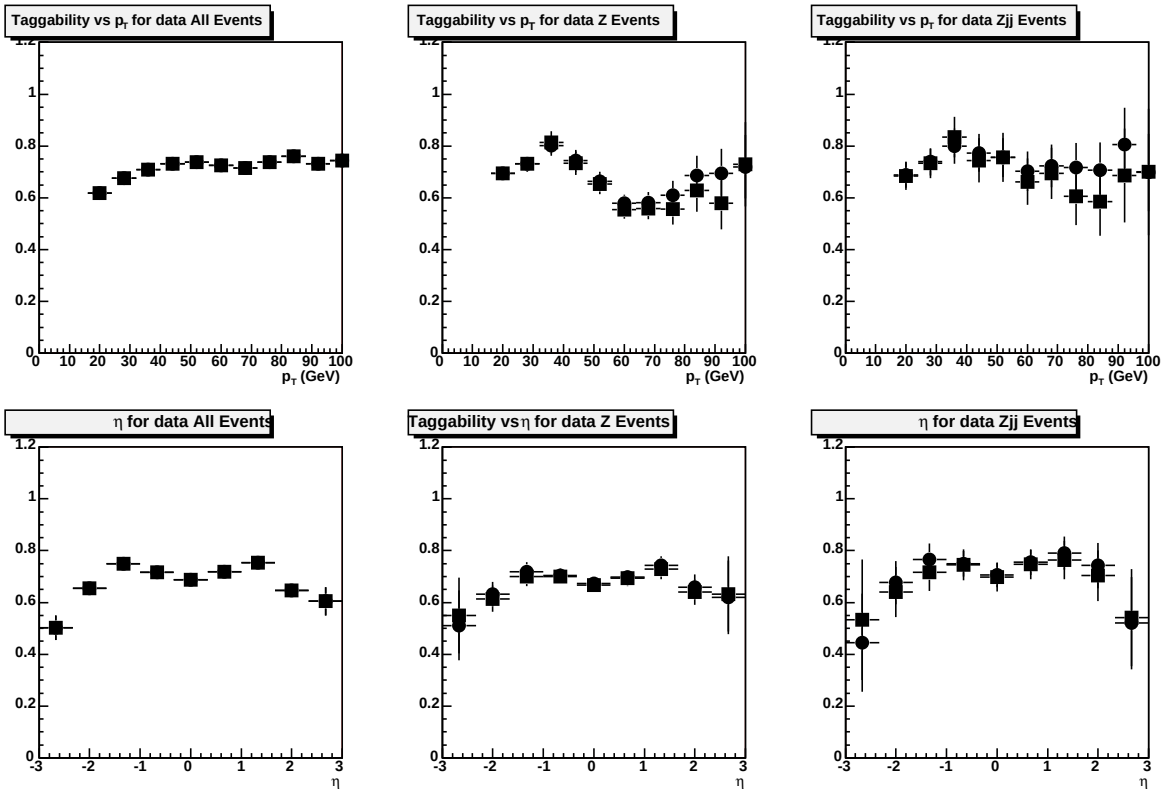

Figure 35: The jet taggability calculated for data without the muon trigger requirement. There is clearly a data/MC difference, especially in the second column. The reason for the taggability drop at high jet p_{T} is due to fact that the muon isolation cut used in this analysis does not explicitly exclude the jet that is close to a muon. The same drop can be seen in Figures 27–29 in a less severe degree. This is due to the Data/MC difference.

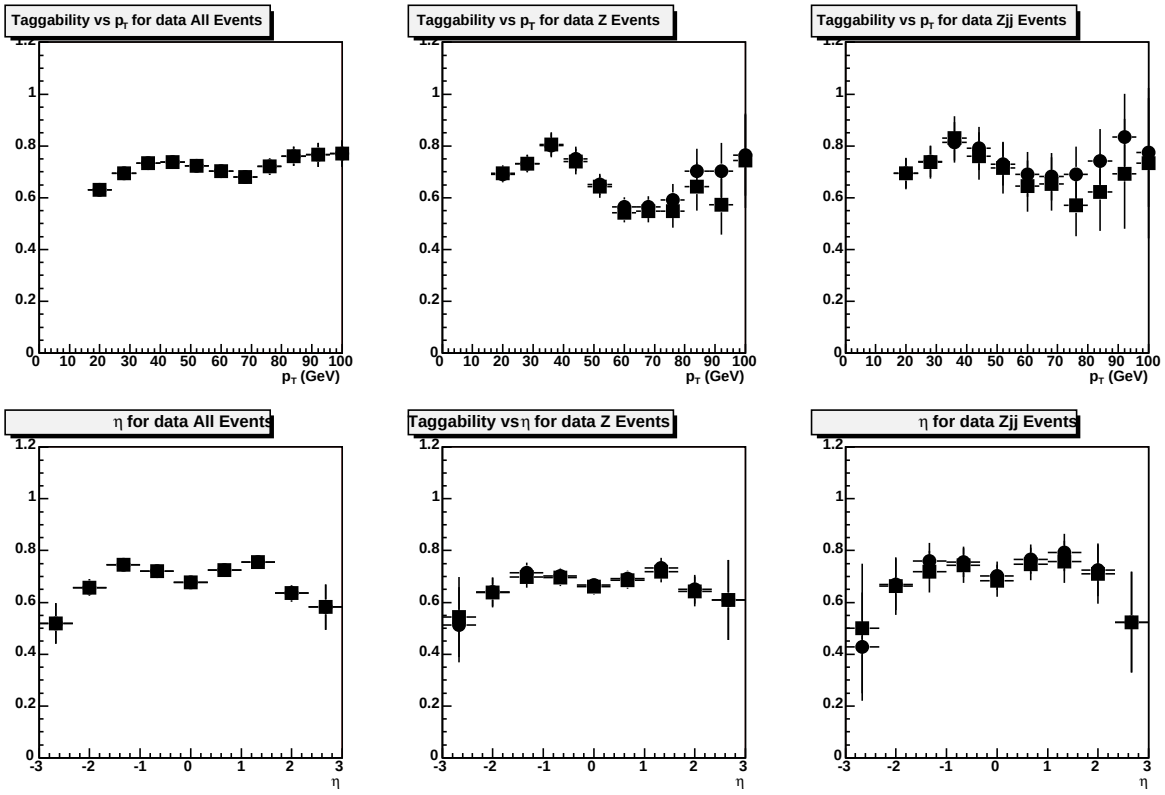

Figure 36: The jet taggability calculated for data with the muon trigger requirement.

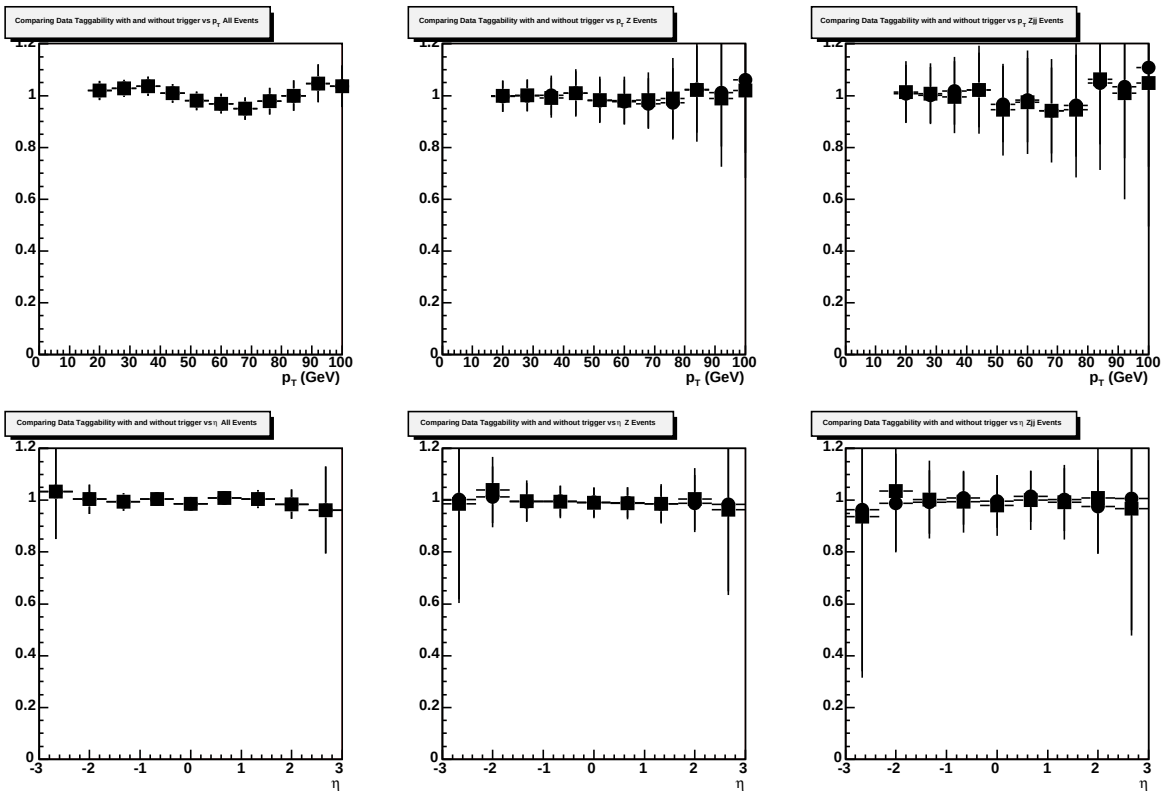

Figure 37: The jet taggability difference between data with and without the muon trigger requirement. Clearly there is no difference within error. So we use the data without trigger requirement to measure the taggability in order to reduce the statistical uncertainty.

the taggability data/MC scale factor by taking the ratio of data taggability in Figure 35 and the MC $Zbb/Zcc/Zqq$ tagabilities in Figure 27 and 28. The combined average is shown in Figure 38.

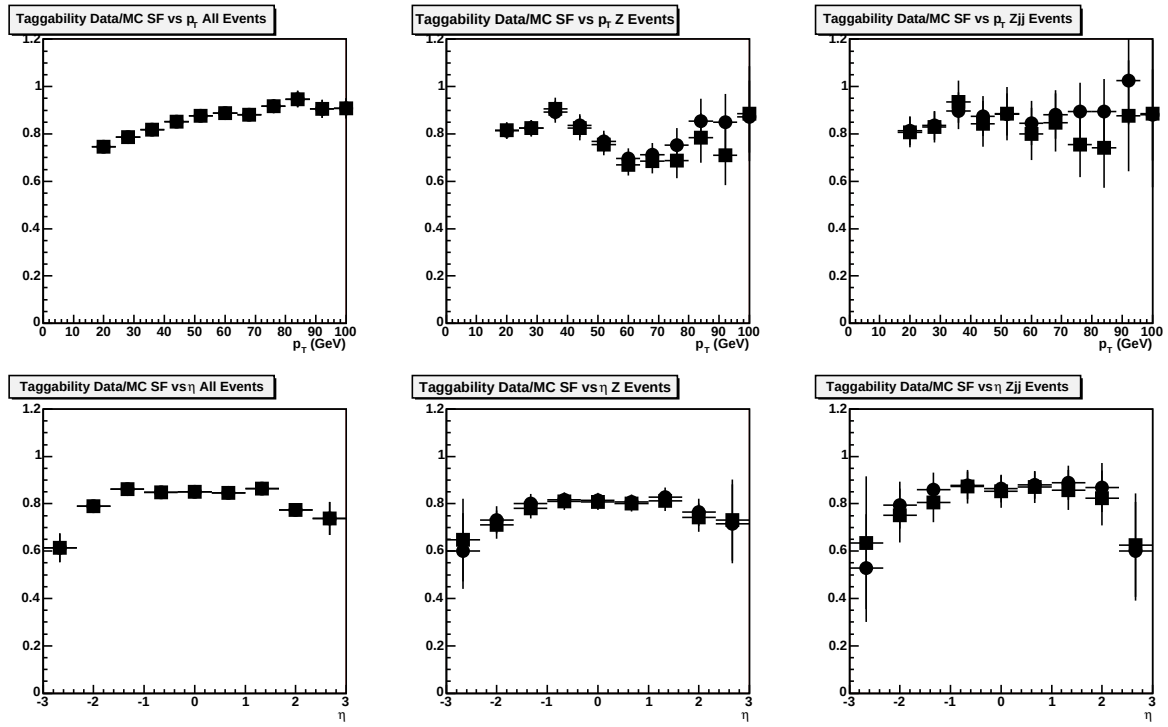

Figure 38: The jet taggability data/MC scale factor. It's combined from data/Zjj, data/Zbb and data/Zcc since these three kinds of events consist most of the selected events in data, and they have the similar scale factor.

Now that both the taggability and b-tag rate data/MC scale factors are available, we simply convolute them[3] over the $Z+2$ jets events to get the event average for the single and double (Taggability×B-tag) efficiencies. The results are listed in Tables 9-10 for all the MC samples.

4.5 Kinematic Acceptance

All the remaining event selection cuts are classified as the kinematic cuts. Their purpose is to confine the jets and the muons in the DØ detector fiducial range, to further reduce

[3]Due to the limited statistics, the ($p_{\rm T}$, η) 2-D taggability is modeled by the product of the tagabilities as 2 functions of $p_{\rm T}$ and η, the function of η is properly normalized so that the overall taggability is not double counted.

Table 9: Event averages of the inclusive single jet taggability and ExtraLoose JLIP b-tag efficiencies for $Z + 2$ jets events for all the MC samples with di-muon isolation cut $f_{iso} = 0.02$. Btag efficiencies include the taggability. The MC efficiencies are simply the ratio of events after/before tag. The data efficiencies and the scale factors are calculated using the convolution method.

Process	Zbb	Zcc	Zjj	$ttdl$	$ttsl$	ZZ	WZ	Z
Data Tag Eff.	0.971	0.971	0.965	0.989	0.997	0.985	0.982	0.95
MC Tag Eff.	0.99	0.993	0.985	0.997	0.995	0.982	0.995	0.977
Data/MC Tag SF.	0.947	0.946	0.941	0.981	0.994	0.968	0.963	0.908
Data B-tag Eff.	0.614	0.323	0.0866	0.8	0.809	0.238	0.165	0.0774
MC B-tag Eff.	0.785	0.413	0.109	0.924	0.884	0.289	0.172	0.095
Data/MC B-tag SF.	0.795	0.757	0.798	0.878	0.892	0.819	0.764	0.747

Process	$ZH(105)$	$ZH(115)$	$ZH(125)$	$ZH(135)$	$ZH(145)$
Data Tag Eff.	0.989	0.989	0.993	0.991	0.989
MC Tag Eff.	0.992	0.998	0.996	0.995	0.993
Data/MC Tag SF.	0.977	0.978	0.98	0.981	0.983
Data B-tag Eff.	0.752	0.768	0.783	0.785	0.77
MC B-tag Eff.	0.883	0.894	0.889	0.885	0.886
Data/MC B-tag SF.	0.854	0.859	0.868	0.875	0.876

Table 10: Event average of the inclusive double jet taggability and ExtraLoose JLIP b-tag efficiency for $Z+2$ jets events for all the MC samples with di-muon isolation cut $f_{iso} = 0.02$.

Process	Zbb	Zcc	Zjj	$ttdl$	$ttsl$	ZZ	WZ	Z
Data Tag Eff.	0.714	0.71	0.685	0.819	0.949	0.783	0.765	0.618
MC Tag Eff.	0.874	0.883	0.841	0.952	0.984	0.92	0.879	0.767
Data/MC Tag SF.	0.696	0.688	0.687	0.792	0.931	0.752	0.741	0.626
Data B-tag Eff.	0.146	0.0325	0.00357	0.304	0.333	0.0435	0.00474	0.00325
MC B-tag Eff.	0.294	0.0617	0.00771	0.516	0.466	0.0801	0.00505	0.00413
Data/MC B-tag SF.	0.538	0.558	0.582	0.628	0.674	0.553	0.541	0.642

Process	$ZH(105)$	$ZH(115)$	$ZH(125)$	$ZH(135)$	$ZH(145)$
Data Tag Eff.	0.817	0.828	0.858	0.845	0.828
MC Tag Eff.	0.95	0.962	0.968	0.964	0.959
Data/MC Tag SF.	0.765	0.775	0.785	0.795	0.808
Data B-tag Eff.	0.255	0.27	0.292	0.291	0.282
MC B-tag Eff.	0.446	0.463	0.48	0.49	0.477
Data/MC B-tag SF.	0.581	0.586	0.604	0.604	0.621

the QCD background and to reduce the cosmic muons. The acceptances of the kinematic cuts are calculated by taking the ratio of the number of events after and before a cut. MC samples are used in doing these calculation, and no data/MC scale factor is used since the MC describes the kinematic variables well. All the kinematic acceptances are measured w.r.t the events where 2 muon and 2 jets presents, no di-muon isolation and b-tagged jets are required. Table 11 lists the acceptances for different MC samples.

Due to the better momentum resolution in MC and the smearing of the muon $\frac{q}{p_{\mathrm{T}}}$, the opposite charge cut has higher efficiency in MC than in the data. The difference is accounted for by a scale factor. The opposite charege cut efficencies of data, MC and the Data/MC scale factor are listed in Table 12

5 QCD Subtraction

This section deals with the QCD subtraction from the selected $Z + 2$jet events in the data. The QCD di-muon isolation efficiency will also be calculated for the events with b-tagged jets. The calculation is based on the the matrix method.

Table 11: Kinematic acceptances $\mathcal{A}_{kine}$ for all MC samples. Measured w.r.t the events in which 2 loose muon with central track match and 2 jet presents.

Process	Zbb	Zcc	Zjj	$ttdl$	$ttsl$	ZZ	WZ	Z
$\mathcal{A}_{kine}$	0.386	0.393	0.392	0.0805	0.00984	0.235	0.156	0.285

Process	$ZH(105)$	$ZH(115)$	$ZH(125)$	$ZH(135)$	$ZH(145)$
$\mathcal{A}_{kine}$	0.511	0.521	0.53	0.538	0.529

Table 12: Di-muon opposite charge data, MC efficiencies and the data/MC scale factor. The MC efficiency is the average of Zjj, Zcc, Zbb MC samples.

Data	MC	Data/MC SF
0.96 ± 0.01	0.99 ± 0.01	0.97 ± 0.01

The matrix equation is established by counting the total number of Z candidates with and without the isolation cut:

$$\text{QCD} + \text{DY} + \text{Z} = N_{non-iso} \quad (10)$$

$$\epsilon_{QCD} \cdot \text{QCD} + \epsilon_{DY} \cdot \text{DY} + \epsilon_{Z} \cdot \text{Z} = N_{iso} \quad (11)$$

where Z refers to the Z peak in the distribution which includes all of the processes in Table 2, 3 except for the $t\bar{t}$ processes where no Z peak presents, the "flat" distribution under the Z peak consist of the QCD background(QCD) and non-QCD processes(DY): Drell-Yan process and $t\bar{t}$[4]; $\epsilon_{QCD}, \epsilon_{DY}, \epsilon_{Z}$ are the isolation cut efficiencies of QCD, Drell-Yan and Z signals, $N_{non-iso}$ and N_{iso} are the total number of events within the mass window without and with isolation respectively. According the Table 5, 6, the $t\bar{t}$ has the similar di-muon isolation efficiency as the processes which contain Z boson, so we also include it into Z. The slight difference in the isolation cut efficiency will be accounted for as systematic error.

The equations hold for 0, 1, 2 b-tag cases[5], but due to various reasons discussed in the following section, the equation will be solved differently for each of these cases.

[4]For simplicity we will refer to both of them as Drell-Yan process.

[5]From now on we will study only the inclusive b-tagged event, thus the inclusive single or double btag are referred to as 1, 2 b-tag.

5.1 $Z + 2$jets, 0 b-tag

Due to the kinematic similarity between the Drell-Yan and the Z process, $\epsilon_{DY} = \epsilon_Z$ and it has been calculated using MC and data samples as described in section 4.2.1.

For the Z + 2jet event without b-tag requirement, we have also calculated the di-muon isolation cut efficiency for QCD using 2 evenly distributed random numbers in section 4.2.3. So we can solve the equations for QCD and $(DY + Z)$.

We can also get the Drell-Yan and Z signal ratio. In doing so we need to extract Z by fitting the Z peak in Figure 16, 18, 20 . The Z peak is modeled by Gauss and Breit-Wigner convoluted function, the QCD background+Drell-Yan is fitted with an exponential function[6]. The fittings are shown in Figure 16, 18, 20 for $Z + 2j$ with 0, 1, 2 b-tag without the di-muon isolation cut. The results are listed in Table 13.

Table 13: Fit results of the Z peak and QCD+Drell-Yan background for $Z + 2j$, $Z + 2j$ with 1^+ b-tag and $Z + 2j$ with 2^+ b-tag. No di-muon isolation cut applied.

Process	Z	Drell-Yan + QCD
$Z + 2j$ 0 b-tag	450.87 ± 19.96	253.13 ± 15.43
$Z + 2j$ 1^+ b-tag	53.70 ± 11.03	92.29 ± 8.06
$Z + 2j$ 2^+ b-tag	8.17 ± 4.94	30.83 ± 5.32

Clearly shown in Figure 18, 20, the Z peaks for 1, 2 btagged events are not so pronounced as in Figure 16. We need to find other ways to confirm the fit results are reliable.

We introduce 2 variables:

$$\gamma_1 = \frac{N_{zbj}}{N_{zjj}} \tag{12}$$

$$\gamma_2 = \frac{N_{zbb}}{N_{zjj}} \tag{13}$$

where $N_{zjj}, N_{zbj}, N_{zbb}$ are the total number of events within the Z mass window of selected Zjj with 0, 1, 2 b-tag respectively.

Figures 39 and 40 show the γ_1 and γ_2 as a function of isolation cut. Clearly γ_1 and γ_2 decrease when the isolation cut is tighter (smaller), and at the point when isolation cut is about 0.02,

[6]Although the fittings look good with and without the di-muon isolation cut, we only use the fit which isolation cut is not applied since in this case the QCD + Drell-Yan process has much larger statistics thus is much better modeled.

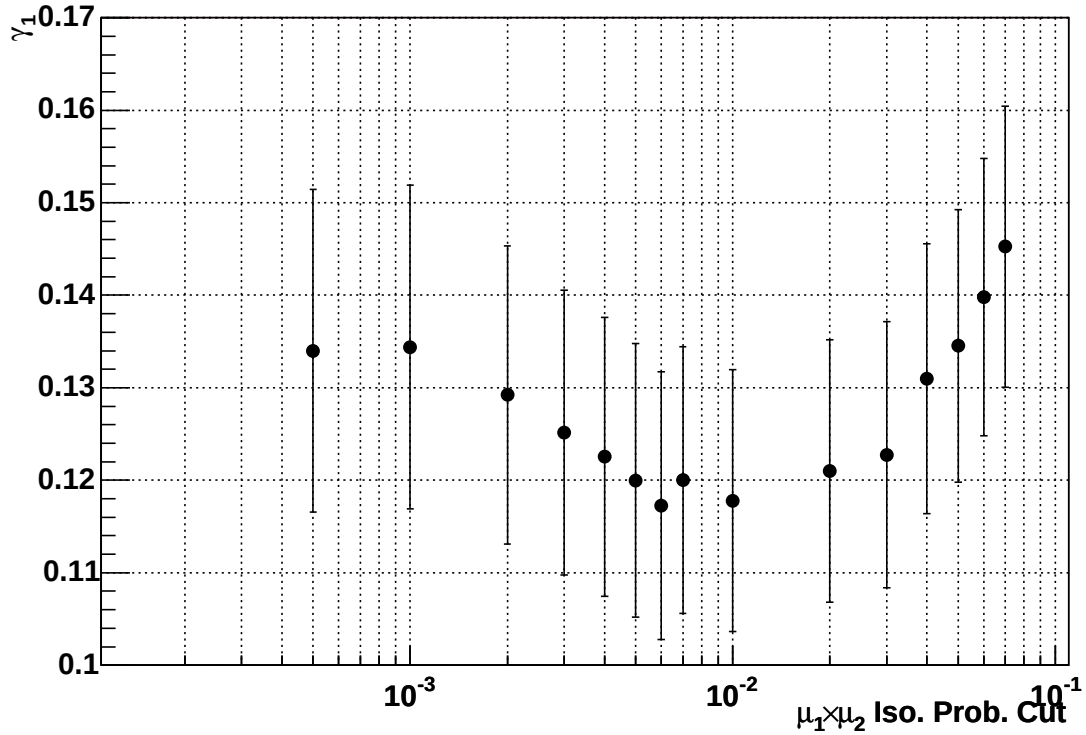

Figure 39: γ_1 as a function of di-muon isolation cut for data. With tighter(smaller) isolation cut, γ_1 decreases until reaching to a plateau. The plateau is the Z + Drell-Yan processes' single btag(including taggability) rate. In practice when the isolation cut is too small($<$ 0.01), the assumption that $Z + 2j, Z + 2c, Z + 2b, t\bar{t}, WZ, ZZ$ has the same isolation cut efficiencies begin not to hold any more, see Figure 22, so the btag rate is only obtained around isolation cut equals 0.01 where the QCD contribution is small enough to be ignored. The plateau is $\gamma_1 = 0.121 \pm 0.014$.

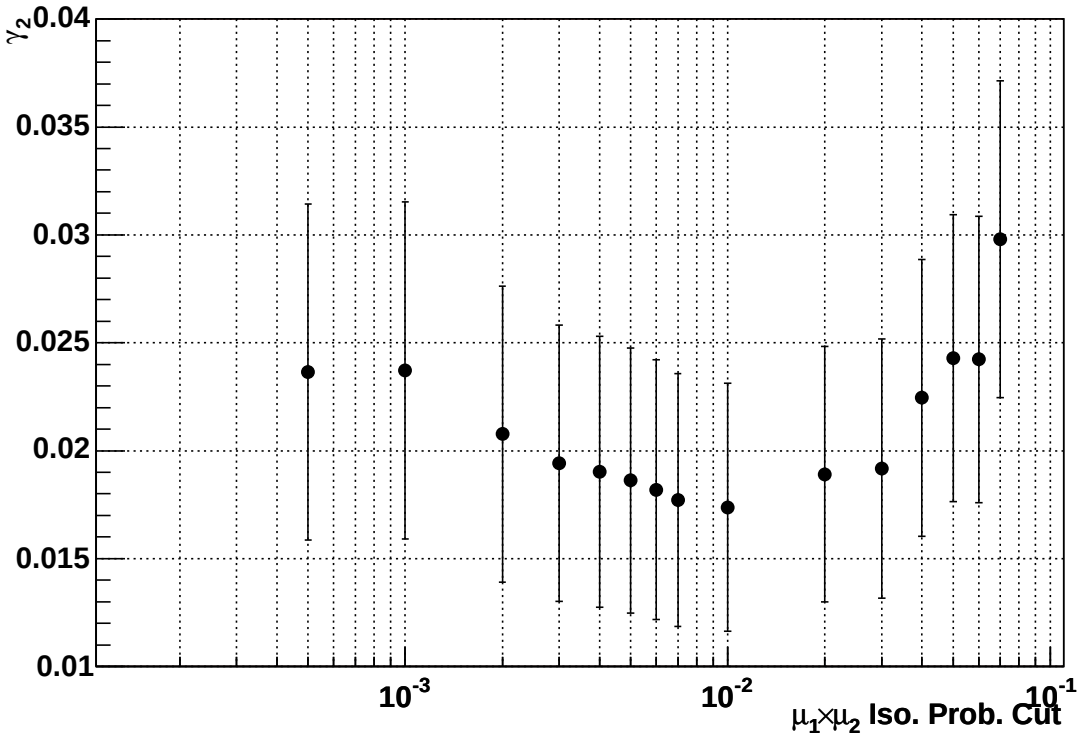

Figure 40: γ_2 as a function of di-muon isolation cut for data. Using the same arguments as for γ_1, the plateau is $\gamma_2 = 0.019 \pm 0.006$.

γ_1 and γ_2 reach to a plateau, and it can be proven that the plateau where isolation cut is very tight is an approximation of the direct measurement of data single b-tag and double b-tag rate for Z+Drell-Yan process:

$$\begin{aligned}
\lim_{IsoCut\to 0}\gamma_1 &= \lim_{IsoCut\to 0}\frac{N_{zbj}}{N_{zjj}} \\
&= \lim_{IsoCut\to 0}\frac{\epsilon_Z\cdot(Z+DY)_{zbj}+\epsilon_{QCD}\cdot QCD_{zbj}}{\epsilon_Z\cdot(Z+DY)_{zjj}+\epsilon_{QCD}\cdot QCD_{zjj}} \\
&= \lim_{IsoCut\to 0}\frac{\epsilon_Z\cdot(Z+DY)_{zbj}}{\epsilon_Z\cdot(Z+DY)_{zjj}} \\
&= \frac{(Z+DY)_{zbj}}{(Z+DY)_{zjj}}=\frac{(Z)_{zbj}}{(Z)_{zjj}} \qquad (14)\\
\lim_{IsoCut\to 0}\gamma_2 &= \frac{(Z+DY)_{zbb}}{(Z+DY)_{zjj}}=\frac{(Z)_{zbb}}{(Z)_{zjj}} \qquad (15)
\end{aligned}$$

At the working isolation cut point 0.02, $\gamma_1 = 0.121 \pm 0.014$ and $\gamma_2 = 0.019 \pm 0.006$. They are in good agreements with the ratio of fitted Z peaks in Table 13. So the fit results are reliable.

The ratio of Z, Drell-Yan and QCD results for $Z + 2j$ without b-tag requirement are listed in Table 14 (Z mass window is included). The combined D-Y/Z ratio g is determined from Figure 41:

$$g = 0.1964 \pm 0.0418 \qquad (16)$$

In [11] the same ratio calculated by PYTHIA is 0.21 when no Z mass window requirement is applied. This agrees with this result as expected because we have the Z mass window requirement in place.

Table 14: QCD subtraction results for $Z + 2j$ data for different dimuon isolation cut.

Isolation Cut	Z+Drell-Yan	Drell-Yan/Z ratio	QCD
0.1	536.98 ± 20.28	0.1970 ± 0.0412	42.02 ± 2.82
0.02	528.87 ± 19.96	0.1946 ± 0.0418	16.13 ± 1.12

5.2 $Z + 2$jets, 1, 2b-tag

For $Z + 2$jet events with b-tag requirements, the method to solve the matrix equation Eq. 10 is different. Because with b-tag requirements, the QCD content in the selected sample

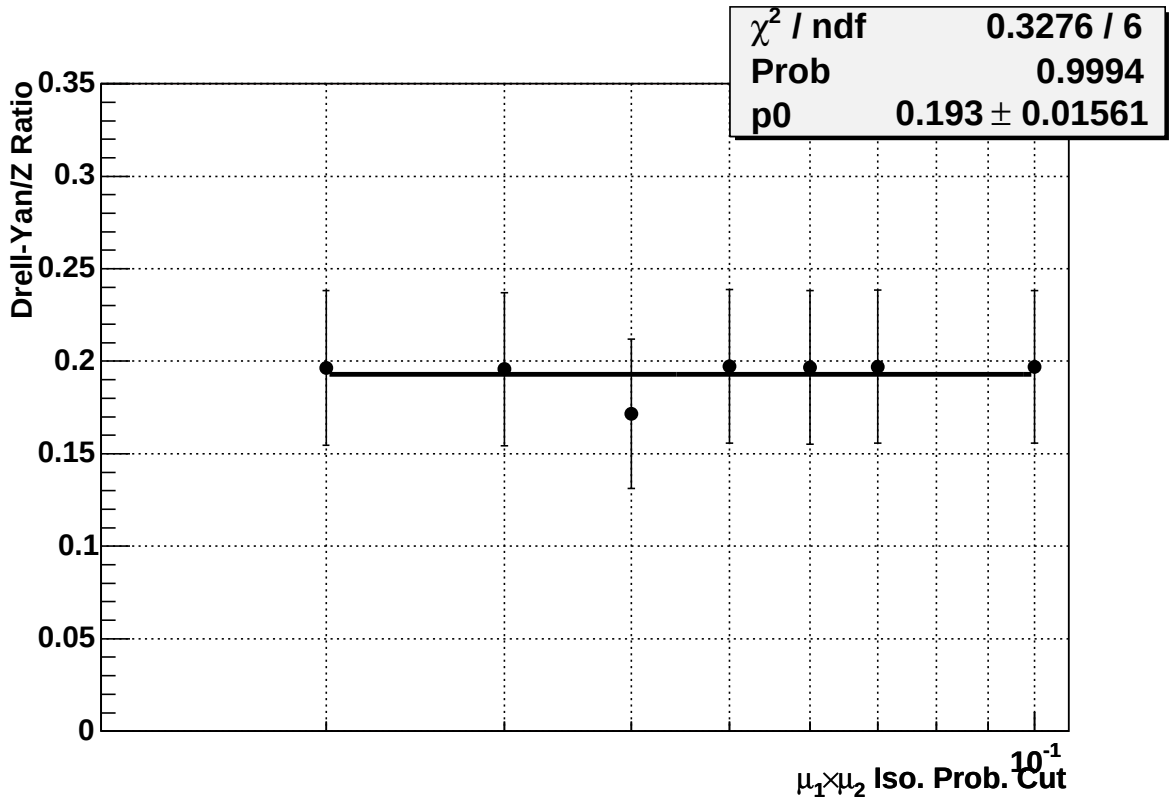

Figure 41: Drell-Yan/Z ratio calculated using the matrix method for the $Z + 2$ jet events without b-tag requirement at different isolation cuts. Z mass window cut is applied. Clearly the ratio is independent of the isolation cut, which confirmed the assumption that Drell-Yan and Z have the same dimuon isolation cut efficiency. The ratio obtained in this analysis is consistent with ratio obtained in the $Z \to \mu\mu$ cross section measurement analysis[11]. This value is slightly lower than the $Z \to \mu\mu$ result because of the Z mass window cut in this analysis.

will have more muons from the b jets and these muons are not isolated, the QCD isolation efficiency will be lower than that without b-tag requirement. There is not a simple way to calculate the isolation cut efficiency for QCD in this case.

The method to solve the equations in this case is to solve for QCD and ϵ_{QCD}. Since we have shown the ϵ_Z is independent of b-tag, we can still use the ϵ_Z in Table 5 in this case. Also, the Drell-Yan and Z ratio should not change with different b-tag, since the di-muon and double b-jet are kinematically uncorrelated with each other. Plugging in the ϵ_Z values from Table 5, Z and Drell-Yan/Z ratio in Table 14, the results of the matrix equations are listed in Table 15, 16.

Table 15: Summary of QCD subtraction results for $Z + 2j$ with 1 b-tag data for different dimuon isolation cut.

Isolation Cut	Z+Drell-Yan	QCD	ϵ_{QCD}
0.1	63.94 ± 7.93	14.06 ± 3.25	0.17 ± 0.09
0.02	63.04 ± 7.89	0.96 ± 3.25	0.01 ± 0.08

Table 16: Summary of QCD subtraction results for $Z+2b$ data for different dimuon isolation cut.

Isolation Cut	Z+Drell-Yan	QCD	ϵ_{QCD}
0.1	9.73 ± 3.23	6.27 ± 1.11	0.21 ± 0.10
0.02	9.59 ± 3.19	0.41 ± 1.11	0.01 ± 0.11

6 Data and MC comparisons

Data is compared with the combined MC samples. The MC samples are normalized to the luminosity and the normalization factor for each of the MC samples is calculated using:

$$s = \frac{\sigma \times \mathrm{BR} \times \mathrm{L}}{N} \times \mathrm{SF} \tag{17}$$

where $\sigma \times$ BR is the cross section times branching ratio of the process, L is the integrated luminosity, N is the total number of MC events after the good data selection and before any event selection cut, SF is the combined Data/MC scale factor of all the event selection cuts, which includes the Jet RECO×ID efficiency Data/MC scale factor, Muon trigger efficiency,

Muon RECO×ID×Tracking×SMT Data/MC scale factor, jet taggability and JLIP btag TRF Data/MC scale factor for events with b-tag requirements. For the other kinematic cuts the Data/MC scale factor is very close to 1 so they are not included in the calculation except for the di-muon opposite charge scale factor. The normalization factors for $Z + 2$ jet events with 0,1,2 b-tag requirements are listed in Table 17.

Table 17: Combined scale factor SF in Eq. 17 for MC $Z + 2$ jet events with 0, 1, 2 b-tag requirements.

Process	Zbb	Zcc	Zjj	$ttdl$	$ttsl$	ZZ	WZ	Z
0 btag	0.48	0.568	0.482	0.892	1.22	0.524	0.637	0.417
1+ btag	0.382	0.429	0.384	0.784	1.09	0.429	0.487	0.312
2+ btag	0.258	0.317	0.28	0.56	0.823	0.29	0.345	0.268

Process	$ZH(105)$	$ZH(115)$	$ZH(125)$	$ZH(135)$	$ZH(145)$
0 btag	0.599	0.641	0.617	0.632	0.649
1+ btag	0.512	0.55	0.536	0.553	0.569
2+ btag	0.348	0.375	0.373	0.382	0.403

Although the top analyzed MC samples have the official muon smearing factors, and the MC Z signals match the data Z signals well, we found the smearing is not good enough for the $Z + 2$ jet events. Thus the true muon momenta were re-smeared by the following equation,

$$\frac{1}{p_T} = \frac{\alpha}{p_T^{MC}} + \text{Gauss}(0, \sigma) \tag{18}$$

where $\alpha = 1.01375, \sigma = 0.00123125$.

Kinematic variable distributions from data are compared to the sum of contributions of MC samples in Figures 42 - 47. The shape of the QCD background in these distributions is determined from the "semi-anti-isolated" $Z + 2j$ events in data, *eg.* we subtract the distribution with the di-muon isolation cut at 0.05 by the same distribution with the di-muon isolation cut at 0.01. From Tables 7, 5 and 14 we can determine the remnant is a mixture of $\sim 70\%$ qcd background and $\sim 30\%$ signal. We do not use the anti-isolated (*eg.* di-muon isolation > 0.02) events to determine the shape because the QCD shape is highly di-muon isolation cut dependent. The remnant is then normalized to the number of QCD events in Tables 14-16. The effect of the signal contamination on the QCD background shape is small and is ascribed to the large QCD background uncertainty.

The breakdown of the MC samples, number of QCD and the number of events in data for

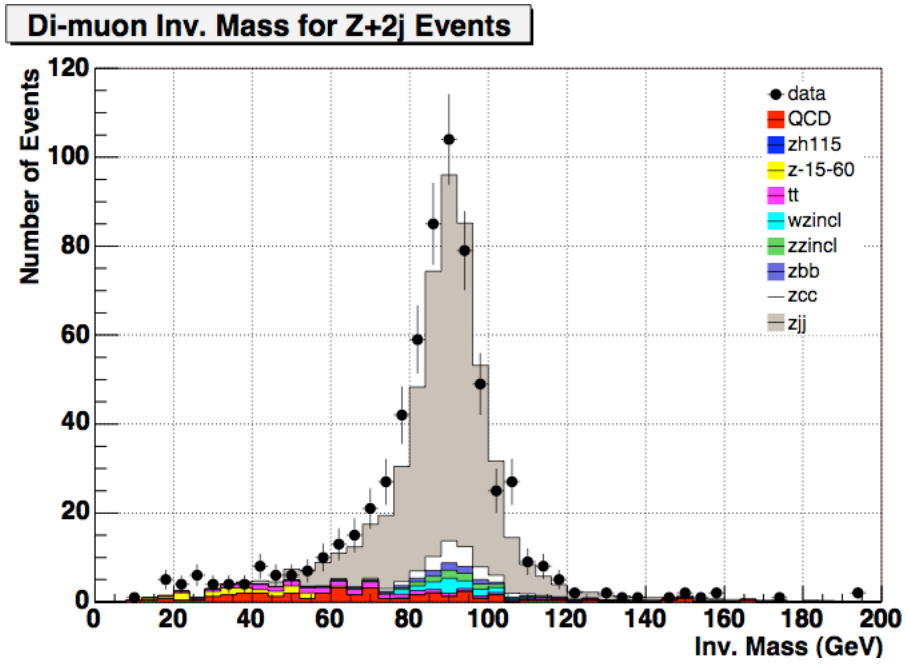

Figure 42: Di-muon invariant mass distribution of the $Z + 2$ jet with 0 btag events.

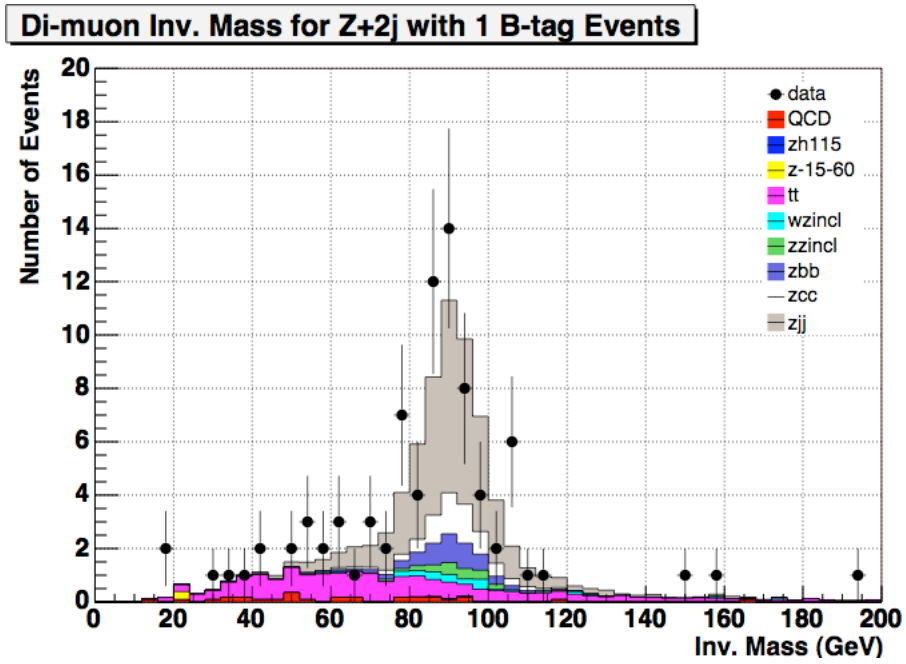

Figure 43: Di-muon invariant mass distribution of the $Z + 2$ jet with 1 btag events.

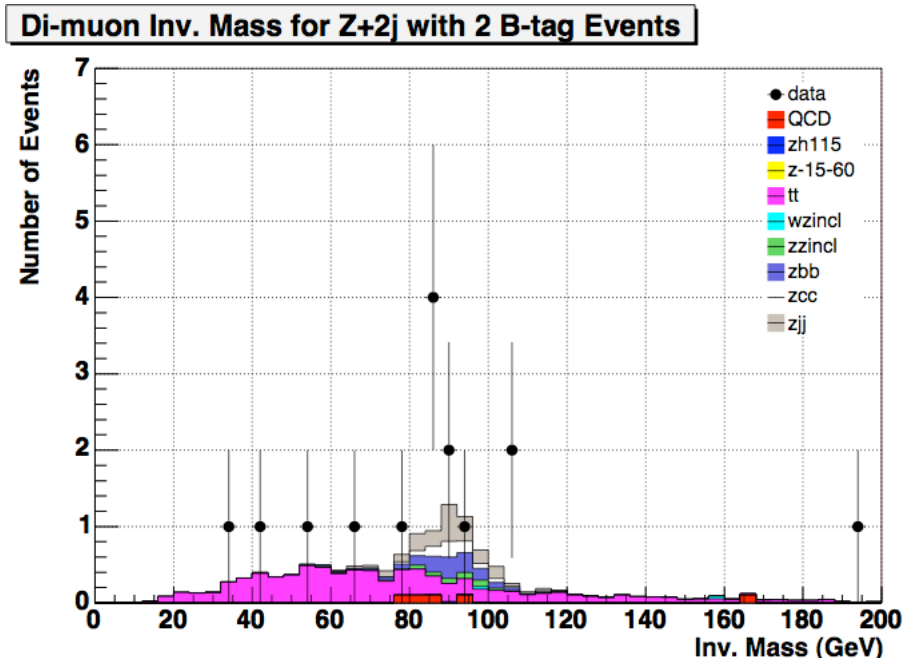

Figure 44: Di-muon invariant mass distribution of the $Z + 2$ jet with 2 btag events.

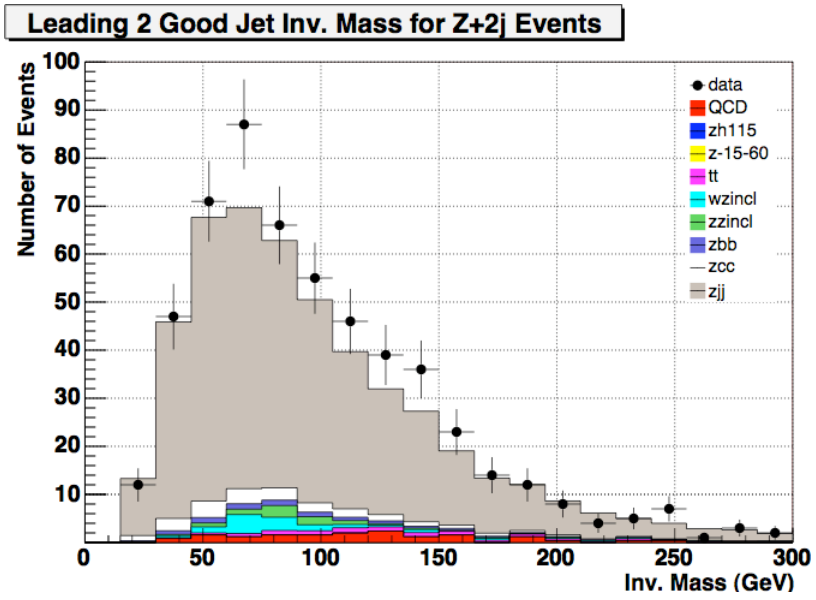

Figure 45: The leading 2 jets' invariant mass distribution for the $Z + 2$ jet events without b-tag requirement. Z mass window cut is applied.

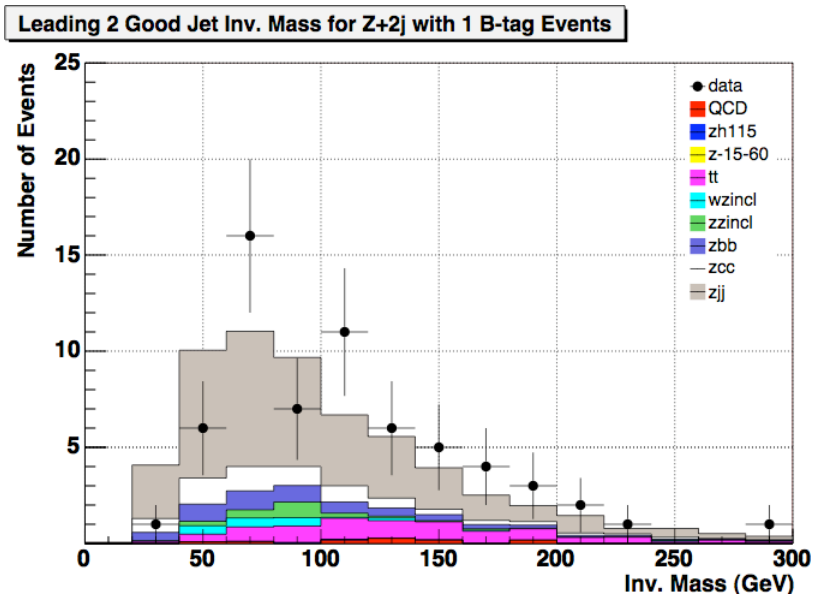

Figure 46: The leading 2 jets' invariant mass distribution for the $Z + 2$ jet events with 1 b-tag requirement. Z mass window cut is applied.

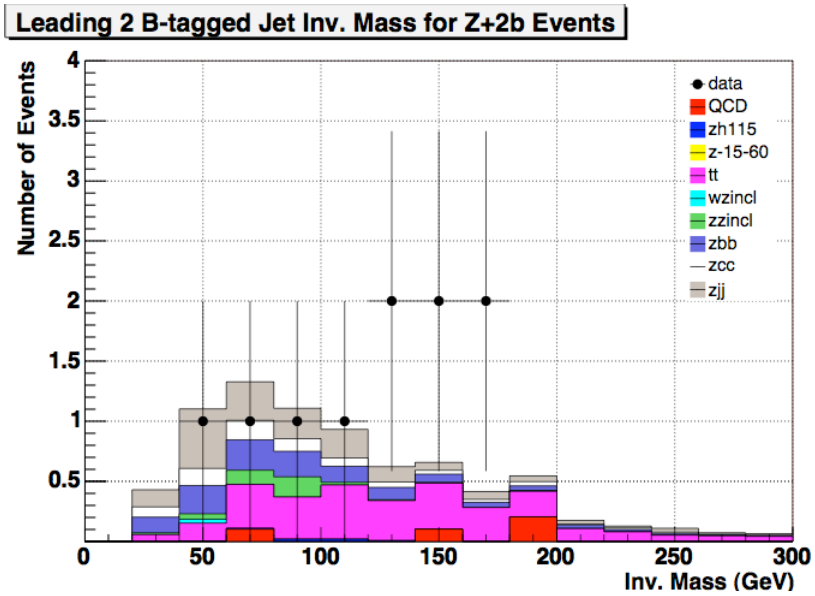

Figure 47: The 2 b jets' invariant mass distribution for the $Z + 2$ jet events double b-tag requirement. Z mass window cut is applied.

$Z+2$ jet events with 0, 1, 2 btags are shown in Table 18. As it is clear MC agrees with data very well.

Table 18: The breakdown of MC samples in $Z+2$ jet events with 0, 1, 2 b-tag requirements. Z mass window cut is applied. $m_H = 105$ GeV. $t\bar{t}$ includes both the single and di-leptonic decay channels.

MC sample	0 btag	1 btag	2btag
Zjj	415	36.2	1.86
Zcc	22.1	6.90	0.76
Zbb	8.32	5.19	1.32
ZZ	8.90	2.11	0.39
WZ	12.5	1.63	0.03
$t\bar{t}$	9.57	7.69	3.06
ZH	0.22	0.17	0.07
QCD	16.13	0.96	0.41
MC Total	493	60.9	7.91
Data	545	64	10

7 Higgs search window

We search for the ZH signal based on the *Standard Model* at 6 Higgs mass points from 105 GeV to 155 GeV. The double b-jet invariant mass distributions of the $Z + 2$ $bjet$ events shown in Figures 48 are fit to Gauss function. For each mass point we apply a mass window cut as 1.5σ of the Higgs mass peak resolution. The Higgs search windows are listed in Table 19.

8 Systematic uncertainties

The sources of systematic uncertainties are listed in Table 20 for ZH signals, Table 21 for QCD background and in Table 22 for each of the non-QCD backgrounds. The contribution of each systematic uncertainty source in ZH and each non-QCD background process is calculated by varying its central value by $\pm\sigma$ and calculating the change of the expected number of $Z+2b$ jet events within the Higgs search window. The uncertainties of Zjj, Zcc, Zbb are treated

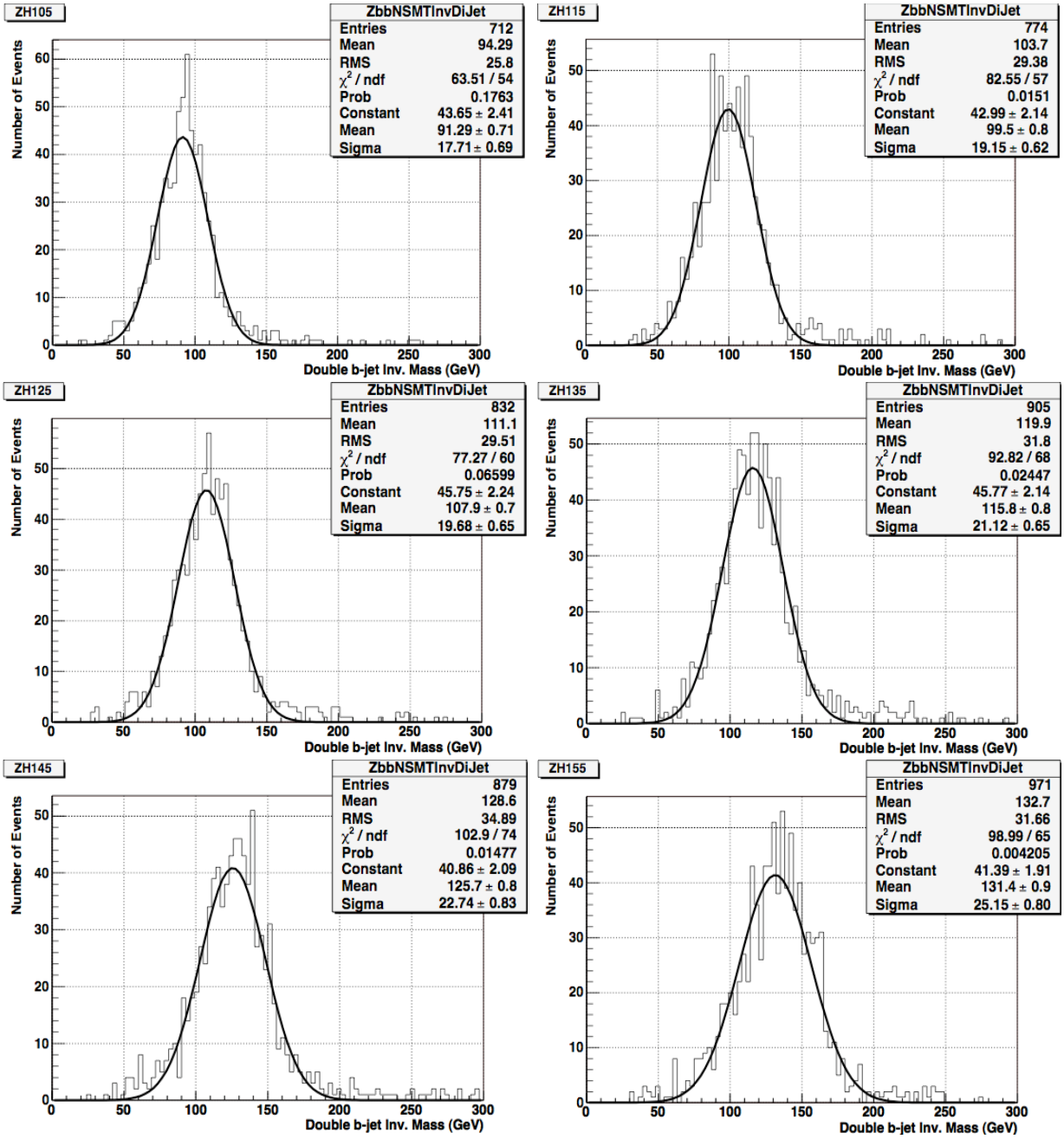

Figure 48: Double b jet invariant mass distribution of *Standard Model ZH* signals at Higgs mass from 105 GeVto 155 GeV, Z mass window cut has been applied. The distributions are fitted to Gauss function. The $\pm 1.5\sigma$ mass window around the peak is set as the Higgs search windows for different Higgs masses.

Table 19: Higgs search window for 6 *Standard Model* Higgs masses of 105 gev to 155 GeV. The resolution is defined as width/mean.

Higgs mass(GeV)	mean(GeV)	width(GeV)	resolution(%)	search window(GeV)
105	91.3	17.7	19.3	65 - 118
115	99.5	19.1	19.2	70 - 128
125	107.9	19.7	18.3	78 - 137
135	115.8	21.1	18.2	84 - 147
145	125.7	22.6	18.0	92 - 160
155	131.4	24.8	18.9	94 - 169

as fully correlated all the other background are assumed to be uncorrelated. All sources of the uncertainties are also treated as uncorrelated so they are added quadratically to get the overall signal and background uncertainties. The uncertainty of QCD is estimated by assuming the the QCD background within the Higgs search window has the same relative uncertainty as the whole QCD background within the Z mass window, so the absolute uncertainty is the whole QCD background uncertainty in Table 16 times the percentage of the QCD that is within the Higgs search window.

9 ZH cross section limit

Using the double b-tagged events, the Bayesian 95% limit[19] on the ZH $\sigma\times$BR are listed in Table 23.

10 Conclusions

We have performed a search for ZH associated production in $\mu\bar{\mu}b\bar{b}$ channel on 370 pb^{-1} data. The upper limit of the cross section at 95% C.L. are set to be between 9.2 to 13.1 pb.

We have introduced optimizations of the signal significance which give two times more signal compared to using the standard muon isolation cut (cut on the track cone and halo) while still controlling the backgrounds at an acceptable level as shown in Figures 49-51.

Table 20: Relative systematic and statistical uncertainties for ZH signals.

Error Source	ZH(105)	ZH(115)	ZH(125)	ZH(135)	ZH(145)	ZH(155)
MuSMTHit	0.022	0.021	0.022	0.022	0.021	0.021
MuTrack	0.102	0.097	0.099	0.097	0.095	0.092
MuID	0.065	0.060	0.061	0.061	0.059	0.057
L3MuTrig	0.053	0.051	0.052	0.051	0.049	0.048
L2MuTrig	0.027	0.026	0.026	0.026	0.027	0.026
L1TrkTrig	0.005	0.005	0.005	0.005	0.005	0.005
L1MuTrig	0.027	0.027	0.026	0.027	0.027	0.026
JetRECOID	0.064	0.060	0.055	0.049	0.045	0.043
JES	0.033	0.031	0.025	0.020	0.016	0.015
Btag TRF	0.086	0.089	0.088	0.091	0.091	0.092
Taggability	0.137	0.137	0.136	0.135	0.133	0.133
SFErrTotal	0.225	0.221	0.219	0.217	0.212	0.210
Cross Section	0.07	0.07	0.07	0.07	0.07	0.07
Luminosity	0.065	0.065	0.065	0.065	0.065	0.065
Total Syst. Err.	0.244	0.230	0.229	0.226	0.222	0.220
Stat. Err.	0.039	0.037	0.035	0.034	0.035	0.032
Acceptance Err.	0.0046	0.0047	0.0049	0.0050	0.0054	0.0052

Table 21: Absolute QCD systematic uncertainties for different Higgs mass.

Higgs Mass (GeV)	105	115	125	135	145	155
Percentage in Higgs window(%)	10.3	10.3	6.90	6.90	10.3	17.2
Absolute Uncertainty	0.115	0.115	0.077	0.077	0.115	0.191

Table 22: Relative systematic and statistical uncertainties for backgrounds. Contributions from WZ, Z(15-60) are negligible.

Error Source	tt	zz	zbb	zcc	zjj
MuSMTHit	0.022	0.024	0.026	0.022	0.029
MuTrack	0.090	0.109	0.122	0.111	0.137
MuID	0.055	0.064	0.073	0.066	0.080
L3MuTrig	0.050	0.059	0.062	0.059	0.067
L2MuTrig	0.027	0.031	0.033	0.031	0.035
L1TrkTrig	0.005	0.006	0.007	0.006	0.007
L1MuTrig	0.027	0.032	0.034	0.033	0.038
JetRECOID	0.047	0.072	0.107	0.112	0.111
JES	0.013	0.045	0.047	0.025	0.046
Btag TRF	0.091	0.085	0.086	0.083	0.047
Taggability	0.132	0.135	0.136	0.133	0.136
SFErrTotal	0.209	0.234	0.258	0.245	0.261
Cross Section	0.08	0.06	0.19	0.19	0.12
Luminosity	0.065	0.065	0.065	0.065	0.065
Total Syst. Err.	0.233	0.250	0.327	0.317	0.295
Stat. Err.	0.084	0.182	0.032	0.111	0.165

Table 23: *Standard Model* $\sigma(p\bar{p} \to ZH) \times Br(H \to b\bar{b})$ limit using Bayesian limit calculator. The acceptances include the $Z \to \mu\bar{\mu}$ branching ratio 3.366%.

m_H (GeV)	105	115	125	135	145
Expected ZH	0.0588	0.0473	0.0327	0.0221	0.0103
Acceptance	0.0014	0.0016	0.0017	0.0019	0.0019
$t\bar{t}$	1.08	1.17	1.13	1.26	1.30
ZZ	0.292	0.278	0.219	0.175	0.088
Zbb	0.545	0.526	0.478	0.436	0.398
Zcc	0.290	0.278	0.232	0.201	0.194
Zjj	0.765	0.685	0.590	0.637	0.590
QCD	0.17	0.16	0.17	0.17	0.20
Total BKGD	3.11	3.09	2.82	2.89	2.77
Total BKGD Syst. Err.	0.57	0.55	0.49	0.50	0.49
Total BKGD Stat. Err.	0.17	0.16	0.14	0.15	0.15
Total BKGD Err.	0.59	0.57	0.51	0.52	0.51
Events in Data	3	3	4	5	6
95% Obs. Limit (pb)	10.5	9.2	10.6	11.1	13.1
95% Exp. Limit (pb)	10.5	9.2	7.3	6.5	6.5
SM results (pb)	0.119	0.083	0.054	0.031	0.015

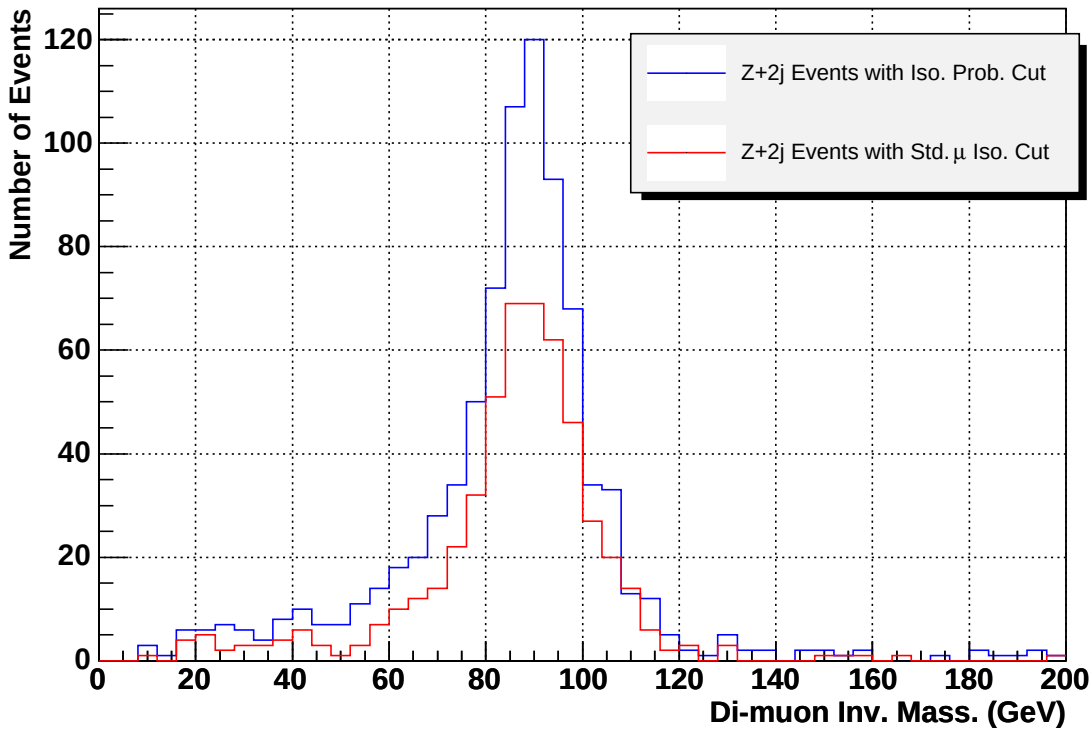

Figure 49: For $Z + 2$ jets events the di-muon invariant mass distribution using optimized di-muon isolation cut (blue line) is compared with that of using the standard muon isolation cut (red line). Clearly by using the di-muon isolation probability cut we get 2 times more signals than using the standard cut, while keep the background at about the same level.

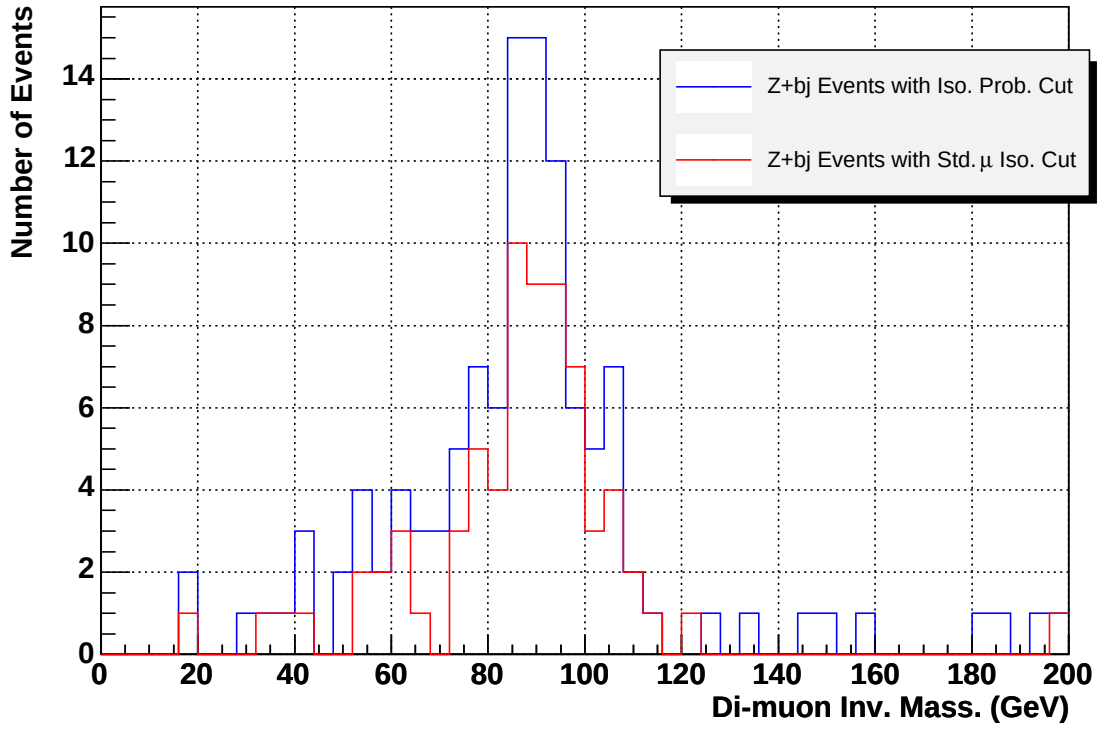

Figure 50: For $Z+2$ jets with 1 or more b-tag events the di-muon invariant mass distribution using optimized di-muon isolation cut (blue line) is compared with that of using the standard muon isolation cut (red line).

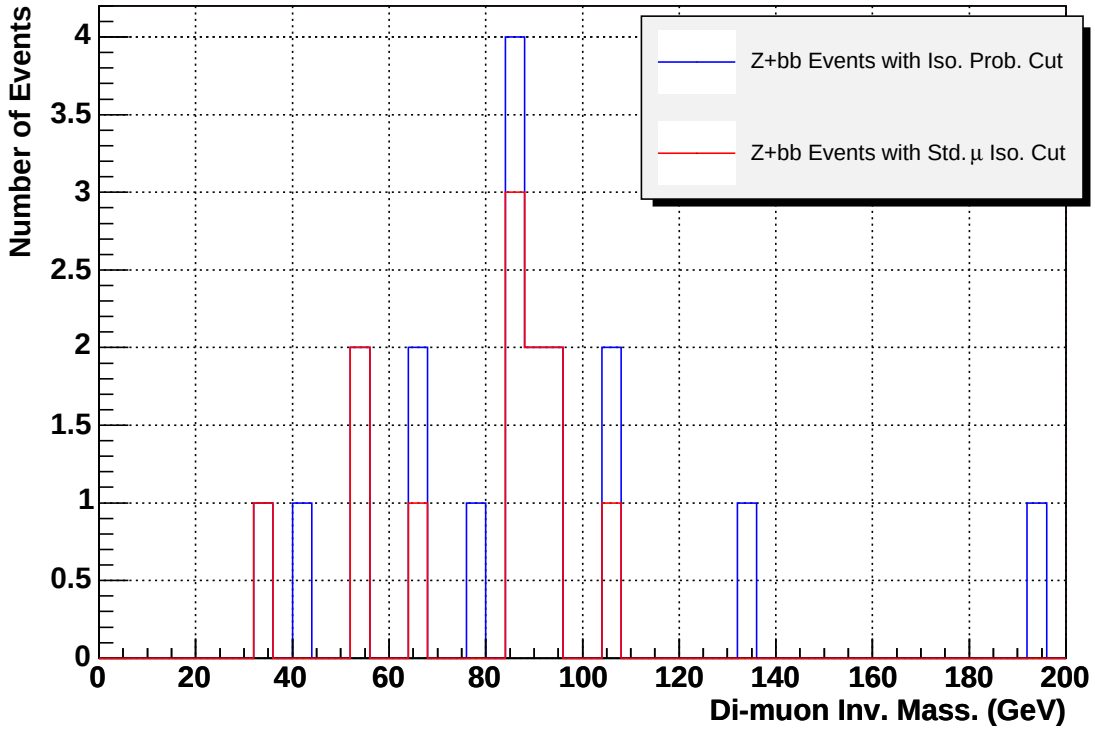

Figure 51: For $Z+2$ jets with 2 or more b-tag events the di-muon invariant mass distribution using optimized di-muon isolation cut (blue line) is compared with that of using the standard muon isolation cut (red line).

A Event average convolution formula

Given the probability ζ of a single object passes some kind of selection criteria, this section will show how to calculate the event average of the probability. Assume in a event there are n such object, the probability that there is 0, 1, 2 such object that pass the selection in this event is show in Eq. 19:

$$P_0(\zeta) = \prod_{i=1}^{n}(1-\zeta_i) \tag{19}$$

$$P_1(\zeta) = \sum_{i=1}^{n}\zeta_i\prod_{j\neq i}^{n}(1-\zeta_j) \tag{20}$$

$$P_2(\zeta) = \sum_{i\neq j}^{n}\zeta_i\zeta_j\prod_{k\neq i,j}^{n}(1-\zeta_k) \tag{21}$$

where the sum is over all the objects in the event before the criteria selection.

The probability that there is $1^+, 2^+$ such object that pass the selection in this event is show below:

$$P_{1^+} = 1 - P_0 \tag{22}$$

$$P_{2^+} = 1 - P_0 - P_1 \tag{23}$$

To calculate the event average, just sum up the probability P interested over all the events in a given sample and divide the summed probability by the total number of events.

B Event Display

The visualization and the event dump of the $Z + 2$ b-tagged jets events from data are shown in this section.

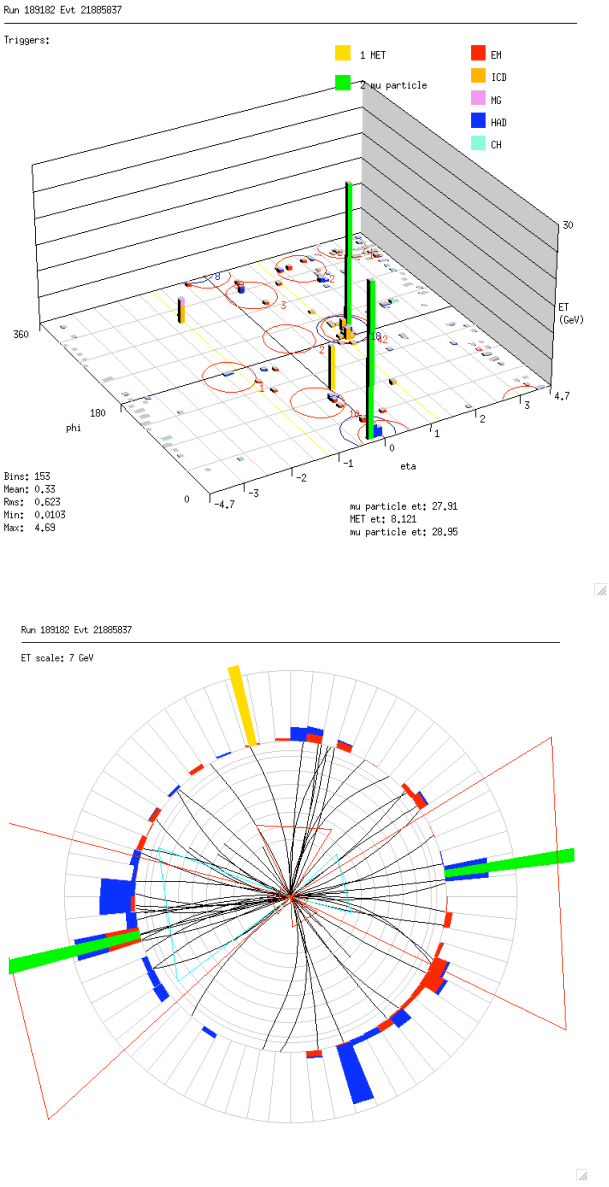

Figure 52: Listed are all muons' p_{T} , *eta*, ϕ, isolation probability, 2-D DCA, A/BC layer time, whether they pass the loose muon ID, all jets' p_{T} , η, ϕ, JLIP probability and whether they are tagable, $E_{\mathrm{T}}^{\mathrm{miss}}$ and it's x/y components and direction. The units in this and the following plots are in GeV, cm, μs and rad.
Di-muon Inv. Mass=77.7, Double b-jet Inv. Mass=152.3;
Muon1: p_{T} =29.0,η=-0.23,ϕ=0.10, iso.prob.=0.052, DCA=0.006,$t_a = -0.730, t_{bc} = 0$, Y;
Muon2: p_{T} =28.4,η=1.41,ϕ=3.40, iso.prob.=0.202, DCA=0.016,$t_a = 0.625, t_{bc} = -0.874$, Y;
Jet1: p_{T} =62.4,η=1.32,ϕ=3.29, JLIP prob.=1.8e-4, taggable;
Jet2: p_{T} =52.0,η=-0.23,ϕ=0.27, JLIP prob.=6.4e-3, taggable;
$E_{\mathrm{T}}^{\mathrm{miss}}$=11.3,$E_{\mathrm{T}}^{\mathrm{miss}}X$=1.78,$E_{\mathrm{T}}^{\mathrm{miss}}Y$=11.1,$E_{\mathrm{T}}^{\mathrm{miss}}$ ϕ=1.41.

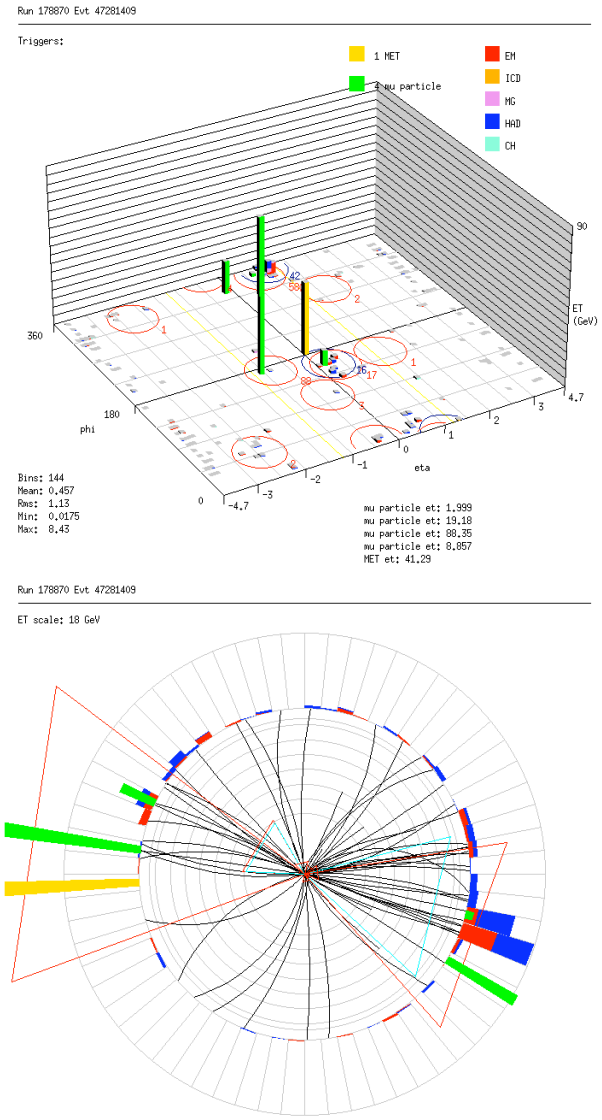

Figure 53: Di-muon Inv. Mass=90.0, Double b-jet Inv. Mass=113.8;
Muon1: $p_{\rm T}$ =88.2,η=-1.04,ϕ=3.00, iso.prob.=0.004, DCA=3.2e-4,$t_a = 0.745, t_{bc} = N/A$, Y;
Muon2:$p_{\rm T}$ =19.4,η=-0.13,ϕ=5.73,iso.prob.=0.034,DCA=-0.008,$t_a = -2.29, t_{bc} = -2.69$, Y;
Muon3: $p_{\rm T}$ =8.81,η= 0.14,ϕ=2.69, iso.prob.=0.933, DCA=-0.011,$t_a = 2.70, t_{bc} = 0.920$, Y;
Muon4: $p_{\rm T}$ =5.49,η= 0.80,ϕ=5.93, iso.prob.=1.000, DCA=-0.081,$t_a = 1.37, t_{bc} = -5.28$, Y;
Muon5: $p_{\rm T}$ =1.20,η= 0.70,ϕ=6.07, iso.prob.=1.000, DCA=-0.093,$t_a = 11.7, t_{bc} = N/A$, Y;
Jet1: $p_{\rm T}$ =63.1,η=0.77,ϕ=5.99, JLIP prob.=4.5e-7, taggable;
Jet2: $p_{\rm T}$ =43.4,η=0.01,ϕ=2.62, JLIP prob.=0.03, taggable;
$E_{\rm T}^{\rm miss}$=23.8,$E_{\rm T}^{\rm miss}X$=23.3,$E_{\rm T}^{\rm miss}Y$=-4.76,$E_{\rm T}^{\rm miss}$ ϕ=6.08.

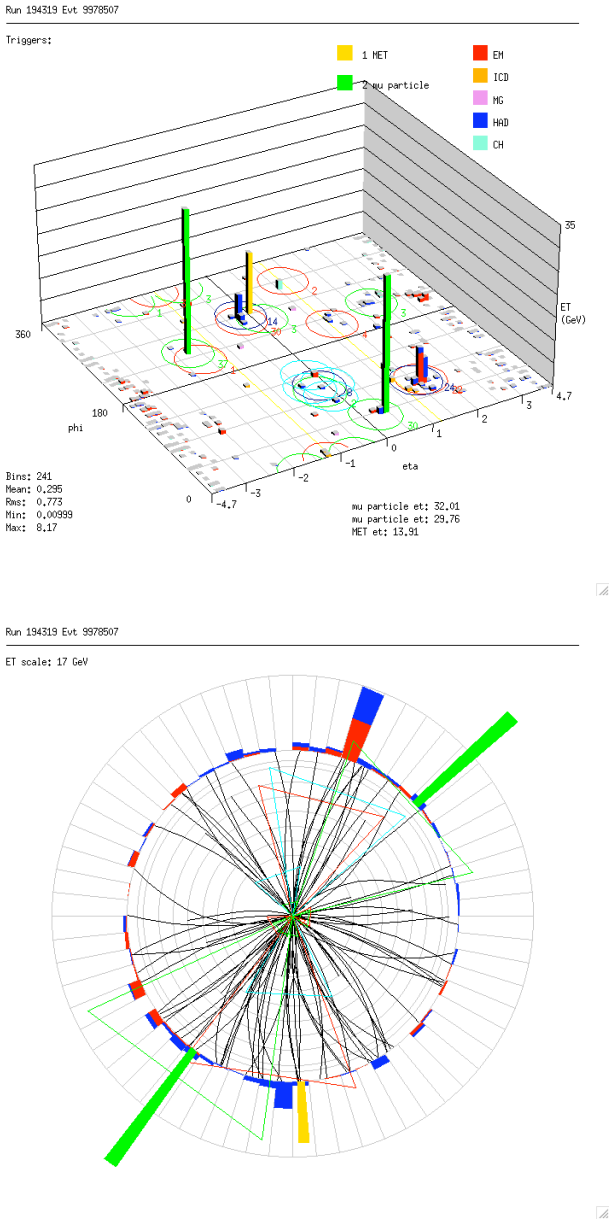

Figure 54:
Di-muon Inv. Mass=106.9, Double b-jet Inv. Mass=76.6;
Muon1:$p_{\rm T}$ =35.7,η=-1.70,ϕ=4.04,iso.prob.=0.021,DCA=-2.2e-4,$t_a = -2.62, t_{bc} = -2.75$, Y;
Muon2: $p_{\rm T}$ =29.9,η=0.45,ϕ=0.70, iso.prob.=0.025, DCA=-0.002,$t_a = -4.67, t_{bc} = -7.37$, Y;
Muon3: $p_{\rm T}$ =15.7,η=1.58,ϕ=1.26, iso.prob.=0.114, DCA=0.008,$t_a = N/A, t_{bc} = N/A$, N;
Jet1: $p_{\rm T}$ =34.1,η=1.61,ϕ=1.21, JLIP prob.=0.023, taggable;
Jet2: $p_{\rm T}$ =20.7,η=-0.18,ϕ=4.63, JLIP prob.=0.014, taggable;
Jet3: $p_{\rm T}$ =12.0,η=-0.18,ϕ=1.95, JLIP prob.=99, un-taggable;
$E_{\rm T}^{\rm miss}$=11.8,$E_{\rm T}^{\rm miss}X$=-0.02,$E_{\rm T}^{\rm miss}Y$=-11.8,$E_{\rm T}^{\rm miss}$ ϕ=4.71.

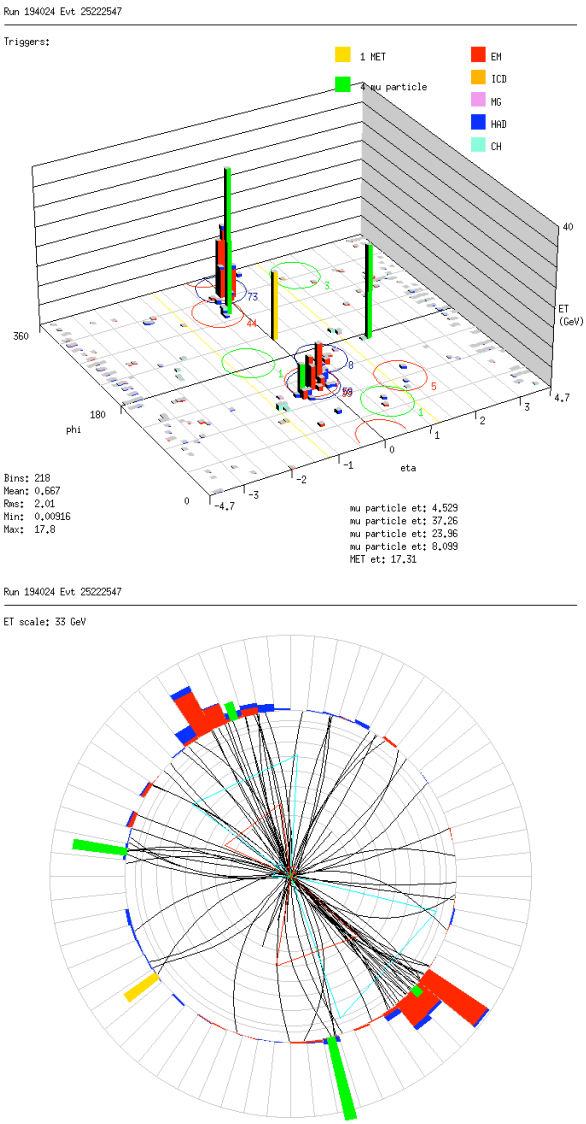

Figure 55: . Di-muon Inv. Mass=84.3, Double b-jet Inv. Mass=166.8;
Muon1: $p_{\rm T}$ =37.3,η=-0.23,ϕ=4.99, iso.prob.=0.075, DCA=-6.7e-4,$t_a = N/A, t_{bc} = -4.33$, Y;
Muon2: $p_{\rm T}$ =24.5,η=1.69,ϕ=2.98, iso.prob.=0.0, DCA=-1.8e-4,$t_a = -0.376, t_{bc} = 0.376$, Y;
Muon3: $p_{\rm T}$ =11.4,η=-0.05,ϕ=2.09, iso.prob.=0.918, DCA=0.096,$t_a = N/A, t_{bc} = N/A$, N;
Muon4: $p_{\rm T}$ =8.20,η=-0.57,ϕ=1.95, iso.prob.=0.765, DCA=0.066,$t_a = -2.58, t_{bc} = 0$, Y;
Muon5: $p_{\rm T}$ =4.53,η=0.20,ϕ=5.58, iso.prob.=1.0, DCA=-4.5e-4,$t_a = -0.435, t_{bc} = N/A$, Y;
Jet1: $p_{\rm T}$ =91.5,η=0.20,ϕ=5.53, JLIP prob.=0.003, taggable;
Jet2: $p_{\rm T}$ =74.9,η=0.04,ϕ=2.05, JLIP prob.=9.3e-6, taggable;
Jet3: $p_{\rm T}$ =13.1,η=0.67,ϕ=2.68, JLIP prob.=0.34, taggable;
$E_{\rm T}^{\rm miss}$=22.6,$E_{\rm T}^{\rm miss}X$=5.94,$E_{\rm T}^{\rm miss}Y$=-21.8,$E_{\rm T}^{\rm miss}$ ϕ=4.98.

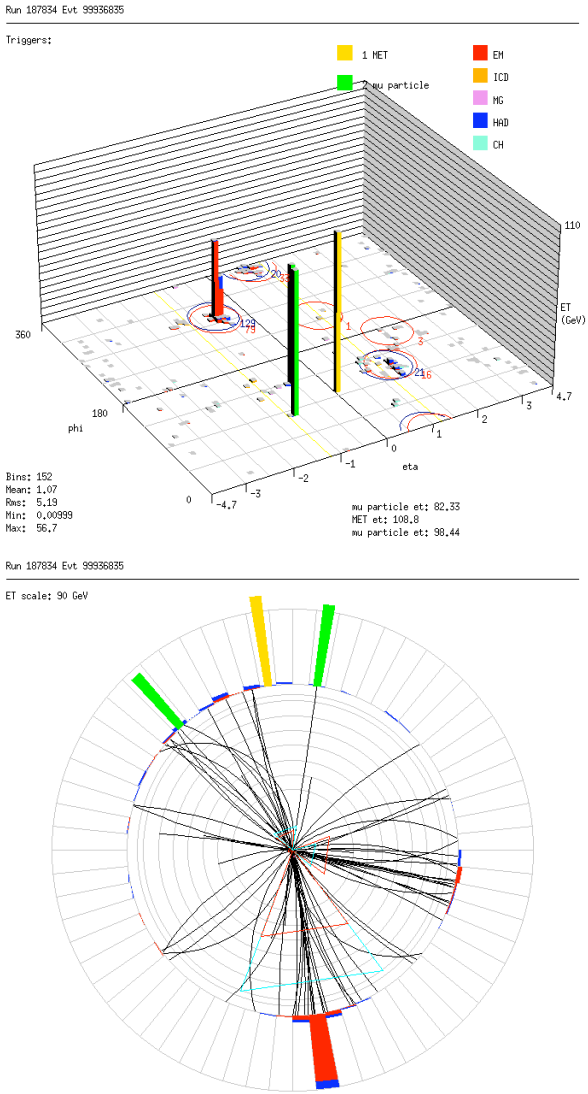

Figure 56: Di-muon Inv. Mass=88.6, Double b-jet Inv. Mass=142.8;
Muon1: $p_{\rm T}$ =95.0,η=-1.07,ϕ=1.42, iso.prob.=0.0, DCA=-3.0e-4,$t_a = 3.87, t_{bc} = -0.376$, Y;
Muon2: $p_{\rm T}$ =83.7,η=-0.59,ϕ=2.32, iso.prob.=0.0, DCA=8.6e-4,$t_a = -1.65, t_{bc} = -1.93$, Y;
Muon3: $p_{\rm T}$ =59.9,η=-0.45,ϕ=4.84, iso.prob.=0.323, DCA=-0.007,$t_a = N/A, t_{bc} = N/A$, N;
Muon4: $p_{\rm T}$ =4.53,η=1.58,ϕ=1.85, iso.prob.=0.643, DCA=-0.004,$t_a = N/A, t_{bc} = N/A$, N;
Muon5: $p_{\rm T}$ =0.95,η=1.41,ϕ=2.58, iso.prob.=0.798, DCA=0.023,$t_a = N/A, t_{bc} = N/A$, N;
Jet1: $p_{\rm T}$ =160.7,η=-0.46,ϕ=4.84, JLIP prob.=7.3e-4, taggable;
Jet2: $p_{\rm T}$ =31.2,η=1.50,ϕ=1.94, JLIP prob.=0.19, taggable;
Jet3: $p_{\rm T}$ =31.7,η=1.00,ϕ=6.08, JLIP prob.=0.007, taggable;
$E_{\rm T}^{\rm miss}$=25.9,$E_{\rm T}^{\rm miss}X$=18.2,$E_{\rm T}^{\rm miss}Y$=-18.5,$E_{\rm T}^{\rm miss}$ ϕ=5.49.

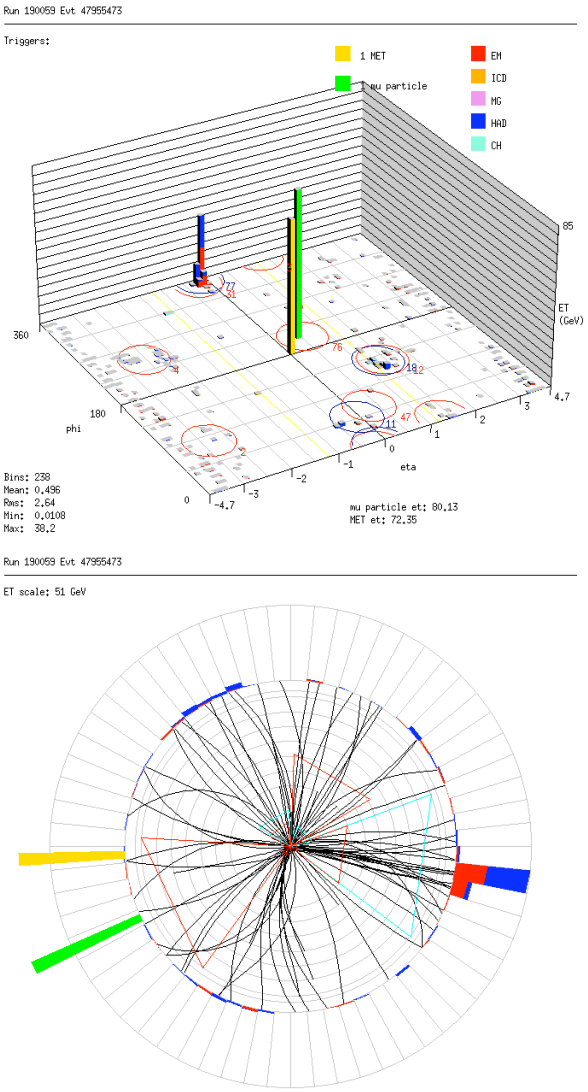

Figure 57: Di-muon Inv. Mass=105.3, Double b-jet Inv. Mass=135.0;
Muon1: $p_{\rm T}$ =76.0,η=0.48,ϕ=3.63, iso.prob.=0.011, DCA=-7.0e-4,$t_a = 5.40, t_{bc} = -1.44$, Y;
Muon2: $p_{\rm T}$ =38.7,η=0.35,ϕ=0.99, iso.prob.=0.070, DCA=-2.2e-4,$t_a = N/A, t_{bc} = 3.63$, Y;
Muon3: $p_{\rm T}$ =12.1,η=-0.27,ϕ=6.13, iso.prob.=0.893, DCA=-2.7e-4,$t_a = N/A, t_{bc} = N/A$, N;
Muon4: $p_{\rm T}$ =5.15,η=1.41,ϕ=2.03, iso.prob.=0.405, DCA=-0.008,$t_a = N/A, t_{bc} = N/A$, N;
Muon5: $p_{\rm T}$ =2.17,η=1.22,ϕ=2.34, iso.prob.=0.966, DCA=0.057,$t_a = N/A, t_{bc} = N/A$, N;
Jet1: $p_{\rm T}$ =96.7,η=-0.27,ϕ=6.11, JLIP prob.=0.008, taggable;
Jet2: $p_{\rm T}$ =28.3,η=1.35,ϕ=2.07, JLIP prob.=0.029, taggable;
Jet3: $p_{\rm T}$ =16.2,η=-0.19,ϕ=0.77, JLIP prob.=0.390, un-taggable;
$E_{\rm T}^{\rm miss}$=34.0,$E_{\rm T}^{\rm miss}X$=-26.1,$E_{\rm T}^{\rm miss}Y$=21.8,$E_{\rm T}^{\rm miss}$ ϕ=2.44.

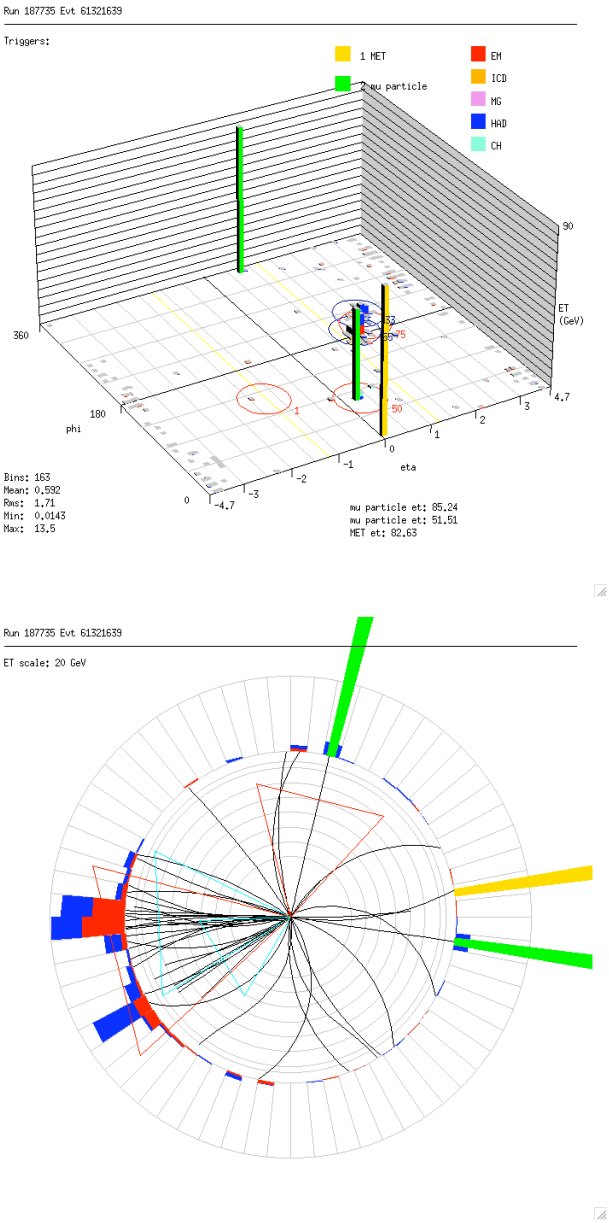

Figure 58: Di-muon Inv. Mass=94.1, Double b-jet Inv. Mass=44.3;
Muon1: $p_{\rm T}$ =85.2,η=0.77,ϕ=6.13, iso.prob.=0.0, DCA=-3.9e-4,$t_a = -3.60, t_{bc} = -5.10$, Y;
Muon2:$p_{\rm T}$ =50.3,η=0.30,ϕ=1.34,iso.prob.=0.006,DCA=-1.2e-4,$t_a = -3.97, t_{bc} = -7.58$, Y;
Muon3: $p_{\rm T}$ =3.99,η=1.92,ϕ=3.60, iso.prob.=0.946, DCA=-0.046,$t_a = N/A, t_{bc} = N/A$, N;
Jet1: $p_{\rm T}$ =72.4,η=1.53,ϕ=3.14, JLIP prob.=2.75e-7, taggable;
Jet2: $p_{\rm T}$ =45.0,η=1.97,ϕ=3.70, JLIP prob.=3.37e-4, taggable;
$E_{\rm T}^{\rm miss}$=14.5,$E_{\rm T}^{\rm miss}X$=10.3,$E_{\rm T}^{\rm miss}Y$=-10.2,$E_{\rm T}^{\rm miss}$ ϕ=5.51.

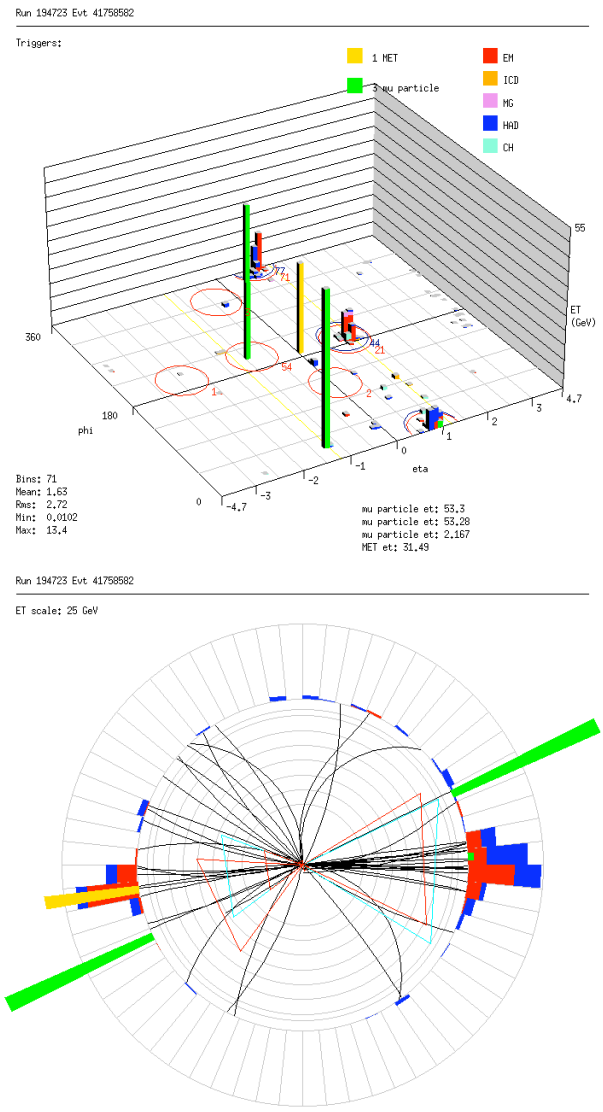

Figure 59: Di-muon Inv. Mass=85.9, Double b-jet Inv. Mass=169.8;
Muon1: $p_{\rm T}$ =53.2,η=-0.92,ϕ=3.54, iso.prob.=0.020, DCA=-0.001,$t_a = -3.06, t_{bc} = 1.79$, Y;
Muon2: $p_{\rm T}$ =34.0,η=-1.19,ϕ=0.46, iso.prob.=0.009, DCA=-0.001,$t_a = 1.88, t_{bc} = -0.50$, Y;
Muon3: $p_{\rm T}$ =9.42,η=0.75,ϕ=6.14, iso.prob.=0.998, DCA=5.3e-5,$t_a = N/A, t_{bc} = N/A$, N;
Muon4: $p_{\rm T}$ =3.61,η=-0.03,ϕ=2.72, iso.prob.=0.865, DCA=-0.049,$t_a = N/A, t_{bc} = N/A$, N;
Muon5: $p_{\rm T}$ =2.17,η=0.93,ϕ=0.01, iso.prob.=1.0, DCA=-0.003,$t_a = N/A, t_{bc} = N/A$, Y;
Muon6: $p_{\rm T}$ =0.99,η=0.43,ϕ=3.03, iso.prob.=0.860, DCA=0.022,$t_a = N/A, t_{bc} = N/A$, N;
Jet1: $p_{\rm T}$ =107.0,η=0.82,ϕ=6.27, JLIP prob.=1.12e-6, taggable;
Jet2: $p_{\rm T}$ =65.2,η=1.05,ϕ=3.27, JLIP prob.=0.003, taggable;
$E_{\rm T}^{\rm miss}$=21.5,$E_{\rm T}^{\rm miss}X$=-20.2,$E_{\rm T}^{\rm miss}Y$=7.24,$E_{\rm T}^{\rm miss}$ ϕ=2.80.

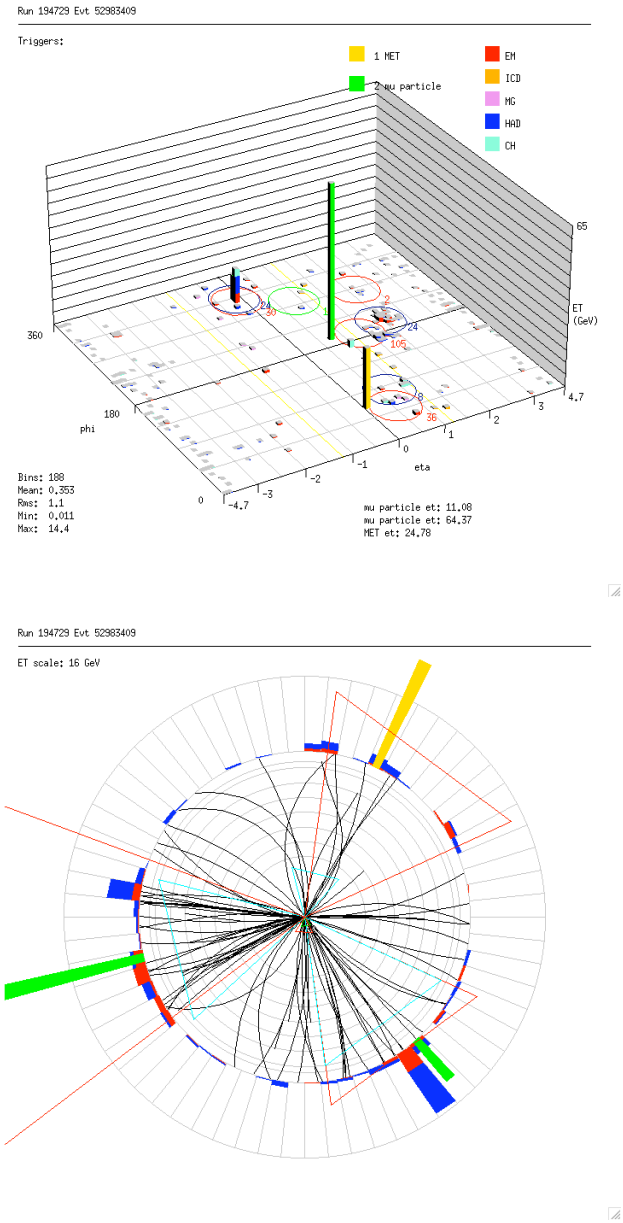

Figure 60: Di-muon Inv. Mass=86.5, Double b-jet Inv. Mass=133.7;
Muon1: $p_{\rm T}$ =60.4,η=0.76,ϕ=3.42, iso.prob.=0.023, DCA=-0.003,$t_a = -1.33, t_{bc} = -1.52$, Y;
Muon2: $p_{\rm T}$ =35.2,η=0.53,ϕ=1.03, iso.prob.=0.017, DCA=-0.011,$t_a = -1.79, t_{bc} = N/A$, Y;
Muon3: $p_{\rm T}$ =11.1,η=-0.18,ϕ=5.44, iso.prob.=0.967, DCA=0.122,$t_a = -1.69, t_{bc} = 2.36$, Y;
Jet1: $p_{\rm T}$ =55.3,η=-0.23,ϕ=5.32, JLIP prob.=0.022, taggable;
Jet2: $p_{\rm T}$ =32.1,η=1.97,ϕ=3.40, JLIP prob.=0.023, taggable;
$E_{\rm T}^{\rm miss}$=85.8,$E_{\rm T}^{\rm miss}X$=61.9,$E_{\rm T}^{\rm miss}Y$=59.3,$E_{\rm T}^{\rm miss}$ ϕ=0.76.

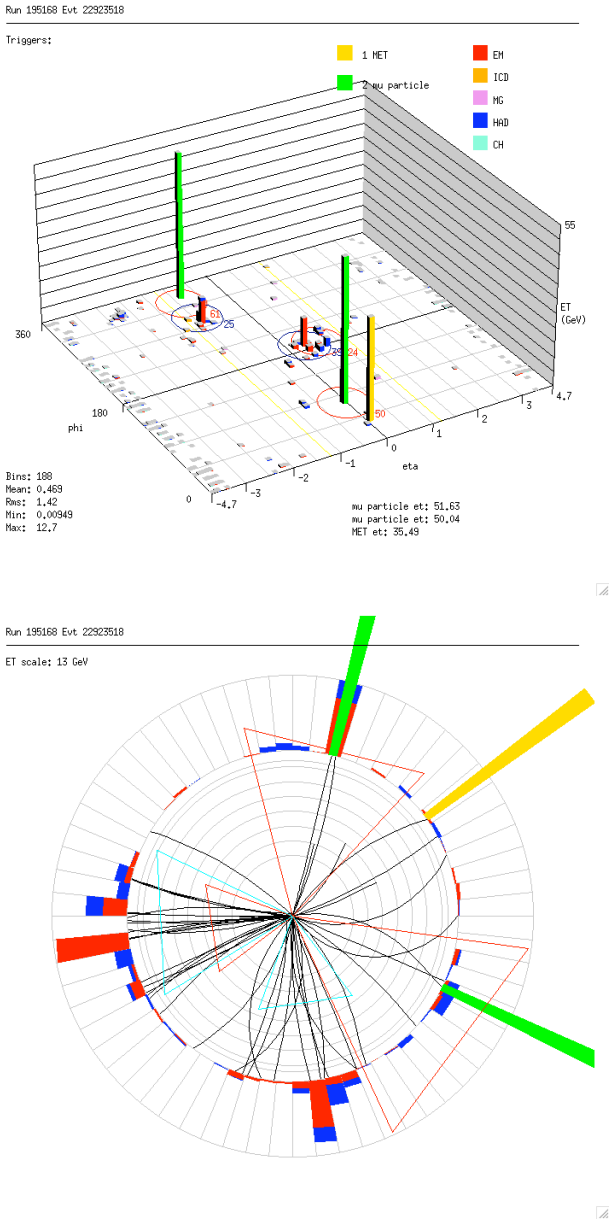

Figure 61: Di-muon Inv. Mass=87.1, Double b-jet Inv. Mass=96.0;
Muon1: $p_{\rm T}$ =51.9,η=-0.82,ϕ=5.88, iso.prob.=0.008, DCA=-4.8e-4,$t_a = 1.67, t_{bc} = 1.01$, Y;
Muon2:$p_{\rm T}$ =49.4,η=-0.04,ϕ=1.33,iso.prob.=0.005,DCA=-0.002,$t_a = -1.65, t_{bc} = -1.72$, Y;
Muon3: $p_{\rm T}$ =6.84,η=0.49,ϕ=3.15, iso.prob.=0.985, DCA=-0.025,$t_a = N/A, t_{bc} = N/A$, N;
Muon4: $p_{\rm T}$ =1.04,η=-0.22,ϕ=3.11, iso.prob.=0.997, DCA=0.828,$t_a = N/A, t_{bc} = N/A$, N;
Jet1: $p_{\rm T}$ =51.9,η=0.40,ϕ=3.19, JLIP prob.=0.038, taggable;
Jet2: $p_{\rm T}$ =38.7,η=-0.96,ϕ=4.89, JLIP prob.=2.7e-4, taggable;
$E_{\rm T}^{\rm miss}$=19.3,$E_{\rm T}^{\rm miss}X$=-17.0,$E_{\rm T}^{\rm miss}Y$=9.24,$E_{\rm T}^{\rm miss}$ ϕ=2.64.

References

[1] M. Carena, *et al.* Report of the Tevatron Higgs Working Group, hep-ph/0010338

[2] Y.D. Mutaf, Topological Analysis Method and High Efficiency Event Selection for $Z(\mu\bar{\mu} + b\bar{b})$, DØ note 4587

[3] MCFM Cross Section, http://www-clued0.fnal.gov/%7Enunne/cross-sections/mcfm_cross-sections.html

[4] Monte Carlo for FeMtobarn processes, http://mcfm.fnal.gov

[5] MCFM Cross Section for CAPS Production, http://www-clued0.fnal.gov/∼nunne/cross-sections/caps_xsect.html

[6] Particle Data, Phys. Lett. B Vol.592/1-4(2004) 1-1110

[7] http://www-d0.fnal.gov/Run2Physics/cs/skimming/pass2.html

[8] M. Klute, L. Phaf, D. Whiteson, TopAnalyze–A Framework Analze Package For Top Group Analyses, DØ note 4122

[9] http://d0-france.fnal.gov/Run2Physics/cs/index.html

[10] http://www-d0.fnal.gov/d0dist/dist/packages/lm_tools/devel/doc/

[11] DØ note 4284, Emily Nurse, Paul Telford

[12] http://www-d0.fnal.gov/∼d0upgrade/d0_private/software/jetid/jetid.html

[13] D. Bloch, B. Clement, Update of the JLIP b-tagger Performance in p14/pass2 with Jes5.3, DØ note in preparation

[14] Muon Identification in p14, DØ note in preparation.

[15] F. Deliot, E. Nurse, muo_cert package, http://www-d0.fnal.gov/d0dist/dist/releases/development/muo_cert

[16] The p14-pass2 muo_cert sample skimmed from the 1MUloose by Gavin. See http://www-d0.fnal.gov/computing/algorithms/muon/data2.html sample 1

[17] PhD thesis of Y. D. Mutaf, Measurement of the Ratio of Inclusive Cross Sections $\sigma(p\bar{p} \to Z + b\text{-jet})/\sigma(p\bar{p} \to Z + \text{jet})$ at $\sqrt{s} = 1.96$ TeV, p153.

[18] James Heinmiller, Nikos Varelas, Jet Reconstrucion Efficiency, DØ note in preparation

[19] V.Buescher *et al.* Recommendation of the Ad-Hoc Committee on Limit-Setting Procedure to be used by DØ in RunII, DØ note 4629